

Comparative Phylogenetic and Molecular Analysis of Plant TIR Domain Proteins

Inaugural-Dissertation

zur

Erlangung des Doktorgrades

der Mathematisch-Naturwissenschaftlichen Fakultät

der Universität zu Köln

vorgelegt von

Oliver Johandrees

aus Lippstadt

Köln, September 2022

Die vorliegende Arbeit wurde am Max-Planck-Institut für Pflanzenzüchtungsforschung in Köln in der Abteilung für Pflanze-Mikroben Interaktionen (Direktor: Prof. Dr. Paul Schulze-Lefert), Arbeitsgruppe Prof. Dr. Jane E. Parker durchgeführt.



MAX-PLANCK-GESELLSCHAFT

Gutachter*innen: Prof. Dr. Jane E. Parker
Prof. Dr. Gunther Döhlemann

Prüfungsvorsitzender: Prof. Dr. Stanislav Kopriva

Tag der mündlichen Prüfung: Mittwoch, 16.11.2022

Publications

Differential *EDSI* requirement for cell death activities of plant TIR-domain proteins

Oliver Johanndrees, Erin L. Baggs, Charles Uhlmann, Federica Locci, Henriette L. Läßle, Katharina Melkonian, Kiara Käufer, Joram A. Dongus, Hirofumi Nakagami, Ksenia V. Krasileva, Jane E. Parker, Dmitry Lapin

(2021) *bioRxiv* (submitted)

Molecular innovations in plant TIR-based immunity signaling

Dmitry Lapin, Oliver Johanndrees, Zhongshou Wu, Xin Li, Jane E. Parker

(2022) *The Plant Cell*

A conserved module regulates receptor kinase signalling in immunity and development

Thomas A. DeFalco, Pauline Anne, Sean R. James, Andrew C. Willoughby, Florian Schwanke, Oliver Johanndrees, Yasmine Genolet, Paul Derbyshire, Qian Wang, Surbhi Rana, Anne-Marie Pullen, Frank L. H. Menke, Cyril Zipfel, Christian S. Hardtke, Zachary L. Nimchuk

(2022) *Nature Plants*

Abstract

Toll/Interleukin 1 receptor (TIR) domains are found across kingdoms of life, where they serve as integral components in immune and cell death pathways. TIRs occur as single-domain proteins and parts of larger protein receptor complexes with common sets of associated domains. Self-association and enzymatic activity are common TIR features, conserved across kingdoms. In plants, TIRs constitute N-terminal signaling domains of intracellular nucleotide-binding leucine-rich repeat receptors (NLRs), which form an important part of the plant immune system to detect pathogen interference. Activated TIR-NLRs (TNLs) produce distinct enzymatic metabolites that serve as second messengers in immunity. While in plants, all studied TIR signaling requires the ENHANCED DISEASE SUSCEPTIBILITY 1 (EDS1) protein family, TIR domains were predicted in plant species with an incomplete or missing EDS1 family. It remains unknown whether TIRs and EDS1 family members co-evolved in plants, and how TIRs evolved in plants without EDS1.

The work presented here provides a large-scale phylogenetic analysis of TIR domains from 39 algae and land plant species, which identified four conserved TIR groups shared by multiple plant clades. Using the phylogeny, this study provides a comprehensive phylogeny-based nomenclature for plant TIRs. Among the conserved groups is a TIR-only group, which highly correlates with EDS1 in tested species and induces *EDS1*-dependent cell death. In contrast, a member of the most widespread group of TIR-NB-TPR (TNP) proteins, which persisted in plants without EDS1, induces *EDS1*-independent cell death. This is the first reported incidence of *EDS1*-independent cell death, induced by a plant TIR domain protein to date, and is in striking contrast to the majority of studied TIRs, including TNLs. This study furthermore provides a comprehensive set of conserved TIR-only and TNP mutants, generated by CRISPR/Cas9 mutagenesis, to study involvement of conserved TIRs in immune signaling pathways.

Table of Contents

Publications	I
Abstract	II
Table of Contents	III
Abbreviations	V
1. Introduction	1
1.1. Surface and intracellular immune receptors in plants	2
1.2. EDS1 signaling branches in plant TIR-mediated immunity.....	5
1.3. Conservation of TIR domains across kingdoms of life	7
1.4. TIR domain self-associations and enzymatic activities.....	10
1.5. Plant TIR metabolites selectively induce EDS1-RNL complexes	13
1.6. Thesis Aims	14
2. Results	15
2.1. Reconstruction of plant TIR domain evolution	16
2.1.1. TIR proteins have radiated in Eudicots and Conifers.....	16
2.1.2. Land plants have evolved four conserved TIR groups.....	18
2.1.3. Conserved TIRs show distinct co-occurrence patterns with the EDS1 family	23
2.1.4. TIR-associated NB-ARC phylogeny reflects conserved TIR groups	23
2.1.5. Catalytic glutamate residues are conserved across TIR groups	25
2.1.6. Conserved <i>TIR-ONLYs</i> are transcriptionally upregulated in immunity	26
2.2. Exploring the involvement of conserved TIR proteins in plant immunity.....	30
2.2.1. Conserved Monocot TIR-onlys induce <i>EDS1</i> -dependent cell death.....	30
2.2.2. Conserved TIR-onlys do not contribute to bacterial resistance in <i>A. thaliana</i>	32
2.2.3. Conserved TIR-onlys do not potentiate TNL signaling in <i>N. benthamiana</i>	36
2.2.4. Maize <i>ZmTNP-IIa</i> induces <i>EDS1</i> -independent cell death in <i>N. tabacum</i>	41
2.2.5. <i>Botrytis</i> -infected <i>N. benthamiana tnp</i> mutants develop smaller necrotic lesions	45
3. Discussion	51
3.1. TIR phylogeny reveals four interspecific conserved groups	51
3.1.1. Advantages of a phylogeny-based TIR protein grouping	51
3.1.2. Potential implications of TIR protein radiation.....	52
3.1.3. Using phylogeny to predict TIR-EDS1 co-evolutionary patterns	53

3.2.	Differential EDS1 requirements for plant TIR-induced cell death.....	55
3.2.1.	Conserved monocot TIR-onlys induce cell death dependent on <i>EDS1</i>	55
3.2.2.	<i>ZmTNP-IIa</i> is an autoactive <i>EDS1</i> -independent cell death inducer	56
3.3.	High-order conserved TIR mutants to identify potential functions.....	58
3.3.1.	TIR-onlys might act redundantly in immunity.....	58
3.3.2.	TNPs likely have immune-unrelated functions.....	59
3.4.	Co-evolutionary patterns and potential origins of plant TIRs	62
3.5.	Future Perspectives.....	64
4.	Material and Methods.....	65
4.1.	Material.....	65
4.1.1.	Species and Proteomes	65
4.1.2.	HMMs	67
4.1.3.	Public RNAseq datasets	68
4.1.4.	Oligonucleotides.....	68
4.1.5.	Vectors	72
4.1.6.	Plant Material	73
4.1.7.	Bacterial Strains	74
4.1.8.	Antibiotics	74
4.1.9.	Antibodies	75
4.1.10.	Media.....	75
4.2.	Methods	76
4.2.1.	Bioinformatic Methods	76
4.2.2.	Biochemical Methods.....	78
4.2.3.	Molecular Biological Methods.....	80
4.2.4.	Bacterial Methods	89
4.2.5.	Plant Methods.....	91
5.	References	96
	Acknowledgements	106
	Eidesstattliche Erklärung.....	107

Abbreviations

%	percent
°C	degree Celsius
μF	micro Farad
μl	microliter(s)
μm	micrometer(s)
μM	micromolar
aa	amino acid(s)
ADP	adenosine diphosphate
ADPr-ATP	ADP-ribosylated ATP
ADR1	ACTIVATED DISEASE RESISTANCE 1
ARM	Armadillo motif
<i>At</i>	<i>Arabidopsis thaliana</i>
ATP	adenosine triphosphate
ATR1	A.THALIANA RECOGNIZED 1
<i>At</i> TIR	<i>Arabidopsis thaliana</i> conserved TIR-only
Avr-protein	avirulence protein
BAK1	BRI1-ASSOCIATED RECEPTOR KINASE 1
<i>Bd</i>	<i>Brachypodium distachyon</i>
<i>Bd</i> TIR	<i>Brachypodium distachyon</i> conserved TIR-only
<i>Bgh</i>	<i>Blumeria graminis</i> f.sp. <i>hordei</i>
BIK1	BOTRYTIS-INDUCED KINASE 1
BLAST	Basic Local Alignment Search Tool
bp	base pair(s)
BPSS	Bayesian partitioning with pattern selection
<i>Ca</i>	<i>Capsicum annuum</i>
Ca ²⁺	Calcium
cADPR	cyclic ADP-ribose
Cas9	CRISPR-associated protein 9
CC	coiled-coil domain
cDNA	complementary DNA
CDS	coding sequence
CFU	colony-forming unit(s)
C-JID	C-terminal jelly roll/Ig-like domain
cm	centimeter(s)
CNL	CC-domain NLR
Col-0	<i>Arabidopsis thaliana</i> accession “Columbia 0”
CRISPR	Clustered Regularly Interspaced Short Palindromic Repeats
C-terminus	carboxyl terminus
cv.	cultivar

ddH ₂ O	double-distilled water
di-ADPR	ADP-ribosylated ADPR
DMSO	dimethyl sulfoxide
DNA	deoxyribonucleic acid
dpi	day(s) post infection
DTT	dithiothreitol
EDS1	ENHANCED DISEASE SUSCEPTIBILITY 1
EDTA	ethylenediaminetetraacetic acid
eFP	electronic fluorescent protein browser
EP-domain	EDS1-PAD4 domain
ETI	effector-triggered immunity
EV	empty vector
flg22	22 amino acid epitope of flagellin
FLS2	FLAGELLIN SENSING 2
f. sp.	forma specialis
fw	forward
gDNA	genomic DNA
GFP	green-fluorescent protein
gRNA	guide RNA
GW	Gateway® cloning
h	hour(s)
HMM	Hidden-Markov-Model
hpi	hour(s) post infection
HRP	horse radish peroxidase
<i>Hs</i>	<i>Homo sapiens</i>
<i>Hv</i>	<i>Hordeum vulgare</i>
<i>Hv</i> TIR	<i>Hordeum vulgare</i> conserved TIR-only
Hz	Hertz
IgG	Immunoglobulin G
IL-1R	Interleukin-1 receptor
IP	immunoprecipitation
kb	kilobase(s)
kDa	kilo Dalton
kV	kilo Volt(s)
l	liter(s)
LRR	leucine-rich repeat domain
<i>Lu</i>	<i>Linum usitatissimum</i>
M	molar
Mal	Myd88 adaptor-like
MAPK	mitogen-activated protein-kinase
mg	milligram(s)
min	minute(s)

ML	maximum-likelihood
ml	milliliter(s)
mm	millimeter(s)
mM	millimolar
mRNA	messenger RNA
ms	millisecond(s)
Myd88	Myeloid differentiation primary response 88
NA	not available
NAD ⁺	nicotinamide adenine dinucleotide
<i>Nb</i>	<i>Nicotiana benthamiana</i>
NB-ARC	nucleotide-binding, shared by Apaf-1, R-proteins and CED-4
NB	nucleotide-binding domain
ng	nanogram(s)
nlp	necrosis and ethylene-inducing peptide 1-like
nlp20	20 amino acid epitope of fungal nlp
nlp24	24 amino acid epitope of fungal nlp
NLR	nucleotide-binding and leucine-rich repeat
nm	nanometer(s)
nM	nanomolar
NOD	nucleotide-binding-oligomerization domain
NRG1	N REQUIREMENT GENE 1
<i>Nt</i>	<i>Nicotiana tabacum</i>
nt	nucleotide(s)
N-terminus	amino terminus
o/n	overnight
OD ₆₀₀	optical density at 600 nm
<i>Os</i>	<i>Oryza sativa</i>
<i>Os</i> TIR	<i>Oryza sativa</i> conserved TIR-only
PAD4	PHYTOALEXIN-DEFICIENT 4
PAGE	polyacrylamide gel electrophoresis
PAMP	pathogen-associated molecular pattern
PBL2	PBS1-LIKE KINASE 2
PBL31	PBS1-LIKE 31
PCR	polymerase chain reaction
pRib-ADP	2'-(5''-phosphoribosyl)-5'-adenosine diphosphate
pRib-AMP	2'-(5''-phosphoribosyl)-5'-adenosine monophosphate
PRR	pattern-recognition receptor
<i>Pst</i>	<i>Pseudomonas syringae</i> pv. <i>tomato</i>
PTI	pattern-triggered immunity
pv.	pathovar
RBA1	RECOGNITION OF HOPBA1
RBOHD	RESPIRATORY BURST OXIDASE HOMOLOGUE D

RK	receptor kinase
RLP	receptor-like protein
RLP23	RECEPTOR-LIKE PROTEIN 23
RNA	ribonucleic acid
RNAi	RNA-interfering
RNAseq	RNA-sequencing
RNL	RPW8-like CNL
Roq1	RECOGNITION OF XOPQ 1
ROS	reactive oxygen species
rpm	round(s) per minute
RPP1	RECOGNITION OF PERONOSPORA PARASITICA 1
RPS2	RESISTANT TO P. SYRINGAE 2
RPS4	RESISTANT TO P. SYRINGAE 4
RPW8	RESISTANCE TO POWDERY MILDEW 8
RRS1	RESISTANT TO RALSTONIA SOLANACEARUM 1
RT	room temperature
RT-PCR	reverse-transcriptase PCR
rv	reverse
SAG101	SENESCENCE-ASSOCIATED GENE 101
SARM1	STERILE ALPHA AND TIR MOTIF CONTAINING 1
SDS	sodium dodecyl sulfate
sec	second(s)
SH	Strep-HA protein tag
SNC1	SUPPRESSOR OF NPR1-1, CONSTITUTIVE 1
SOBIR1	SUPPRESSOR OF BIR1 1
SRA	Sequence Read Archive
TBS	TRIS-buffered saline
T-DNA	Transfer DNA from <i>Agrobacterium tumefaciens</i>
TEMED	tetramethylethylenediamine
TIR	Toll/interleukin-1 receptor
TIRAP	TIR adaptor protein
TLR	Toll-like receptor
TMV	tobacco mosaic virus
TN	TIR-NB protein
TNL #1	conserved TNL group #1
TNL #2	conserved TNL group #2
TNL	TIR-NLR protein
TNP	TIR-NB-TPR protein
tpm	transcripts-per-kilobase-million
TPR	Tetratricopeptide repeat
TRIS	tris(hydroxymethyl)aminomethane
TX	TIR-X protein

UV	ultraviolet light
V	Volt(s)
v/v	volume per volume
v-cADPR	variant cADPR
w/v	weight per volume
WsB	<i>Arabidopsis thaliana</i> accession “Wassilewskija”
WT	wild type
x	times
Xcv	<i>Xanthomonas campestris</i> pv. <i>vesicatoria</i>
xg	relative centrifugal force
XTNX	X-TIR-NB-X protein
YFP	yellow-fluorescent protein
ZAR1	HOPZ-ACTIVATED RESISTANCE 1
Zm	<i>Zea mays</i>

1. Introduction

The Toll/Interleukin-1 Receptor (TIR) domain is present across all three domains of life, including prokaryotes such as Archaea and bacteria as well as eukaryotes like mammals and plants. Across organisms, TIR domains can be associated with various other protein domains and engage in signaling pathways, often linked to cell death and immune responses. Within their pathways, TIRs can provide protein-protein interaction hubs, act as homomeric signaling devices, or engage in large protein complexes. Over the past few years, landmark studies have reported a TIR-catalyzed enzymatic activity, which marked the starting point of research aimed at identifying activation mechanisms, enzymatic properties, and downstream signaling activities of TIR domains. Phylogenetic studies have investigated the evolution of TIRs, both at the very broad scale utilizing cross-kingdom domain comparisons, and in more detail within smaller groups of organisms. These studies have defined major functionally conserved features within groups of TIR proteins. Past research on plant TIR proteins has largely focused on their roles within immune receptors. However, recent studies have ascribed multiple enzymatic activities to plant TIRs. These enzymatic activities yield multiple products that may subsequently engage different downstream signaling branches. The assortment of TIR-products may account for downstream signal divergence between various TIR domains. However, it remains poorly understood how plant TIR domains evolved and to what extent they co-evolved with their downstream signaling partners in plant immunity.

1.1. Surface and intracellular immune receptors in plants

Unlike most animals, which possess professional and often motile immune cells, plants rely entirely on cell-autonomous innate immunity to perceive and counter invading microbes. Accordingly, all plant cells are capable of microbial perception and the initiation of downstream immune responses. Plants are able to sense the presence of conserved microbial molecules called pathogen-associated microbial patterns (PAMPs) using surface-localized receptors, which constitute the first layer of immunity against a broad range of invading pathogens. These so-called pattern-recognition receptors (PRRs) are plasma-membrane bound receptor kinases (RKs) or receptor-like proteins (RLPs) (Couto & Zipfel, 2016). Both PRR types have an extracellular ligand-binding domain and a single pass transmembrane portion. Furthermore, RKs contain an intracellular kinase domain, which RLPs lack (Couto & Zipfel, 2016). An example of RKs is FLAGELLIN-SENSING 2 (FLS2) from *Arabidopsis thaliana*, which contains a leucine-rich repeat (LRR) ectodomain for detection of bacterial flagellin (a 22 amino acid epitope called flg22) (Zipfel *et al.*, 2004). Upon flg22 binding, FLS2 forms a heterocomplex with its co-receptor BRI1-ASSOCIATED RECEPTOR KINASE 1 (BAK1), which is stabilized by incorporation of the PAMP (Sun *et al.*, 2013). BAK1 is a common co-receptor that is used by several RKs and RLPs (Couto & Zipfel, 2016). Activated PRRs use cytoplasmatic kinases, which in the case of FLS2 is BOTRYTIS-INDUCED KINASE 1 (BIK1). In the resting state, BIK1 associates with FLS2, and upon elicitation with flg22 it is phosphorylated by BAK1 leading to dissociation of activated BIK1 from the complex (Lu *et al.*, 2010; Zhang *et al.*, 2010). Activated BIK1 then phosphorylates RESPIRATORY BURST OXIDASE HOMOLOGUE D (RBOHD) resulting in production of reactive oxygen species (ROS) (Kadota *et al.*, 2014; Li *et al.*, 2014). In general, PAMP-induced ROS bursts are among the earliest immune responses against pathogens, being induced within several minutes of PAMP perception (Couto & Zipfel, 2016). BIK1 also activates processes further downstream, including mitogen-activated protein kinase (MAPK) phosphorylation, transcriptional reprogramming, and Ca²⁺ influx into the cell (Kadota *et al.*, 2014). Taken together, the responses induced by PRRs provide a first barrier against a multitude of pathogens, which was termed pattern-triggered immunity (PTI).

A well-studied RLP contributing to PTI is RECEPTOR-LIKE PROTEIN 23 (RLP23), which possesses an extracellular LRR domain that binds the conserved 20 or 24 amino acid epitopes of necrosis and ethylene-inducing peptide 1-like (nlp) proteins (nlp20 or nlp24) (Albert *et al.*, 2015;

Seidl & Van den Ackerveken, 2019). RLP23 lacks an intracellular kinase domain, but constitutively associates with the RLK SUPPRESSOR OF BIR1 1 (SOBIR1). Upon nlp binding, BAK1 is recruited to form a tripartite complex at the plasma membrane as well (Albert *et al.*, 2015). In contrast to FLS2, RLP23 downstream signaling is mediated by the cytoplasmatic kinase PBS1-LIKE31 (PBL31) (Pruitt *et al.*, 2021). While BIK1 induces a strong ROS burst via activation of RBOHD (Kadota *et al.*, 2014; Li *et al.*, 2014), PBL31 leads to a pronounced ethylene induction and a weaker ROS burst (Pruitt *et al.*, 2021). BIK1 was shown to negatively regulate RLP23-PBL31-mediated PTI responses.

While PTI provides a robust layer of defense against an array of opportunistic pathogens, professional host-adapted pathogens have evolved ways to manipulate the plant immune system by interfering with host processes. Similar to animal pathogens, professional plant pathogens secrete a plethora of so-called effector molecules, which generally consist of small proteins, peptides, or metabolites (Toruno *et al.*, 2016). These effectors directly interfere with plant immunity or alter host metabolic processes or developmental programs to enhance pathogen colonization. In order to counter host-adapted pathogens, plants have evolved a second layer of immunity, which perceives pathogens via effector surveillance programs (Jones & Dangl, 2006). This surveillance is carried out by intracellular nucleotide-binding LRR receptors (NLRs), which resemble mammalian nucleotide-binding-oligomerization domain (NOD)-like receptors. Plant NLRs have a central nucleotide-binding domain (NB) (further classified as Apaf1/R/CED4-like NB (NB-ARC) domain) and are divided into two categories based on their variable N-terminal domains namely TIR-NLRs (TNLs) and coiled-coil (CC) domain NLRs (CNLs) (Jones *et al.*, 2016). These NLRs directly bind effectors or indirectly detect their manipulation of host processes to induce immunity (Monteiro & Nishimura, 2018; Tamborski & Krasileva, 2020).

Many direct interactions between NLRs and effectors were described, including the *A. thaliana* and *Nicotiana benthamiana* TNLs RECOGNITION OF PERONOSPORA PARASITICA 1 (*AtRPP1*^{WsB}) and RECOGNITION OF XOPQ 1 (*NbRoq1*), which recognize the effectors A.THALIANA RECOGNIZED 1 (*ATR1*^{Emoy2}) and XopQ from the oomycete *Hyaloperonospora parasitica* and bacterium *Xanthomonas campestris* pv. *vesicatoria* (*Xcv*), respectively (Krasileva *et al.*, 2010; Schultink *et al.*, 2017). Upon direct effector recognition, these TNLs oligomerize to induce downstream responses (Ma *et al.*, 2020; Martin *et al.*, 2020). However, it became obvious that there are NLRs that monitor host manipulation in different ways. In addition to the directly

recognized effectors, some NLRs sense perturbations in effector-modified host proteins, called guardees, or by trapping effectors using so-called decoys, which resembles functional effector targets (van der Hoorn & Kamoun, 2008). The *A. thaliana* CNL HOPZ-ACTIVATED RESISTANCE 1 (ZAR1) for example recognizes an effector-manipulated form of the pseudokinase decoy PBS1-LIKE KINASE 2 (PBL2) (Wang *et al.*, 2015), leading to formation of a pentameric ring (Wang *et al.*, 2019a; Wang *et al.*, 2019b). Upon activation, ZAR1 is likely inserted into the plasma membrane, where it acts as a Ca²⁺-permeable channel (Wang *et al.*, 2019a; Wang *et al.*, 2019b). This represents the first example of plant-pathogen perception via identification of an effector-modified host protein at the molecular level. The ZAR1-like mechanism was proposed for additional CNLs (Adachi *et al.*, 2019), and gave a first answer to the long standing question of NLR activation. Activated NLRs lead to a strong immune response oftentimes including programmed host cell death which provides a robust layer of defense against adapted pathogens, called effector-triggered immunity (ETI) (Jones & Dangl, 2006).

1.2. EDS1 signaling branches in plant TIR-mediated immunity

While the mechanism of TNL activation has only recently been solved, the downstream signaling pathways establishing TNL-mediated ETI have been subject to research for the past three decades. Strikingly, all studied plant TIR proteins signal via ENHANCED DISEASE SUSCEPTIBILITY 1 (EDS1) and its two interacting protein partners (Lapin *et al.*, 2020; Venugopal *et al.*, 2009; Wirthmueller *et al.*, 2007). Together with PHYTOALEXIN-DEFICIENT 4 (PAD4) and SENESCENCE-ASSOCIATED GENE 101 (SAG101), EDS1 forms a conserved family of lipase-like proteins, defined by their C-terminal EDS1-PAD4 (EP) domain (Wagner *et al.*, 2013). Outside the EDS1 family, no other proteins are described to contain EP domains (Wiermer *et al.*, 2005). The EP domain contributes to formation of exclusive EDS1-PAD4 and EDS1-SAG101 heterodimers (Wagner *et al.*, 2013).

In plants, TIR and EDS1 heterodimer signaling depends on a class of conserved CNLs, also termed “helper NLRs” with a RESISTANCE TO POWDERY MILDEW 8 (RPW8)-like CC domain (RNLs). The RNLs ACTIVATED DISEASE RESISTANCE 1 (ADR1) and N REQUIREMENT GENE 1 (NRG1) co-function with EDS1-PAD4 and EDS1-SAG101 heterodimers, respectively (Sun *et al.*, 2021; Wu *et al.*, 2021). The two *A. thaliana* TNLs RESISTANT TO *P. SYRINGAE* 4 (*AtRPS4*) and RESISTANT TO *RALSTONIA SOLANACEARUM* 1 (*AtRRS1*) sense the presence of the bacterial effector protein AvrRps4 together as an NLR-pair and were used as ETI triggers in extensive genetic studies on the two emerging EDS1 signaling branches. In *AtRPS4-AtRRS1*-mediated immunity, the EDS1-PAD4-ADR1 branch is required to induce transcriptional reprogramming without visible host cell death, while the EDS1-SAG101-NRG1 branch mainly mediates host cell death induction (Bonardi *et al.*, 2011; Castel *et al.*, 2019; Lapin *et al.*, 2019; Saile *et al.*, 2020; Sun *et al.*, 2021; Wu *et al.*, 2019). In contrast, TNL-mediated immunity and cell death are both dependent on EDS1-SAG101-NRG1 in *N. benthamiana* (Gantner *et al.*, 2019; Qi *et al.*, 2018).

Historically, PTI and ETI have been regarded as separate layers, individually triggered during stages of immunity. However, it was recently shown that components of both immune sectors overlap and form a more complex network. Both TNL- and CNL-mediated ETI was shown to depend on PTI components such as RBOHD, indicating that ETI can be regarded as enhanced PTI (Ngou *et al.*, 2021; Tian *et al.*, 2021; Yuan *et al.*, 2021). At the same time, the EDS1-PAD4 heterodimer, a classical component of ETI, was shown to be involved in nlp20-triggered immune

responses (Pruitt *et al.*, 2021). EDS1-PAD4 are also known to contribute to resistance against virulent *Pseudomonas syringae* strains in *A. thaliana* that are not recognized by known TNLs (Cui *et al.*, 2017; Cui *et al.*, 2015; Dongus & Parker, 2021), an immune response that was termed “basal resistance”. The crosstalk between PTI and ETI, as well as the functional overlap of immune pathways suggest a far more complicated immune network in plants and argue against a strict division between PTI and ETI responses (Ngou *et al.*, 2021).

1.3. Conservation of TIR domains across kingdoms of life

Apart from appearing in plant TNLs, TIR domains are also found across all forms of cellular life (Toshchakov & Neuwald, 2020). Despite varying primary sequences and associated protein domains, a conserved flavodoxin-like α/β -fold is shared between bacterial, animal and plant TIRs (Bayless & Nishimura, 2020; Lapin *et al.*, 2022; Nimma *et al.*, 2021), defining the domain across kingdoms. The first TIRs were recognized as domains shared by *Drosophila melanogaster* Toll and human Interleukin-1 receptor (IL-1R) proteins (Gay & Keith, 1991). Both are involved in innate immunity, but Toll is also indispensable for *D. melanogaster* embryogenesis (Anderson *et al.*, 1985; Lemaitre *et al.*, 1996). As first plant TIR homolog, the *N. benthamiana* N resistance protein was described, which resembles a TNL mediating resistance against tobacco mosaic virus (TMV) (Whitham *et al.*, 1994). Structurally, TIRs consist of a central β -sheet surrounded by five alphabetically named α -helices (Toshchakov & Neuwald, 2020). Plant TIRs differ from those studied in bacteria and animals in an extended α -helical D region (Bernoux *et al.*, 2011; Lapin *et al.*, 2022). This plant-specific feature was implicated in cell death signaling and enzymatic activity of plant TIRs.

Plant TIR domain containing proteins contribute to diverse signaling pathways, and additional domains appear to specify the function of individual TIR proteins. Certain common TIR protein architectures have been functionally defined and grouped via phylogenetic analyses in the past. TIR-containing proteins mostly have one of the following domain architectures: (1) short TIR-only proteins with at most additional short domains, (2) TIR domains directly fused to repeat domains, and (3) TIR domains connected to an NB and variable repeat domains (Lapin *et al.*, 2022). The integration of TIR domains into various full-length proteins and diverse signaling pathways marks the importance of this signaling domain across phylogenetic groups of organisms.

The first group of TIR proteins was described in bacteria, oomycetes, animals, and plants. They can either be complete stand-alone TIRs or contain additional short domains, for example transmembrane portions, but TIR domains occupy most of their sequence. This is the most widespread domain architecture for TIR-containing proteins in plants (Lapin *et al.*, 2022; Meyers *et al.*, 2002; Sun *et al.*, 2014), and is also a feature of several effector proteins secreted by human and plant bacterial pathogens (Eastman *et al.*, 2021; Nanson *et al.*, 2020). Also, part of this group are the human Myeloid differentiation primary response 88 (Myd88) and Myd88 adaptor-like (Mal) proteins, which provide a protein-protein interaction hub in innate immunity (O'Neill & Bowie,

2007). A characterized plant TIR-only protein is RECOGNITION OF HOPBA1 (*AtRBA1*) from *A. thaliana*, which induces immune defenses in response to the *P. syringae* effector HopBA1 (Nishimura *et al.*, 2017). Although mostly lacking other prominent protein domains, these TIR proteins fulfill a large variety of functions across different organisms. The most prominent members of the ‘TIR + repeat’ architecture are animal LRR-containing Toll-like receptor (TLR) proteins. TLRs detect the presence of extracellular PAMPs (Kawasaki & Kawai, 2014; O’Neill & Bowie, 2007), showing a functional overlap with plant PRRs. In contrast to plant PRRs however, TLRs induce downstream signaling to induce a cell death response upon PAMP binding (Kawasaki & Kawai, 2014). So far, no analogous TIR-containing PAMP receptors have been described in plants. The third group of TIR proteins has a ‘TIR-NB-repeat’ architecture and was identified in prokaryotes and plants. Common C-terminal repeat domains include LRR, WD40 or Tetratricopeptide repeat (TPR) domains, which vary across different organisms (Lapin *et al.*, 2022; Sarris *et al.*, 2016). TIR-NB-TPR proteins are present in bacteria and plants (Lapin *et al.*, 2022). Fungi contain HET-NB-TPR proteins with the HET domain resembling TIRs at the sequence level (Dyrka *et al.*, 2014).

Two major trends can be observed in the evolution of TIRs, resulting both in high copy number variation of certain TIRs and simultaneous maintenance of a small cadre of evolutionarily conserved TIRs. In animals, Myd88 and Mal proteins were kept in low copy numbers and show a high degree of conservation across species (Kumar *et al.*, 2017; O’Neill & Bowie, 2007; Toshchakov & Neuwald, 2020), while the number of TLRs per genome can vary drastically (Liu *et al.*, 2021). A similar trend was observed in plants, where TNL numbers in most Eudicots expanded, most likely to specialize in the detection of diverse pathogenic effectors. At the same time, Monocots and aquatic flowering plants lost full-length TNLs completely and members of the Caryophyllales order within Eudicots have a reduced TNL repertoire (Baggs *et al.*, 2020; Lapin *et al.*, 2019; Liu *et al.*, 2021; Monteiro & Nishimura, 2018; Shao *et al.*, 2016; Tamborski & Krasileva, 2020). To date, the mechanisms that balance the persistence or loss of TNLs in plant genomes are not fully understood. Phylogenetically conserved TIR proteins were also described in plants, in the form of TIR-NB-TPR proteins (TNPs, also known as XTNX), which exist in most land plants (Meyers *et al.*, 2002; Nandety *et al.*, 2013; Zhang *et al.*, 2017b). A phylogenetic study reported their presence in land plants ranging from Bryophytes to Angiosperms, encompassing most land plants (Zhang *et al.*, 2017b). They were described to exist in two major clades, which potentially originated from ancient genome duplications (Zhang *et al.*, 2017b).

Using a method called Bayesian partitioning with pattern selection (BPSS) (Neuwald, 2014), groups of TIRs were identified across prokaryotes, animals, and plants in a computationally affordable way (Toshchakov & Neuwald, 2020). TIRs were divided mostly into kingdom-specific protein groups, representing functionally diverging TIR proteins. For example, the largest animal-specific group contained TLR receptors, and the largest plant group is comprised of TNLs (Toshchakov & Neuwald, 2020). While inter-kingdom studies like this provide a valuable resource to classify TIRs across kingdoms and highlight overarching trends in structural diversification, they lack resolution at the single protein level. For instance, ~1000 plant TIR-containing proteins could not be classified based on BPSS (Toshchakov & Neuwald, 2020). In contrast, phylogenetic studies on a subset of TIR proteins or at the level of individual species can provide a higher-resolution classification (Meyers *et al.*, 2002; Nandety *et al.*, 2013; Zhang *et al.*, 2017b). However, there have been no studies that explicitly compare all TIRs found in plants, to discover plant specific TIR evolutionary trends, using the latest set of available genomes.

1.4. TIR domain self-associations and enzymatic activities

In addition to their common structural elements and similar trends in evolution, TIR domains are also functionally conserved across kingdoms. Two conserved aspects of TIR functions are the formation of intermolecular TIR-TIR protein interactions and their consequential enzymatic activity, which are both shared by most TIR domains.

The existence of TIR-TIR interactions was described for animal and plant proteins alike and is crucial for direct and indirect TIR signaling activities. By interacting with TIRs of activated TLR receptors, animal TIR adaptor proteins like Myd88 and TIRAP form complexes at the plasma membrane, which provide signaling platforms for activated PAMP signaling leading to protein kinase activation and transcriptional reprogramming (Clabbers *et al.*, 2021; Fields *et al.*, 2019; O'Neill & Bowie, 2007). Interestingly, this pathway is itself targeted by TIR domain effectors from pathogenic bacteria, which can form heterodimers with the mammalian signaling components to interfere with immunity (Cirl *et al.*, 2008; Nanson *et al.*, 2020; Yadav *et al.*, 2010). This is a striking example of inter-kingdom conservation of TIR-TIR interactions. TIR-TIR interactions were also described for the human STERILE ALPHA AND TIR MOTIF CONTAINING 1 (*HsSARM1*) protein, which is involved in inducing axonal cell death. Upon activation, *HsSARM1* TIRs come into close proximity, which is important for neurodegeneration (Shi *et al.*, 2022).

In plants, studies of TIR-TIR interactions were first based on the crystal structures of TIR domains from the *Linum usitatissimum* (flax) and *A. thaliana* TNL receptors *LuL6* and *AtRPS4-AtRRS1* pair, respectively (Bernoux *et al.*, 2011; Williams *et al.*, 2014). Separated from their NB-ARC and LRR domains, their TIRs induce autoactive cell death that does not require the presence of their cognate effectors (Zhang *et al.*, 2017a) but is still dependent on EDS1 in *N. benthamiana* (Wan *et al.*, 2019). The structures showed TIR homodimers, resolving important interaction surfaces that also influence the function of their full-length receptor proteins. In the *LuL6*^{TIR} dimer, a self-association interface between the α D and α E helices (DE interface) was reported (Bernoux *et al.*, 2011), while the *AtRPS4*^{TIR}-*AtRRS1*^{TIR} interaction was mainly mediated by the α A and α E helices (AE interface) (Williams *et al.*, 2014). Later, it was shown that plant TIRs including the ones from *A. thaliana* TNLs SUPPRESSOR OF NPR1-1, CONSTITUTIVE 1 (*AtSNC1*) and *AtRPP1*^{WSB} interact via both AE and DE interfaces and that mutations in either of the interfaces impairs signaling and cell death functions (Zhang *et al.*, 2017a). The importance of the DE interface in cell

death induction was later confirmed for the *A. thaliana* and *Brachypodium distachyon* TIR-only proteins *AtRBA1* and *BdTIR*, respectively (Nishimura *et al.*, 2017; Wan *et al.*, 2019).

TIR-TIR interactions are required for recently discovered TIR-enzymatic activity, marking the second conserved attribute of TIRs. Apart from the TIRs of TLRs and TIR adaptor proteins, which likely evolved into purely structural protein-protein interaction domains, most investigated TIRs are enzymatically active (Bayless & Nishimura, 2020; Horsefield *et al.*, 2019). This activity was first shown for *HsSARM1*, which is able to hydrolyze NAD^+ (Essuman *et al.*, 2017). *HsSARM1* lowers intracellular NAD^+ levels likely leading to an energy imbalance and consequent neuronal cell death (Essuman *et al.*, 2017). A similar enzymatic activity was later shown for bacterial and archaeal TIRs (Essuman *et al.*, 2018), as well as plant TNL TIRs and the TIR-onlys *AtRBA1* and *BdTIR* (Wan *et al.*, 2019). TIR domains are active NADases in *in vitro* experiments showing that no other intrinsic signaling components or enzymes are required. Mutations in the AE and DE interfaces of plant TIRs disrupted NADase activities (Wan *et al.*, 2019), again highlighting the importance of TIR-TIR interactions. Apart from self-association, a single glutamate residue is required for NADase activity of all of the tested TIRs, which is conserved across organisms (Essuman *et al.*, 2018; Wan *et al.*, 2019; Whitham *et al.*, 1994). This glutamate resides in the αC helix and forms part of the catalytic site that was identified in the plant TIRs.

The structures of full-length *AtRPP1*^{WsB} and *NbRoq1* TNLs in complex with their cognate effectors ATR1 and XopQ, respectively, have been solved using cryo electron-microscopy (EM) (Ma *et al.*, 2020; Martin *et al.*, 2020). These so-called plant resistosomes form tetrameric structures, consisting of four TNLs and four effector proteins in complex. Upon effector binding, the resistosomes assemble and sections of the TNL NB-ARC domains around a region called “P-loop” assist in complex formation via contact points with the TIR domains (Ma *et al.*, 2020). This leads to stable tetramer formation, in which four TIRs are brought into close proximity. The P-loop region is important for a multitude of NLRs and mutations can lead to loss-of-function or autoactive versions of NLRs, as was shown for P-loop variants in *AtRPP1*^{WsB} and *AtNRG1* (Jacob *et al.*, 2021; Krasileva *et al.*, 2010). Upon complex assembly, TIRs in *AtRPP1*^{WsB} and *NbRoq1* form two symmetric and two asymmetric dimers, with the asymmetric TIR domains forming the catalytic center, required for NAD^+ hydrolysis. A loop connecting the βB sheet and αB helix (called BB-loop) comes into contact with the opposing TIR domain and forms the active center, resulting in two catalytic centers per TNL-effector tetramer (Ma *et al.*, 2020; Martin *et al.*, 2020). BB-loop

regions are conserved structural elements in other TIR domains and were shown to be required for TNL-mediated cell death (Ma *et al.*, 2020). Effectors are directly bound to the TNLs via interactions with the LRR domains as well as the C-terminal jelly roll/Ig-like domain (C-JID). C-JIDs are oftentimes present in TNLs that directly recognize effectors and were shown to be essential for both *AtRPP1*^{W^sB} and *NbRoq1* TNL-effector complex formation (Ma *et al.*, 2020; Martin *et al.*, 2020). Since C-JID-containing TNLs are widespread in plants (Lapin *et al.*, 2022; Ma *et al.*, 2020) it is likely that the *AtRPP1*^{W^sB} and *NbRoq1* resistosomes will form a basis to characterize functions and activities of other TNLs.

It was shown that molecular crowding alone, which leads to induced proximity of TIRs, can enhance their activities (Horsefield *et al.*, 2019), which underlines the importance of close TIR-TIR contacts. Consequential, in untriggered states TIRs have to be kept apart to avoid autoactivation. Different mechanisms have evolved to keep TIRs inactive. For example, in *HsSARM1* autoinhibitory armadillo motif (ARM) domains prohibit TIR-TIR contacts in the inactive octameric complex (Figley *et al.*, 2021; Shen *et al.*, 2021; Sporny *et al.*, 2020). By nicotinamide outcompeting NAD⁺ bound to the ARM domains, they likely change conformation and set TIR domains free allowing interactions and subsequent enzymatic activity. Similarly, it was shown for the *AtRPS4-AtRRS1* pair that binding to bacterial effectors relieves a self-inhibited state, allowing enzymatically active *AtRPS4* TIR domains to interact (Guo *et al.*, 2020).

1.5. Plant TIR metabolites selectively induce EDS1-RNL complexes

While NAD⁺ hydrolysis emerged as a common feature of enzymatically active TIR domains, the identity of resulting products varies between different organisms and TIR domains. *HsSARM1* mainly cleaves NAD⁺ into nicotinamide and cyclic ADP-Ribose (cADPR) (Essuman *et al.*, 2017). Nicotinamide and cADPR are also produced by prokaryotic and plant TIRs, which were additionally shown to produce a variant cADPR (v-cADPR) (Wan *et al.*, 2019). It is hypothesized that v-cADPR is the active signaling compound in the bacterial Thoeris system, which mediates antiphage resistance in a variety of bacteria (Ofir *et al.*, 2021). In the *Bacillus subtilis* Thoeris system, catalytic products from the TIR protein ThsB trigger the downstream NADase ThsA, which leads to NAD⁺ depletion and thereby induced resistance against invading phages (Ofir *et al.*, 2021). In plants, studies have hypothesized that v-cADPR might also be the signaling compound inducing cell death, however a study expressing a bacterial TIR that produces v-cADPR showed it is not sufficient to induce cell death in tobacco (Duxbury *et al.*, 2020), removing v-cADPR from the list of candidate TIR metabolites for downstream signaling in plants.

Instead, two studies identify the TIR catalytic metabolites ADP-ribosylated ATP (ADPr-ATP), ADP-ribosylated ADPR (di-ADPR) and 2'-(5''-phosphoribosyl)-5'-adenosine mono- or diphosphate (pRib-AMP/pRib-ADP) as active signaling compounds in plants (Huang *et al.*, 2022; Jia *et al.*, 2022), explaining the link between TIR activation and downstream immune signaling via EDS1 heterodimers, which has been puzzling for the last decades. The TIR-catalyzed metabolite pRib-AMP preferably binds EDS1-PAD4 (Huang *et al.*, 2022), while ADPr-ATP and di-ADPR are more likely to be incorporated into the EDS1-SAG101 complex (Jia *et al.*, 2022). Binding of the specific TIR metabolites induces EDS1 heterodimer associations with the respective RNLs, via a conformational change in PAD4 and SAG101 within the heterodimers (Huang *et al.*, 2022; Jia *et al.*, 2022). It is likely that activated ADR1 and NRG1 work as Ca²⁺ channels, in a ZAR1-like fashion, since homologous residues within their CC domains are crucial for their RNL cell death activity (Bi *et al.*, 2021; Jacob *et al.*, 2021) and the autoactive variant of *At*NRG1 was shown to induce Ca²⁺ influx into human HeLa cells, which is P-loop dependent (Jacob *et al.*, 2021). While these recent findings provided a direct link between TIR activation, enzymatic activity, and specification of downstream signaling, it still remains unknown how the formation of heterodimers is controlled so the plant can balance immune responses with and without induction of programmed cell death, as activated TIRs produced all three metabolites simultaneously (Huang *et al.*, 2022; Jia

et al., 2022). In addition to the NADase reaction products that induce specific EDS1-RNL interactions, plant TIRs were shown to catalyze a second reaction. Cryo-EM structures of flax *LuL7^{TIR}* bound to DNA revealed that plant TIRs can engage in signaling via cooperative assembly formation (SCAF), which was previously described for animal TIRs (Nanson *et al.*, 2020; Nimma *et al.*, 2021). SCAF leads to accumulation of TIRs by formation of long filaments, likely potentiating enzymatic activities. *LuL7^{TIR}* was shown to hydrolyze DNA and synthesize 2',3'-cyclic nucleotide monophosphates (cNMPs) to promote cell death (Yu *et al.*, 2022). While self-association was required for cNMP synthesis, a cysteine residue neighbouring the catalytic glutamate of *LuL7^{TIR}* is crucial for this second enzymatic activity (Yu *et al.*, 2022). While these studies provide more and more candidate metabolites, it remains unknown how TIR-generated signals are integrated during immune responses.

1.6. Thesis Aims

With an ever-increasing body of publications pointing to the importance of TIR domain containing proteins in plant immunity, providing a phylogeny-based annotation for plant TIRs is of major interest to allow selected analyses on different TIR groups. This study aimed to provide a solely phylogeny-based TIR annotation using TIRs from a comprehensive set of plant species. As the EDS1 signaling node is a major signaling partner for plant TIRs, investigating potential co-evolutionary patterns of TIRs and EDS1 in plants was a second aim. Testing the expression of identified conserved groups of TIR domains was another aim, which led to the identification of immune-related TIRs for further analyses.

The molecular analysis focused on confirming TIR-EDS1 co-evolutionary trends and to test whether TIR-EDS1 co-occurrence dictates EDS1-dependent functions of major TIR groups. Finally, CRISPR/Cas9 mutants were generated to test for involvement of conserved TIRs in plant immune responses and to establish if *TIR*-less plants are viable. Host plants were selected to represent a variety of EDS1 family protein sets to reflect natural variation within this important TIR signaling pathway.

2. Results

The results presented in this thesis are split into two major parts. The first part describes the establishment of a bioinformatic pipeline for TIR domain identification, copy number comparison and phylogenetic reconstruction of TIR evolution in plants. The resulting large-scale TIR phylogeny was then used to derive a phylogeny-based grouping of conserved TIR domains. Additionally, bioinformatic tools were utilized to analyze the immune-related expression of conserved TIR protein groups in a variety of plants. The second part deals with the molecular characterization of the two most conserved plant TIR protein groups identified in the first part, while highlighting their distinct *EDS1*-dependencies. Furthermore, the second part describes *A. thaliana* and *N. benthamiana* CRISPR/Cas9 mutants that were generated to investigate possible conserved TIR functions in and outside of immunity.

Most of the included data were also assembled into a publication, that can currently be found on bioRxiv (Johannndrees *et al.*, 2021). While all major findings are included in this thesis, I focus on the results that were generated by me during my time as a PhD student. Additional experiments and results taken from the manuscript are indicated using citations.

2.1. Reconstruction of plant TIR domain evolution

2.1.1. TIR proteins have radiated in Eudicots and Conifers

One of the aims of this thesis was to reconstruct plant TIR domain phylogeny and to find evolutionary trends among TIR domains, as well as possible co-evolutionary traces between TIRs and the EDS1 family. For an unbiased and novel view of plant TIR evolution, I did not rely on previously published sets of TIR proteins, but tried to gather TIRs directly from published proteomes, which are the result of protein predictions on sequenced and assembled genomes. The depth of information within such a phylogenetic analysis is always dependent on the amount and phylogenetic spread of the species chosen for the analysis. To get the most information possible, I decided to use species ranging across multiple phylogenetic clades within green plants. These included green algae (Chlorophyta and Streptophyta), non-vascular mosses and liverworts (Bryophytes) as well as vascular plants from Lycophytes, Gymnosperms (Conifers), Magnoliids, Monocots and finally multiple orders of the Eudicots (Rosids, Asterids, Caryophyllales). For all of these clades, I selected species, that had a genome and derived proteome available, either from a public database, or directly from publications (Table 1). In total, 39 plant species were selected for the TIR phylogenetic analysis.

First, I wanted to get an overview of how diverse TIR numbers would be amongst plants and across phylogenetic clades. For this, I established a bioinformatic pipeline to search the proteomes of all selected plants using Hidden-Markov Models (HMMs) deposited in the public Pfam protein domain database. Because there are multiple TIR and TIR-related HMMs (TIR, TIR_2, TIR-like, DUF1863 and SEFIR, Table 2), I combined the results of all of these, considering the different regions being identified and keeping only the longest predicted domains. As there is no functional distinction known between the different TIR “types”, I termed all of the identified protein domains TIR domains and combined them into one dataset. For the purpose of better readability, I will only state the genus names for phylogenetic analysis, the full species names can be found in Table 1. With a few exceptions within the tested algae (*Chara*, *Ostreococcus* and *Coccomyxa*), all tested plants contained predicted TIR domains, however numbers varied drastically, ranging from a single TIR in *Marchantia*, *Selaginella* and some algae (*Chlamydomonas*, *Volvox*, *Micromonas*), to 385 and 417 TIRs in the Conifer *Pinus* and Eudicot *Eucalyptus*, respectively (Figure 1). Generally, TIR numbers were the highest in Conifers and Eudicots and lower in Monocots and non-vascular plants.

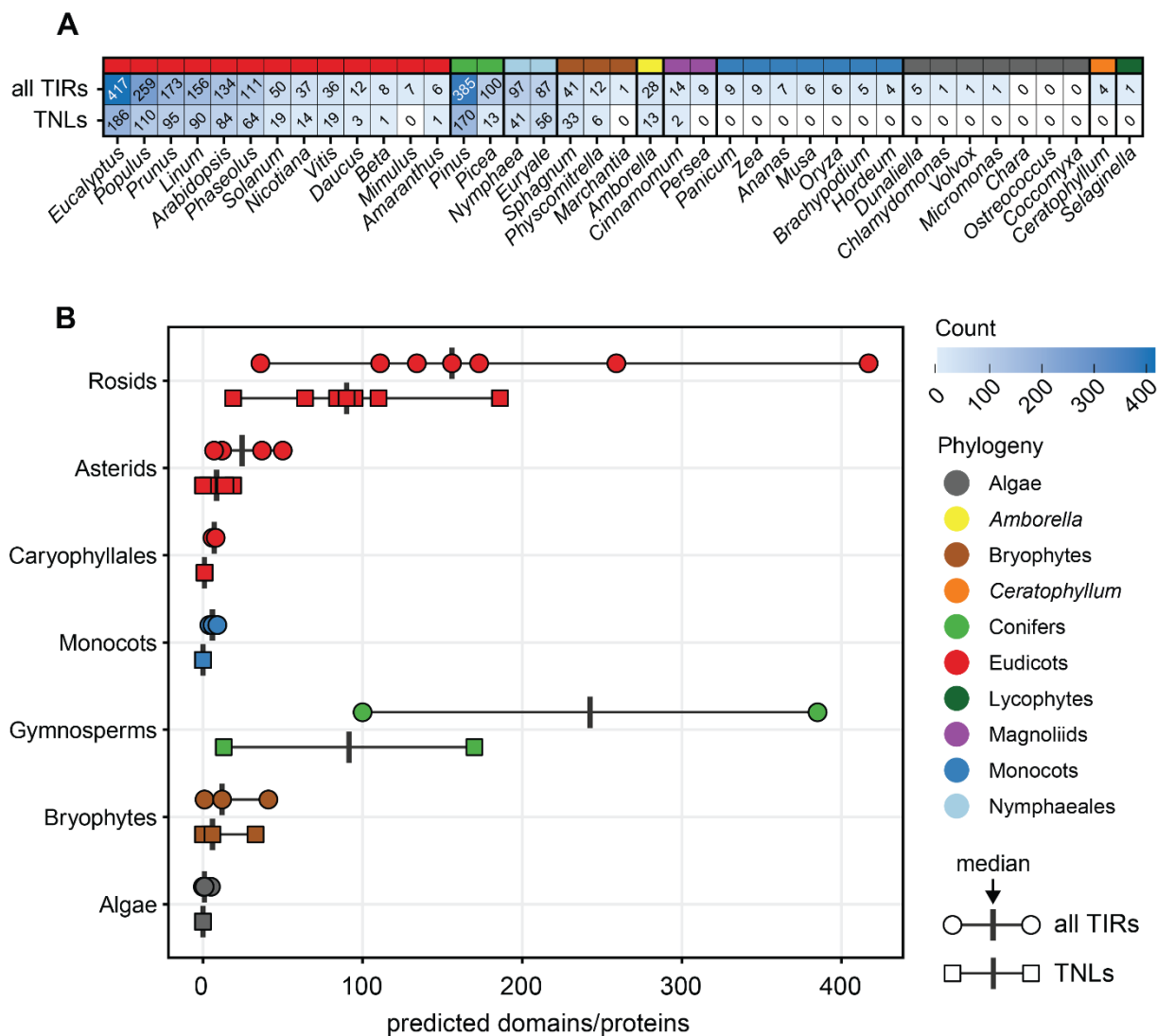


Figure 1: Variation of TIR domain and TNL protein numbers across 39 plants

A Total TIR domains and TNL proteins identified in 39 different plant proteomes. Colors on top indicate phylogenetic clade of the source plant. Numbers in squares indicate numbers of all TIR domains identified using TIR HMMs (TIR, TIR2, TIR-like, DUF1863, SEFIR, Table 2), TNL proteins were identified using additional NB-ARC and LRR HMMs. Blue color shades illustrate copy number differences. A list of full taxonomic names as well as the proteome information can be found in Table 1.

B TIR domain and TNL counts summarized per broader taxonomic clades (families for Eudicots). Dots (all TIR domains identified by HMMs) and squares (TNLs identified by additional HMMs found in Table 2) each represent a single species falling into the broader taxonomic clade, which is indicated by different colors. Horizontal lines show the spread of copy numbers within different taxonomic unit, the vertical bars show respective medians.

A similar trend was observed when comparing numbers of the most commonly TIR-associated protein domain architecture, being full-length TNL proteins. These were predicted using the same proteomes of the 39 plant species, with additional HMMs for NB-ARC and LRR domains (Table 2). Bioinformatic prediction of LRR domains was not as trivial as TIR or NB-ARC prediction, since there is a multitude of different LRR HMMs available in the Pfam database, mainly distinguished by the number of LRRs, so the combined results of the LRR HMMs listed in Table 2 were used for TNL annotation, together with the NB-ARC results (Figure 1). As expected, full-length TNLs were not predicted in the proteomes of algae and *Selaginella* and Monocots, while some Eudicot and Conifer species contain more than 100 TNLs (Figure 1). To gain a more detailed insight into TIR distributions, I also looked at distributions of TIRs and TNLs within the Eudicots and compared it to the other tested plant clades. It is apparent that within the Eudicots, Rosids contain the most TIRs and TNLs, Asterids have lower numbers, and the tested Caryophyllales *Amaranthus* and *Beta* have similar overall TIR domain numbers, comparable to Monocots, and only a single predicted full-length TNL within both proteomes (Figure 1). This illustrates the striking range of TIR and TNL numbers and shows possible signs of TIR radiation within the Conifers and Eudicots, with a much stronger accumulation of TIRs and TNLs in Rosids and Asterids, which did not occur in Caryophyllales. However, these numbers do not yet consider the TIR domain phylogeny and are simply based on protein domain annotations and HMM predictions.

2.1.2. Land plants have evolved four conserved TIR groups

The current TIR nomenclature in plants is mainly influenced by protein domains attached to the TIR domains, for example NB-ARC or LRR domains in TIR-NB-ARC (TN) or TNL proteins. Protein domain architectures have been used in the past to name proteins, for example in the *A. thaliana* TN or TIR-X (TX) proteins (Meyers *et al.*, 2002). However, nomenclatures like these do not reflect the phylogenetic relationship of the TIR domains within those protein groups and can therefore overlook larger evolutionary trends, by naming all proteins with the same full-length domain arrangement in a similar way. To introduce an unbiased and purely phylogeny-based nomenclature of plant TIRs, I constructed a maximum likelihood (ML) phylogenetic tree for a total 2,348 identified TIR domains from the 39 tested plant species (Johandrees *et al.*, 2021), to look for the presence of phylogenetically conserved TIR groups. Because of the algal TIR proteins showing very long branches on that initial tree, which did not fall into concise monophyletic

groups, they were excluded from further phylogenetic analyses. Also, to reduce the overall calculation time (the initial 2,348 sequence tree took ~2 months to calculate), I selected representative TIR domain sequences from the main phylogenetically distinct groups, resulting in a set of 307 TIRs that were used to generate a representative ML tree (Figure 2). This tree had a much shorter calculation time (~1 week), allowing me to modify the phylogenetic searches and add or remove outlier TIRs, while retaining the global phylogenetic grouping of TIRs on the tree (Figure 2). The presence of the same conserved groups on both the initial full tree as well as the reduced representative trees suggest importance of the recovered groups. It also highlights that many of the Conifer and Eudicot TIR domain sequences are very similar on a phylogenetic level, but do not contribute to a better resolution on the ML trees. This points towards radiation of TIRs within these clades, leading to a high number of similar TIR domains in each species. Four highly conserved groups were defined as TIR domain groups with a bootstrap support greater than 90, that contain TIRs from more than one species and or broader phylogenetic clade (Figure 2). The identified groups were therefore solely based on their TIR domain phylogeny, excluding possible attached domains or functions of the full-length proteins to bias their annotation.

To try and add more information and possibly annotate the full-length proteins containing conserved TIR domains, additional HMM searches were performed using NB-ARC, LRR, C-JID and TPR HMMs (Table 2). Two of the conserved TIR groups mostly contain TNL proteins, which is why they were termed TNL #1 and TNL #2 (Figure 2). TNL #1 was previously identified as “NLR family 31” in studies focusing on NB-ARC phylogeny (Liu *et al.*, 2021; Zhang *et al.*, 2016). They were not predicted to contain common C-terminal TNL domains, such as C-JID domains, which were identified in the effector-recognizing TNLs *AtRPP1* and *NbRoq1* (Figure 2, (Ma *et al.*, 2020; Martin *et al.*, 2020)). TNL #1 proteins can be found in most Eudicot proteomes, including Caryophyllales, which have lost most other full-length TNLs, and all together showed a reduced TIR and TNL repertoire (Figure 1, Figure 2). Additionally, TNL #1 proteins are present in the Magnoliid *Cinnamomum*, but not in Monocots, Conifers, *Amborella* or Nymphaeales (Figure 2), suggesting that this TIR group likely emerged in Mesangiosperms before the Monocot-Eudicot split and was likely lost in Monocots.

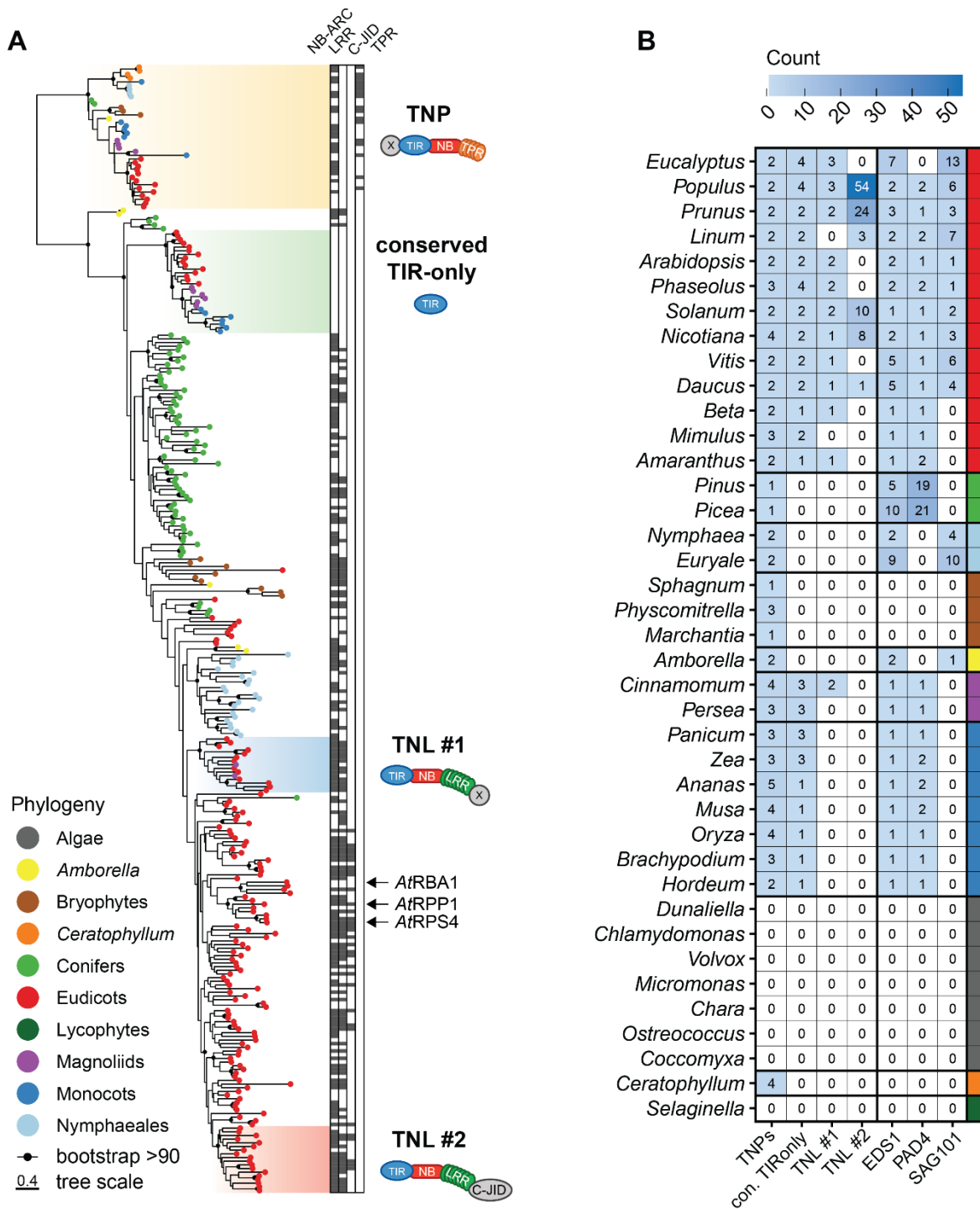


Figure 2: Phylogeny of representative TIR domains identified in 39 selected plant species

A Maximum-Likelihood phylogenetic tree (generated using IQ-TREE) of 307 representative TIR domain sequences. TIR domains were predicted from 39 plant proteomes using TIR HMMs (TIR, TIR2, TIR-like, DUF1863, SEFIR, Table 2). Dots represent individual TIR domains, their color shows their phylogenetic origin. Branches with bootstrap support >90 are marked with black dots. Black boxes next to the individual TIR domains indicate presence of additional protein domains (NB-ARC, LRRs, C-JID and TPRs), which were identified using their respective HMMs (Table 2). Conserved groups with TIR domains from more than one species or clade are marked with rectangular boxes and their predominant full-length protein domain architectures are depicted as cartoons next to them.

B Conserved TIR domain and EDS1 family counts per plant species. Colors on the right side indicate phylogenetic clade of the source plant. Numbers in squares indicate numbers of conserved TIR domain groups as well as EDS1, PAD4 and SAG101. Conserved TIR proteins were identified on the complete phylogenetic tree (Johannrees *et al.*, 2021), EDS1 family proteins were identified by prediction of the EP-domain using an HMM and running a subsequent phylogenetic tree to separate EDS1, PAD4 and SAG101 sequences (as described in (Johannrees *et al.*, 2021)). Blue color shades illustrate copy number differences. A list of full taxonomic information as well as the proteome information can be found in Table 1.

The TNL #2 group, previously called “NLR family 10” based on NB-ARC phylogeny (Zhang *et al.*, 2016), was identified only in Eudicots, interestingly being absent from *Eucalyptus* and *Arabidopsis*, which otherwise have extended TIR repertoires (Figure 2). In contrast to TNL #1 proteins, which are maintained at 1-3 copies per proteome, TNL #2 numbers have drastically expanded in some proteomes (54 in *Populus* and 24 in *Prunus*) (Figure 2). Interestingly, TNL #2 proteins comprise around 50 % of predicted TNLs in *Populus*, *Nicotiana* and *Solanum*. Many TNL #2 proteins were identified to have additional post-LRR C-JID domains, possibly indicating effector-binding capabilities, which would suggest a role in immunity (Figure 2). However, neither TNL #1 nor TNL #2 groups contain any functionally annotated proteins.

A third conserved TIR group (referred to as “conserved TIR-only”) relates to a family of ~200 aa-long proteins, without additional domains except their TIRs. Conserved TIR-onlys are maintained at 1-4 copies per tested proteome and interestingly they are present in all analyzed Eudicots, Magnoliids and Monocots, in striking contrast to TNL #1, which are absent from Monocots (Figure 2). Conserved TIR-onlys were not identified in any other plant clade, suggesting their emergence in Mesangiosperms (Figure 2). Importantly, this group does not include the described TIR-only *AtRBA1* from, which recognizes the bacterial HopBA1-effector (Figure 2, (Nishimura *et al.*,

2017)), or the multitude of Conifer TIR-onlys, highlighting the difference between TIR-only domain architecture, which can be found in proteins across the phylogeny and the phylogenetically conserved TIR-only group identified here.

While C-terminal LRR repeat domains are generally present in full-length TNL proteins, TPR repeats were only predicted in a single conserved TIR protein group (Figure 2). This group marks the most taxonomically widespread TIR group, present in all tested land plants (except *Selaginella*). Proteins within this group were previously named XTNX proteins (Meyers *et al.*, 2002), due to their X-TIR-NB-X domain architecture, where Xs stand for unknown or non-conserved domains. Using additional TPR HMMs, I could show that the C-terminal domain in these proteins is most often represented by a TPR domain, which is why these proteins were renamed into TNPs, where P stands for Tetratricopeptide repeat, to differentiate it from the N-terminal TIR domain. Prediction of TPRs has the same drawback of LRRs with many available HMMs (Table 2), which is why results were combined again. However, this annotation could miss single TPRs in the full set of proteins. TNPs do not contain C-JID domains but have frequently been identified to contain NB-ARC domains (Figure 2). The TNP group comprises previously studied *AtTN17* and *AtTN21*, the two *A. thaliana* TNPs (Nandety *et al.*, 2013), again showing the downside of purely domain-based annotations, which do not take into account the special nature of these two proteins. While TNPs are still present in the aquatic flowering plant *Wolffia australiana*, with a drastically reduced NLR repertoire (Baggs *et al.*, 2020; Baggs *et al.*, 2022; Johandrees *et al.*, 2021), data presented here show that TNPs are not present in algae, which suggests emergence of the TNP group in land plants, including the secondary aquatic plants (Johandrees *et al.*, 2021).

In summary, the four described groups mark the most conserved TIR domain groups found in the 39 analyzed plant species. While their full-length domain architecture was helpful in naming the proteins, it is not sufficient to define individual TIR domain groups on a phylogenetic level. TNL and TIR-only domain architectures are widespread, yet only a small subset of these proteins was contained within the highly conserved phylogenetic groups described here (Figure 2).

2.1.3. Conserved TIRs show distinct co-occurrence patterns with the EDS1 family

Members of the EDS1 protein family are essential signaling components in plant immunity, connecting TIR domain signaling to cell death and immune outputs (Lapin *et al.*, 2020). The intimate connection between TIRs and EDS1 signaling prompted me to investigate potential co-evolutionary patterns between the two immune components. For this, the 39 plant proteomes were screened for EP domains, uniquely marking EDS1, PAD4 and SAG101, using an HMM and subsequently a ML phylogenetic tree was built to define copy numbers of the EDS1 family proteins per species (Table 2, Figure 2, (Johandrees *et al.*, 2021)). In accordance with previous publications, SAG101 was absent from Conifers, Monocots and Caryophyllales, while EDS1 and PAD4 were identified in most other seed plant species. Interestingly, Nymphaeales, *Eucalyptus* and *Amborella* contain SAG101, but not PAD4 (Figure 2). Conserved TIR-onlys show the highest co-occurrence with EDS1 and PAD4, being co-present in most Mesangiosperms, indicating a possible co-evolutionary link between the EDS1/PAD4 heterodimer and conserved TIR-onlys (Figure 2). An opposite evolutionary pattern was observed for the TNPs, which are present across land plants, including non-seed plants and secondary water plants that lost EDS1 (Baggs *et al.*, 2022), indicating an EDS1-independent TNP TIR evolution (Figure 2). These data show that while TIRs and EDS1 have a strong functional link in studied TIR proteins, including TNLs, presence of TIR domains in a plant proteome is not strictly dependent on EDS1.

2.1.4. TIR-associated NB-ARC phylogeny reflects conserved TIR groups

Because TIR domains are oftentimes functionally linked to associated NB-ARC domains, I also investigated the phylogeny of these NB-ARC domains. For this, NB-ARC domains found in TIR proteins from the representative TIR tree (Figure 2) were analyzed in a similar fashion, using HMM searches and subsequently building an ML tree. Strikingly, the resulting NB-ARC ML tree reflects the TIR domain phylogeny, with three conserved groups containing TNP, TNL #1 and TNL #2 proteins (Figure 3). While NB-ARC domains from TNL #1 and TNL #2 proteins are more closely related to canonical TNL proteins, the TNP NB-ARC domains show a high divergence, which is why they are referred to as NB-ARC-like sequences (Figure 3). Further analyses, including alignments to canonical TNL NB-ARCs revealed that important functional residues are conserved within the P-loop of TNPs, pointing towards a functional conservation of these residues, while the overall NB-ARC domains differ (Johandrees *et al.*, 2021). Matching TIR/NB-ARC evolutionary

patterns suggest that TIRs are associated with NB-ARC domains that show a degree of specialization to the TIR protein context they are present in. It further underlines the importance of the four conserved TIR protein groups.

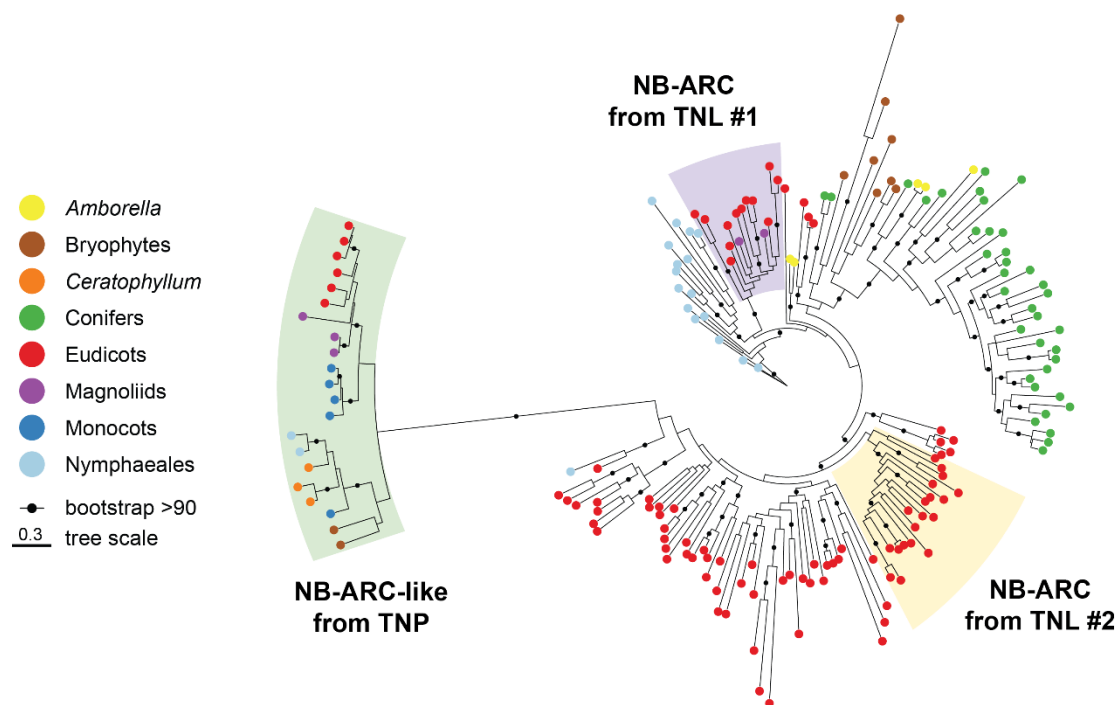


Figure 3: Phylogeny of TIR-associated NB-ARC domains

TIR-associated NB-ARC domains were identified using the respective NB-ARC HMM (Table 2) on all predicted TIR proteins from the tree in Figure 2. The Maximum-Likelihood tree was generated using IQ-TREE. Dots represent individual NB-ARC domains, their color shows the phylogenetic origin. Branches with bootstrap support >90 are marked with black dots. NB-ARC domains originating from observed TIR proteins shown in Figure 2 are marked with colored boxes.

2.1.5. Catalytic glutamate residues are conserved across TIR groups

Glutamate residues were shown to be essential for NADase enzymatic activity of TIR domains across several kingdoms of life (Essuman *et al.*, 2017; Essuman *et al.*, 2018; Wan *et al.*, 2019), which is crucial for several TIR functions. In plants, products of this reaction are important second messengers in immunity and cell death signaling (Huang *et al.*, 2022; Jia *et al.*, 2022). Therefore, it was of interest to assess whether the conserved TIR domains contain these catalytic residues and how the surrounding protein environments evolved. To investigate this, I extracted the TIR domain sequences from the initial 2,348 sequence ML tree (Johanndrees *et al.*, 2021) and aligned the TIRs originating from each conserved group. Subsequently, I generated sequence motifs to easily compare the alignments of different regions within the TIR groups and centered them around the corresponding known residues in *AtRPP1*^{W_sB} (Figure 4). Putative catalytic glutamates can be found in all four conserved TIR groups, including TNPs, which have two adjacent glutamates in that region (Figure 4). While the entire region surrounding the catalytic glutamates is similar in the conserved TIR-onlys as well as the two conserved TNL groups, it differs substantially in the TNPs (Figure 4), indicating a possible functional distinction. In addition to the catalytic glutamates, TIR-TIR self-association interfaces are crucial for TIR activities. The AE interface (comprising an SH amino acid stretch) was shown to be important for the *AtRPP1*^{W_sB} (Zhang *et al.*, 2017a). However, this motif did not show a high degree of conservation across conserved types of TIR domains (Figure 4). In contrast, the DE interface (comprising a central glycine residue) was shown to be important for cell death and NADase activity of *Bd*TIR and *At*RBA1 TIR-only proteins (Wan *et al.*, 2019). This glycine was well maintained across all conserved TIR groups, except the TNPs (Figure 4). Structure prediction of conserved TIR-only proteins from *Oryza sativa* (rice) and *A. thaliana* differed from known plant TIRs in an α D-helical region (Johanndrees *et al.*, 2021), important for cell death activities of TNL receptors *At*RPS4 (Sohn *et al.*, 2014) and *Lu*L6 (Bernoux *et al.*, 2011) and for cNMP synthetase activity found in several plant TIR domains (Yu *et al.*, 2022). However, this amino acid stretch was not conserved enough to draw conclusions for the conserved TIR groups (Figure 4).

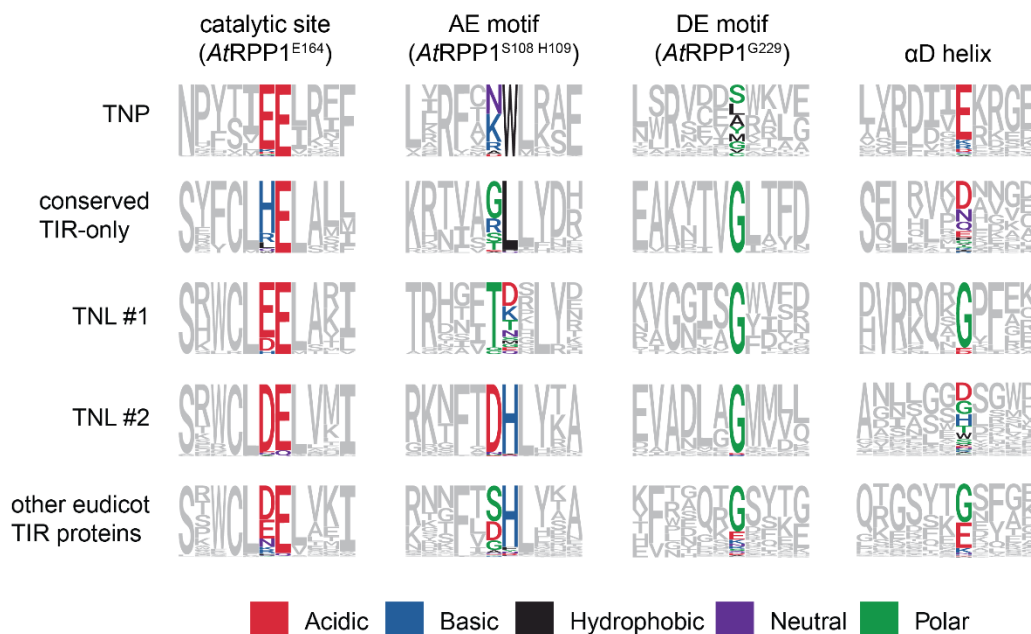


Figure 4: Sequence motifs of known functional motifs within conserved TIR domains

Sets of TIR domains were taken based on the complete phylogenetic tree (Johanndrees *et al.*, 2021), “other eudicot TIR proteins” are TIRs including canonical TNLs, TNs as well as TIR-only proteins, which are outside the conserved group. Sequence motifs were generated for each TIR group to show the level of conservation for the catalytic glutamate region, AE and DE TIR-TIR self-interaction interfaces as well as residues in the αD helix. The *AtRPP1*^{W^{SB}} TIR domain was taken as reference to align the sequence motifs of other TIR domains. Colors illustrate the different chemical attributes of functionally characterized amino acids within the motifs.

2.1.6. Conserved *TIR-ONLYs* are transcriptionally upregulated in immunity

Differential co-occurrence of the conserved TIR groups and EDS1, as well as the broad appearance across clades and presence of some immune-related additional domains in TNL #1, asked the question whether the conserved TIR proteins are responsive to immune-related stresses. For this, diverse public RNAseq datasets were screened for two Eudicots (*A. thaliana* and *N. benthamiana*) as well as two Monocots (*O. sativa* and *Hordeum vulgare* (barley)). Several immune-related RNAseq datasets were recovered (Table 3) and expression of the four conserved *TIR* groups, as well as all predicted *NLRs* was compared between untriggered and triggered tissues, using Z-score normalized expression values that allow comparison between datasets. *NLR* genes were predicted using the published NLR-Annotator software, which relies on identifying *NLR* genes via conserved motifs, including TNLs, CNLs and RNLs (Steuernagel *et al.*, 2020). Across RNAseq samples, *NLRs* were slightly induced by immune triggers, with *H. vulgare* being the exception (Figure 5).

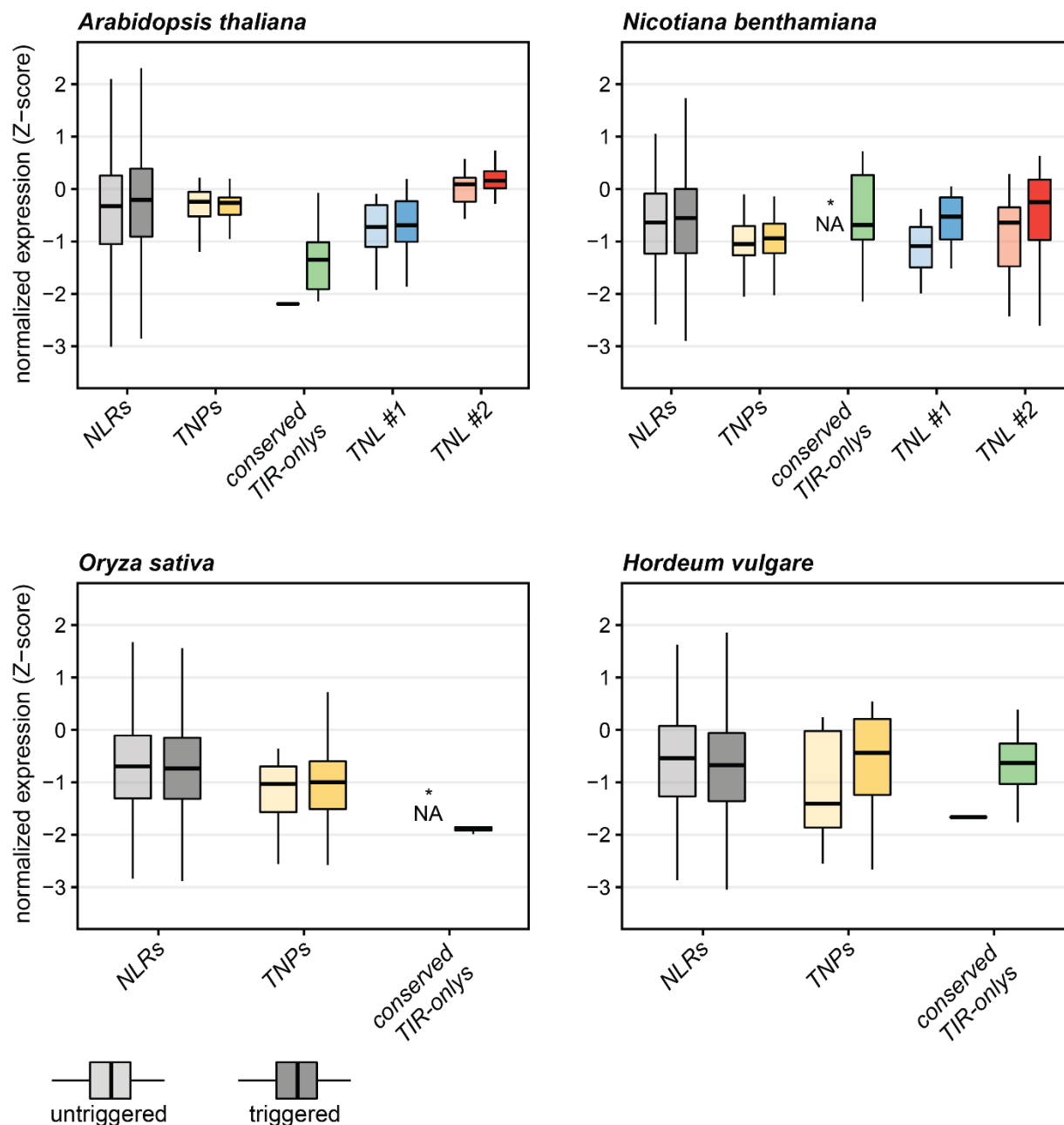


Figure 5: Expression profiles of conserved TIR genes from public RNAseq data

Expression data was gathered from publicly available RNAseq experiments involving infection assays on the plants *Arabidopsis thaliana*, *Nicotiana benthamiana*, *Hordeum vulgare* (barley) and *Oryza sativa* (rice), a full description of all used RNAseq samples can be found in Table 3. Boxplots show Z-score normalized expression of NLR genes (annotated with NLR-Annotator) and the conserved TIR gene groups (coding for proteins shown on the tree in Figure 2). Data are separated into untriggered (opaque boxplots) and untriggered (solid boxplots) tissues. Genes with no detectable expression are marked with “*NA”.

It is difficult to say which *NLRs* are induced, since the annotation is based on NLR-Annotator and only a small fraction of *NLRs* is functionally annotated. Probably, only a few *NLRs* respond to each specific pathogen or treatment. *TNP* genes were generally unresponsive to immune triggers, except for the *H. vulgare* *TNPs*, which showed a trend towards induction (Figure 5). *TNL #1* and *TNL #2* expression was upregulated in *N. benthamiana* samples, where *TNL #2* genes comprise half of the *TNL* repertoire (Figure 2). Strikingly, conserved *TIR-ONLY* genes were either not detected or expressed at a very low level in non-triggered tissues across all tested species but displayed induction in a multitude of triggered samples in both Monocots and Eudicots (Figure 5, (Johandrees *et al.*, 2021)).

To explore the expression of conserved *TIR-ONLY* genes in more detail, two timely resolved datasets were selected for *A. thaliana* and *H. vulgare* and the expression of the responsive *A. thaliana* *TIR-ONLY* AT1G52900 (*AtTIR*), as well as the *H. vulgare* *TIR-ONLY* HORVU2Hr1G039670 (*HvTIR*) plotted on a time axis (Figure 6). For this, the raw data was fetched from the public SRA database, reads quantified per gene and normalized to transcripts per million (tpm) to allow comparison of multiple sequencing runs (3 replicates per time point and treatment) (Figure 6). Both genes are virtually not expressed before the biotic triggers (*Pseudomonas syringae* pv. *tomato* (*Pst*) DC3000 D28E or *Blumeria graminis* f. sp. *hordei* (*Bgh*), RNAseq accessions listed in Table 3), but exhibit induction at early stages of infection (Figure 6). For *AtTIR*, it did not matter whether *Pst* expressed the effector protein HopAM1 or not, since expression peaked at two hours post infection (hpi) in both cases. After 2 hpi, the expression of *AtTIR* quickly decreases back to basal levels (Figure 6). Additional data taken from CNL-triggered ETI suggests induction of *AtTIR* by a multitude of triggers (Johandrees *et al.*, 2021). Similarly, the expression of *HvTIR* peaks at 20 hpi, which relates to an early stage of *Bgh* haustoria formation (Yamaoka *et al.*, 2000), before it drops to close to zero at later stages of infection. Taken together, these observations suggest that *TIR-ONLY* expression is responsive to diverse immune triggers across species. This contrasts with most other conserved *TIR* groups, which were either unresponsive, or showed species-specific upregulation (Figure 6, (Johandrees *et al.*, 2021)). The early time points, at which *TIR-ONLY* expression was upregulated, suggest involvement in surface immunity, rather than downstream signaling or long-time transcriptional reprogramming in defense.

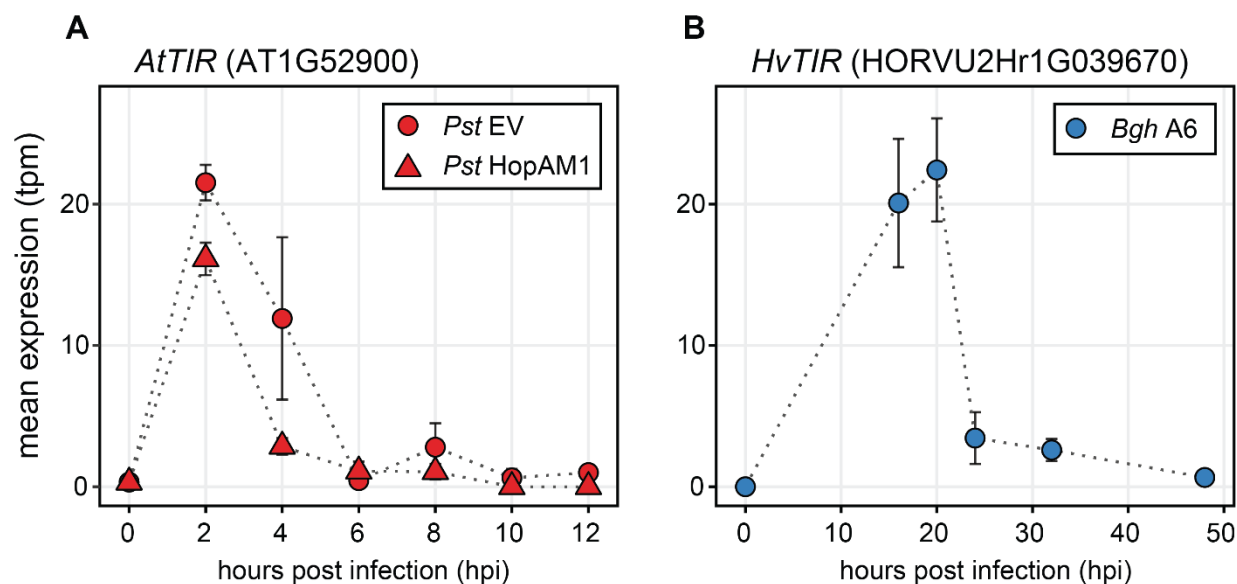


Figure 6: Time-resolved gene expression profiles of conserved *TIR-ONLYs*

A Gene expression of the conserved *Arabidopsis thaliana* *TIR-ONLY* gene AT1G52900 (*AtTIR*) during *Pseudomonas syringae* pv. *tomato* (*Pst*) infection. Data were gathered from a public RNAseq dataset (SRP075162, Table 3). Plants were infected with *Pst* D28E expressing the effector HopAM1 or an empty vector (EV) control strain. Samples were harvested at 0-12 hours post infection (hpi) and mean expression values normalized to transcript per million (tpm). Error bars indicate the standard error of the mean at any given time point.

B Gene expression of the conserved *Hordeum vulgare* *TIR-ONLY* gene HORVU2Hr1G039670 (*HvTIR*) during *Blumeria graminis* f. sp. *hordei* (*Bgh*) infection. Data were gathered from a public RNAseq dataset (SRP111697, Table 3). Plants were infected with *Bgh* isolate carrying the effector AvrA6. Samples were harvested at 0-50 hours post infection (hpi) and mean expression values normalized to transcript per million (tpm). Error bars indicate the standard error of the mean at any given time point.

2.2. Exploring the involvement of conserved TIR proteins in plant immunity

2.2.1. Conserved Monocot TIR-onlys induce *EDS1*-dependent cell death

TIR-signaling is tightly linked to *EDS1* in Eudicots, regarding both cell death and induced resistance against invading pathogens. Overexpression of TIR-only proteins, as well as the isolated TIR domains of canonical TNLs can induce *EDS1*-dependent cell death in *N. benthamiana* leaves, even without an effector protein present (Horsefield *et al.*, 2019; Wan *et al.*, 2019). As conserved TIR-onlys co-occur with *EDS1* and *PAD4* in the tested Mesangiosperms (Figure 2), I sought to determine if their overexpression would also trigger cell death and if it is *EDS1*-dependent. Cell death induction upon overexpression in *N. benthamiana* was already shown for the *B. distachyon* member of the conserved TIR-onlys (*BdTIR*), and required *EDS1* (Wan *et al.*, 2019). To test if the cell death induction is preserved across conserved TIR-onlys, I cloned the *TIR-ONLY* genes from rice (*OsTIR*, Os07G0566800) and barley (*HvTIR*, HORVU2Hr1G039670) into vectors suitable for *Agrobacterium*-mediated transient expression in *N. benthamiana* as fusions to C-terminal YFP tags. Co-expression of YFP-tagged *AtRPP1*^{WsB} with its matching SH-tagged effector *ATR1*^{Emoy2} served as a positive control that induced cell death in WT but failed to do so in an *eds1a* mutant (Figure 7, (Ma *et al.*, 2020)). Cell death was scored as macroscopic lesions on the leaves within the infiltrated areas. Overexpression of YFP, as a negative control, did not induce visual cell death symptoms (Figure 7). Three days after *Agrobacterium* infiltrations (dpi), both *OsTIR* and *HvTIR* induced cell death in WT leaves, but not in the *eds1a* mutant, while the proteins accumulated in both *N. benthamiana* genotypes at 1 dpi, shown on immunoblots (Figure 7). This indicates *EDS1*-dependent cell death and excludes lack of cell death due to low protein accumulation in *eds1a* as a likely explanation. Catalytic glutamates are crucial for induction of cell death by TIRs, which was shown for *BdTIR* (Wan *et al.*, 2019). Substituting the putative catalytic glutamates of the TIR-onlys to alanines (*OsTIR*^{E133A} and *HvTIR*^{E128A}) likewise resulted in complete loss of cell death (Figure 7). Similarly, mutations in the DE interface of the TIR-onlys fully (*OsTIR*^{G188R}) or partially (*HvTIR*^{G183R}) eliminated the cell death response upon overexpression (Figure 7). Importantly, all TIR-only variants were still detectable in *N. benthamiana* leaves by immunoblots (Figure 7). These results indicate dependence of conserved TIR-only induced cell death on *N. benthamiana EDS1*, and both an intact TIR catalytic site and DE interface. In this regard, *OsTIR* as well as *HvTIR* behave like TNLs and the previously characterized *BdTIR*.

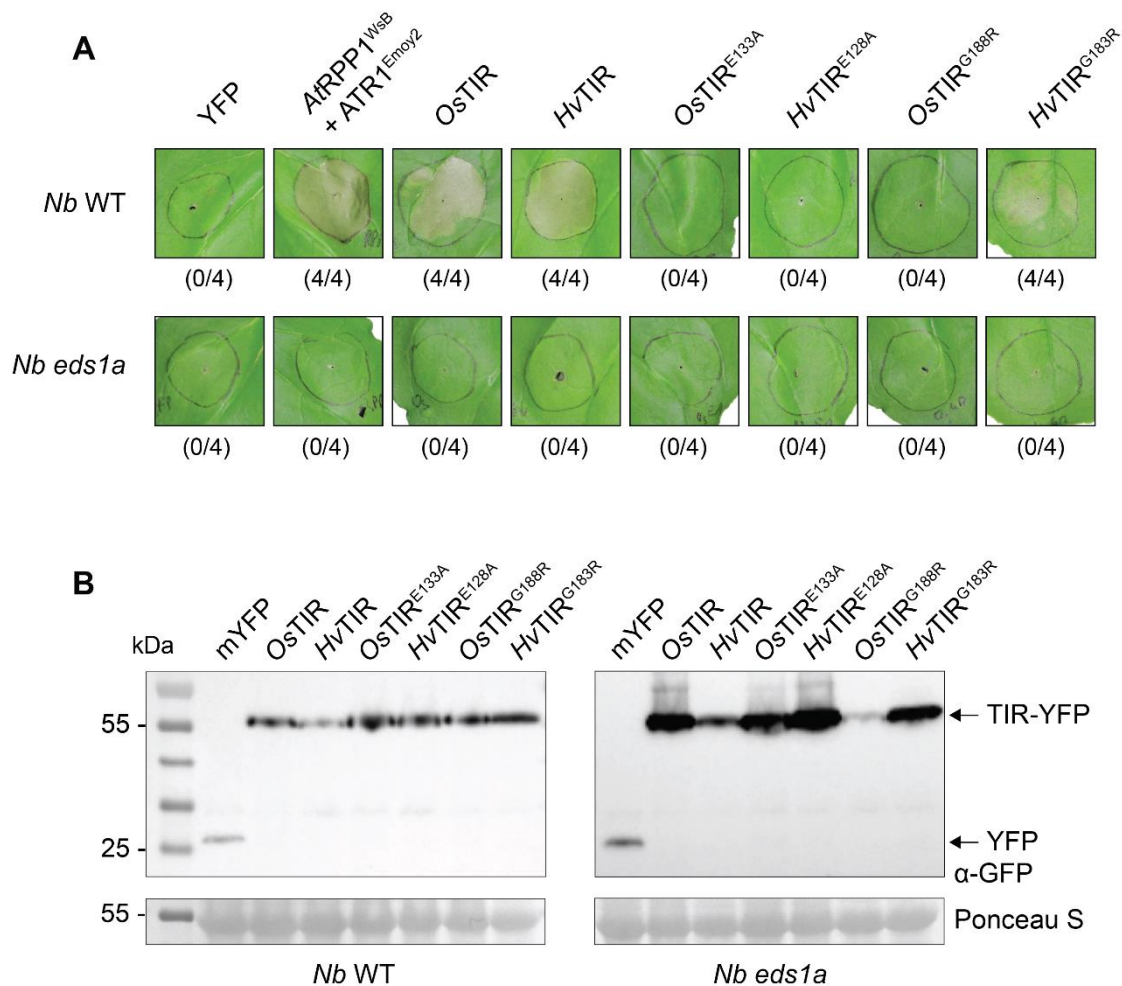


Figure 7: Cell death induced by overexpression of monocot TIR-only proteins

A Macroscopic cell death induced by *Agrobacterium*-mediated overexpression (all constructs were 35S promoter driven) of N-terminally YFP-tagged conserved TIR-only proteins from rice (*OsTIR*) and barley (*HvTIR*) in *Nicotiana benthamiana* (*Nb*) WT and the *eds1a* mutant. Proteins expressed were *OsTIR* and *HvTIR* WT as well as the putative non-catalytic variants (*OsTIR*^{E133A}, *HvTIR*^{E128A}) and DE interface variants (*OsTIR*^{G188R}, *HvTIR*^{G183R}). YFP and *AtRPP1*^{Wsb} together with the recognized effector *ATR1*^{Emoy2} were expressed as negative and positive controls, respectively. Pictures were taken three days after *Agrobacterium* infiltration. In total, four biological replicates were performed, numbers below pictures indicate the number of replicates with cell death symptoms.

B Accumulation of monocot TIR-only variants in *Nb* WT and *eds1a* leaves from experiments in **A** shown on immunoblots using α -GFP antibodies (Table 9). Samples were taken from infiltrated leaf areas one day after *Agrobacterium* infiltration and total proteins extracted. Expected protein sizes are indicated on the right side. Ponceau S staining of the membranes served as control for equal loading. Protein standard sizes in kDa are indicated on the left side. Immunoblots have been repeated with samples from three independent biological replicates, with similar results.

2.2.2. Conserved TIR-onlys do not contribute to bacterial resistance in *A. thaliana*

Due to their conserved transcriptional induction in immunity, the *EDS1*-dependent cell death they induce in *N. benthamiana* and their co-evolutionary pattern with *EDS1* and *PAD4* in Mesangiosperms, I tested whether TIR-onlys are directly involved in immune defenses against bacteria. To test this, I generated mutants in *A. thaliana* and *N. benthamiana* to compare the influence of loss of TIR-onlys in both species. Using the bioinformatic pipeline outlined above, two conserved *TIR-ONLY* genes (AT1G52900 and AT1G61105) were identified in the *A. thaliana* genome, which were confirmed via reciprocal BLAST searches to ensure no genes were missed due to potential incomplete protein annotations in the utilized proteome. These two genes were targeted using a CRISPR/Cas9 system to allow phenotypic analysis and immune assays investigating conserved TIR-only functions. CRISPR/Cas9-mediated mutagenesis provided a suitable method for this, since the two genes both reside in close proximity on chromosome 1, which would make crossing of two individual T-DNA insertion lines difficult due to genomic linkage of the proximate loci. Additionally, the utilized *A. thaliana* CRISPR/Cas9 system was shown to be highly efficient, generating homozygous mutants in the first generation and allowing to integrate multiple guide RNAs (gRNAs) in one vector for plant transformation (Ordon *et al.*, 2020; Ordon *et al.*, 2017). Both *TIR-ONLYs* were targeted with a single gRNA (designed using the CRISPR-P v2.0 online tool), making sure to select gRNAs with a high on-target score as close to the start codon as possible, while manually checking for absence of any off-target sequences via BLAST searches. After plant transformation and harvesting the first generation of mutant seeds, the utilized vectors allow immediate selection for the insert by seed coat fluorescence labeling, which made crossing out the Cas9 enzyme much easier. Only seeds that lost fluorescence, which is a reporter for loss of the Cas9 insert, were further propagated, and genotyped for mutations. Absence of inserted DNA was confirmed by PCR to ensure Cas9-free stable mutants with a lower chance of off-site mutations induced by prolonged Cas9 presence. The resulting *tir-only* double mutants (*tir-only-d1* and *tir-only-d2*) were independent homozygous lines (originating from individual transformants) and propagated until at least the T3 generation before conducting experiments. At the AT1G52900 locus, a 1 nucleotide (nt) deletion or insertion was generated in the *tir-only-d1* and *tir-only-d2* mutant line, respectively (Figure 8). At the AT1G61105 locus, 5 nt were deleted in both double mutants.

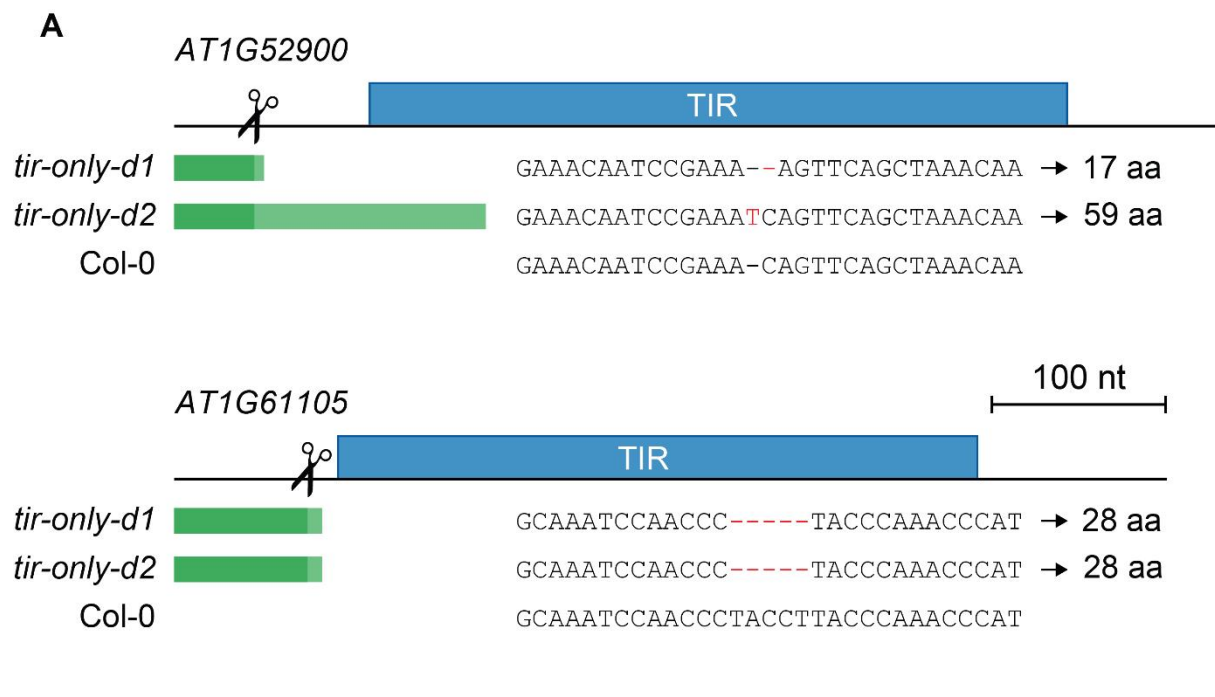
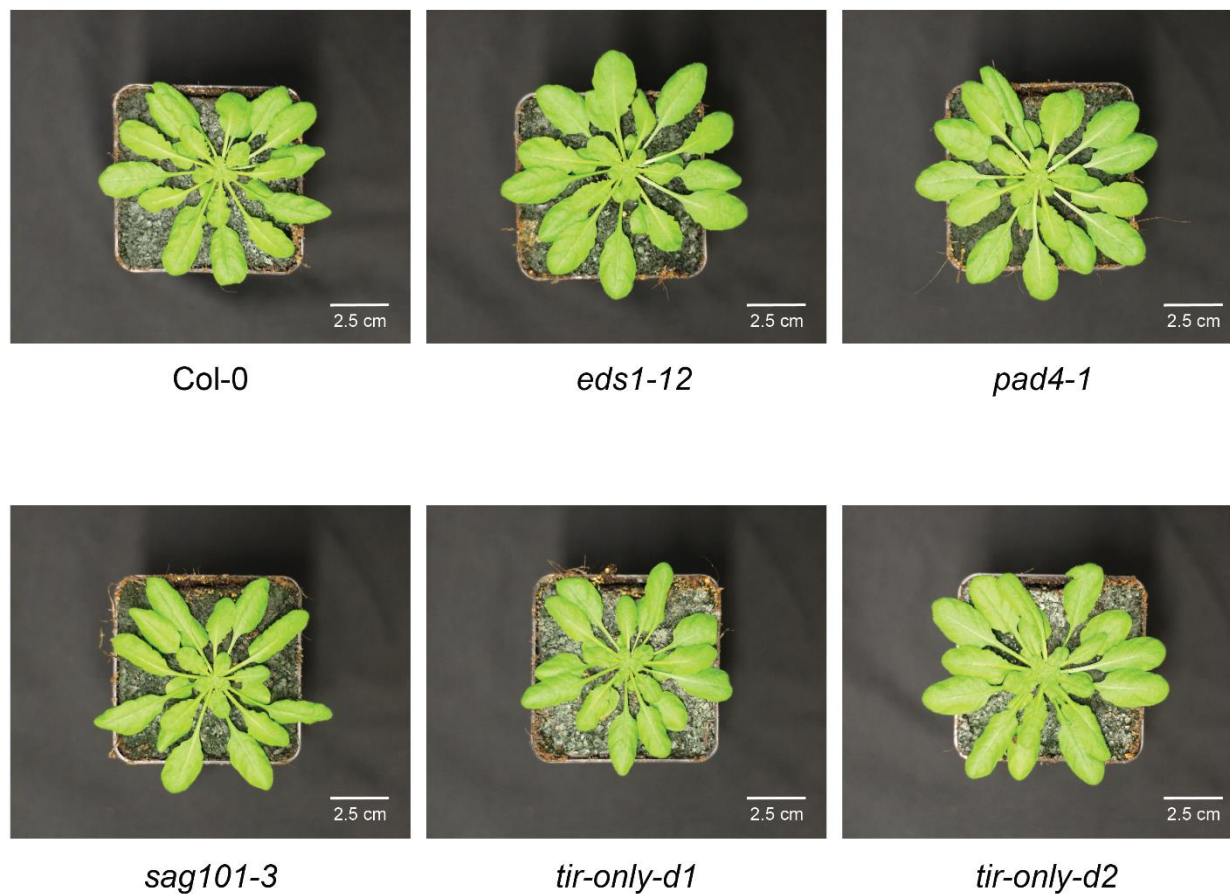
**B**

Figure 8: *Arabidopsis thaliana* tir-only CRISPR/Cas9 mutants

A The two *Arabidopsis thaliana* conserved *TIR-ONLY* genes (AT1G52900 and AT1G61105) targeted by CRISPR/Cas9 are indicated with a black line (representing their coding sequences), including a scale for size determination in nucleotides (nt). The scissor icon shows the gRNA target site in each gene, colored boxes on top indicate the location of the TIR domain. Green bars underneath the genes indicate the “left-over” mRNA that is still translated in the mutants until a stop codon is introduced. The opaque part of the bar represents the frame-shift variant of the mRNA, induced by the mutation at the CRISPR site. The aligned sequences show the induced mutations on the DNA level and resulting protein sizes are indicated in amino acids (aa) for each mutant allele.

B Photographs of 5-week-old *A. thaliana* WT (Col-0), *eds1-12*, *pad4-1*, *sag101-3* and the two independent *tir-only* double mutants (*tir-only-d1*, *tir-only-d2*) described in **A**. Plants were grown under short-day growth-chamber conditions further described in the Material and Methods section.

All mutations lead to frameshifts and early Stop codons, that either completely abort translation before the TIR domain of the mature protein or stop shortly after its beginning (Figure 8). Neither of the lines showed an apparent growth phenotype under greenhouse conditions when compared to Col-0 WT and *EDS1* family mutants (Figure 8).

To test for a possible involvement of conserved TIR-onlys in *A. thaliana* immunity, the two independent *A. thaliana* *tir-only* double mutants (*tir-only-d1* and *tir-only-d2*) described above were screened in a *Pst* DC3000 infection assay. For this, I used *Pst* DC3000 strains expressing AvrRps4 and AvrRpt2 effector proteins, recognized by the TNL pair *AtRRS1S/AtRPS4* and the CNL RESISTANT TO P. SYRINGAE 2 (*AtRPS2*) (Axtell & Staskawicz, 2003; Williams *et al.*, 2014), respectively. Additionally, I included the empty vector (EV) control strain. This setup allowed me to screen the mutants for impairments in basal immunity (*Pst* DC3000 EV), TNL-mediated ETI (*Pst* DC3000 AvrRps4) or CNL-mediated ETI (*Pst* DC3000 AvrRpt2) in a single immune assay. As controls, I included the *A. thaliana* mutants *eds1-12*, *pad4-1* and *sag101-3*, all mutants are in the Col-0 background. It is known that both EDS1 and PAD4 are required for basal resistance against *Pst* DC3000 EV as well as NLR-mediated resistance against the recognized strains (Bhandari *et al.*, 2019) and I wanted to test if the *tir-only* mutants mimic that phenotype, which would prove that they not only co-evolved, but also functionally relate to each other. Both *eds1-12* and *pad4-1* were colonized to a higher extent by *Pst* DC3000 EV, while *sag101-3* showed WT-like CFU values (Figure 9), indicating an involvement of the EDS1-PAD4 heterodimer and not

SAG101 in basal resistance. Both *tir-only* double mutants are indistinguishable of Col-0 when infected with *Pst* DC3000 EV (Figure 9). Similar results were obtained in infections with *Pst* DC3000 AvrRps4, where only the *eds1-12* mutant was less resistant (Figure 9). When infected with *Pst* DC3000 AvrRpt2, *eds1-12* and *pad4-1* show a trend towards higher CFU values, but these are not significantly different from Col-0 (Figure 9). Again, both *tir-only* mutants behaved like Col-0 (Figure 9). Taken together, the infection assay data does not suggest a direct involvement of TIR-onyls in resistance against *Pst* DC3000 or a functional link between EDS1-PAD4 and the conserved TIR-onyls in *A. thaliana*.

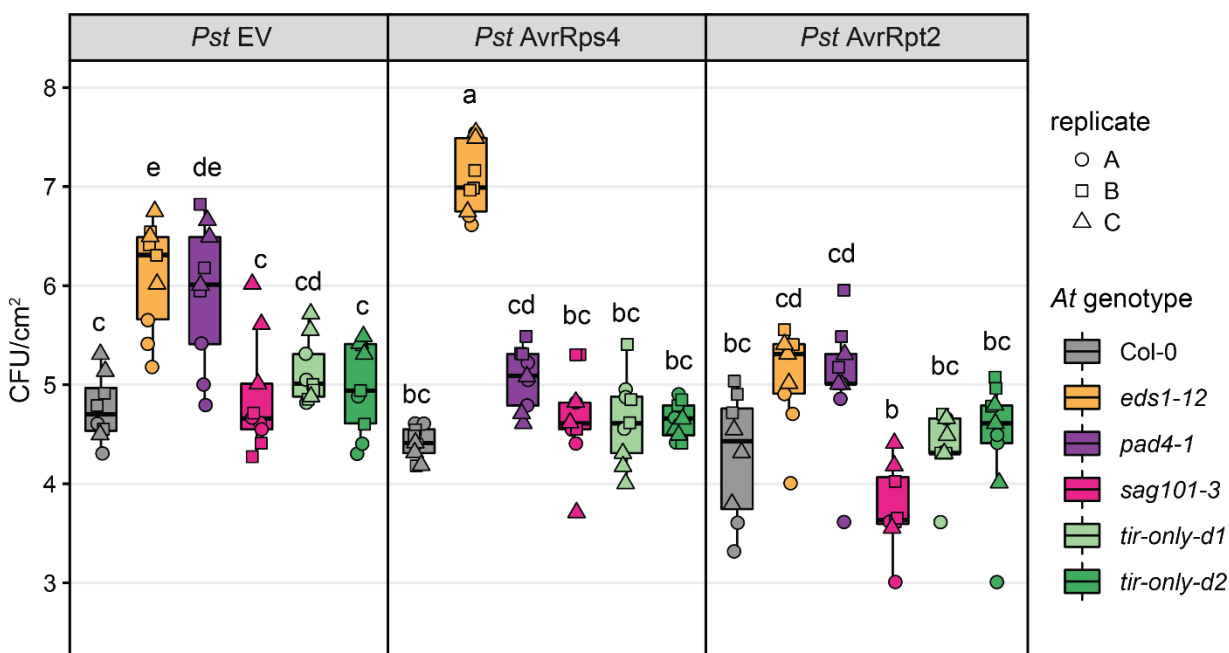


Figure 9: *Arabidopsis tir-only Pseudomonas syringae* immune assay

Pseudomonas syringae pv. *tomato* DC3000 (*Pst*) growth assay in *Arabidopsis thaliana* (*At*) WT (Col-0), *eds1-12*, *pad4-1*, *sag101-3* and the two independent conserved *tir-only* double mutants (*tir-only-d1*, *tir-only-d2*). Leaves were syringe-infiltrated with *Pst* vector empty vector (EV), AvrRps4 and AvrRpt2 strains. Bacterial titers were determined at three days post infection. Boxplots show colony-forming units (CFU)/cm², colors indicate different *At* genotypes. The respective *Pst* strains are shown on top of the boxplots. Shapes plotted on over the boxplots indicate individual CFU/cm² measurements, representing a total of three biological replicates. Genotype-treatment combinations sharing letters above boxplots do not show statistically significant differences (Tukey HSD test, $\alpha = 0.01$, $n = 9$).

2.2.3. Conserved TIR-onlys do not potentiate TNL signaling in *N. benthamiana*

In contrast to *A. thaliana*, which shows EDS1/PAD4-dependent basal resistance against virulent pathogens (Bhandari *et al.*, 2019; Dongus *et al.*, 2022), such a response is not known for *N. benthamiana*, where all tested immune responses against *Xcv* are EDS1/SAG101-dependent (Gantner *et al.*, 2019; Lapin *et al.*, 2019), marking a major difference between the two plants immune systems. Exploiting this difference, I generated *tir-only* mutants in *N. benthamiana*, to compare them to the *A. thaliana* mutants. The *N. benthamiana* genome is predicted to contain three conserved *TIR-ONLY* genes, which were confirmed via reciprocal BLAST. However, in the genome annotation that was used for generation of gRNAs for *N. benthamiana* (draft genome v1.0.1), one of the genes (Niben101Scf34945g00001) was incorrectly annotated as a part of a whole *TIR-ONLY* gene. It is much shorter, and the annotation starts in the middle of a predicted TIR domain, suggesting pseudogenization (Figure 10). Because this was the only annotation available at that time, I still designed a gRNA for this gene to target it together with the other two, fully annotated, conserved *TIR-ONLY* genes (Niben101Scf02391g00012 and Niben101Scf00180g07008). For the mutagenesis, I selected gRNAs with a good on-site score (CRISPR-P v2.0) and without any possible off-targets in the *N. benthamiana* genome. Preferably, good candidates close to the Start codon of each gene were chosen (Figure 10). For the mutagenesis, I employed a set of CRISPR/Cas9 vectors similar to the ones utilized for *A. thaliana* mutagenesis, which were optimized for use in *N. benthamiana* (Ordon *et al.*, 2017; Stuttmann *et al.*, 2021). After stable transformation, plants were checked for absence of the Cas9 insert by a CNL-triggered (*Capsicum annuum* CaBs3-AvrBs3 interaction) cell death assay integrated into the plasmids (Stuttmann *et al.*, 2021). Only plants without the Cas9 insert, which was confirmed by PCRs, were propagated, and sequenced for induced mutations. Two independent triple mutant lines with homozygous mutations at all three *TIR-ONLY* loci were selected (Figure 10). All mutant alleles (except the ones at the Niben101Scf34945g00001 locus) introduce frameshifts and early Stop codons (Figure 10).

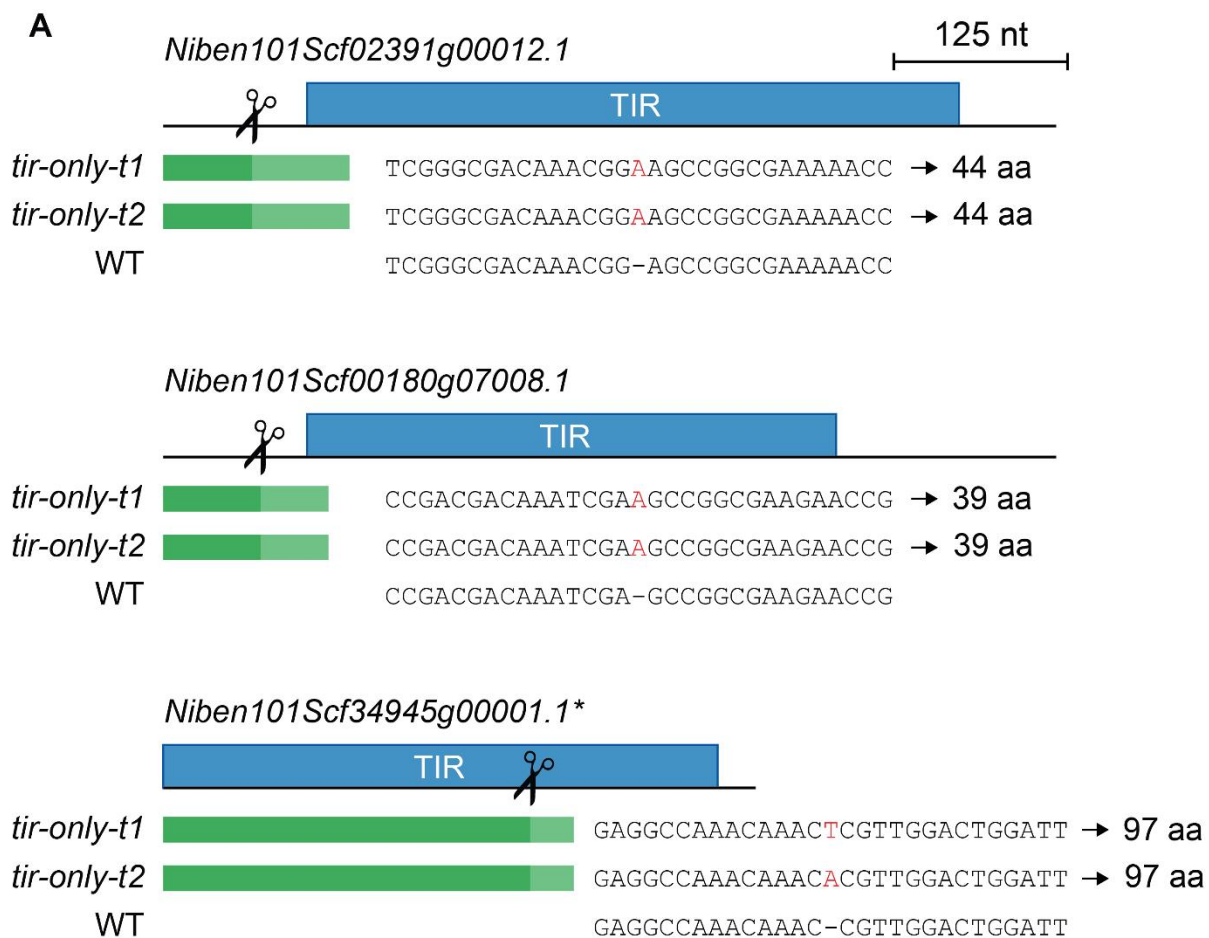
**B**

Figure 10: *Nicotiana benthamiana* tir-only CRISPR/Cas9 mutants

A Schemes of the three *Nicotiana benthamiana* conserved *TIR-ONLY* genes (Niben101Scf02391g00012.1, Niben101Scf00180g07008.1 and Niben101Scf34945g00001.1) targeted by CRISPR/Cas9 indicated with a black line (representing their coding sequences), including a scale for size determination in nucleotides (nt). The gene marked with an asterisk is likely a pseudogene or not correctly annotated. The scissor icon shows the gRNA target site in each gene, colored boxes on top indicate the location of the TIR domain. Green bars underneath the genes indicate the “left-over” mRNA that is still translated in the mutants until a stop codon is introduced. The opaque part of the bar represents the frame-shift variant of the mRNA, induced by the mutation at the CRISPR site. The aligned sequences show the induced mutations on the DNA level and resulting protein sized are indicated in amino acids (aa) after each alignment.

B Pictures of 5-week-old *N. benthamiana* WT, *eds1a*, *pad4*, *sag101ab* and the two independent *tir-only* triple mutants (*tir-only-t1*, *tir-only-t2*) described in **A**. Plants were grown under long-day greenhouse conditions further described in the Material and Methods section.

In *A. thaliana*, SCAF and cNMP production by TIRs were shown to be involved in amplification of immune signals, including cell death (Yu *et al.*, 2022). To test if the *N. benthamiana* conserved *TIR-ONLYs* are directly involved in cell death signaling, I overexpressed the *Xcv* effector protein XopQ, recognized by the TNL *NbRoq1*, which induces EDS1-SAG101-dependent cell death in *N. benthamiana* (Gantner *et al.*, 2019; Lapin *et al.*, 2019). Macroscopic cell death was assessed and YFP was included as a negative control (Figure 11). While the overexpression of YFP did not induce cell death in any of the tested genotypes, XopQ reliably did so in *N. benthamiana* WT, *pad4* and the two *tir-only* mutants (*tir-only-t1* and *tir-only-t2*). However, XopQ did not induce cell death in the *eds1a* and *sag101ab* mutants (Figure 11), underlining the importance of EDS1 and SAG101, but not PAD4 for cell death in *N. benthamiana*. The results indicate that the conserved TIR-onlys are not involved in execution of TNL-triggered cell death in *N. benthamiana*.

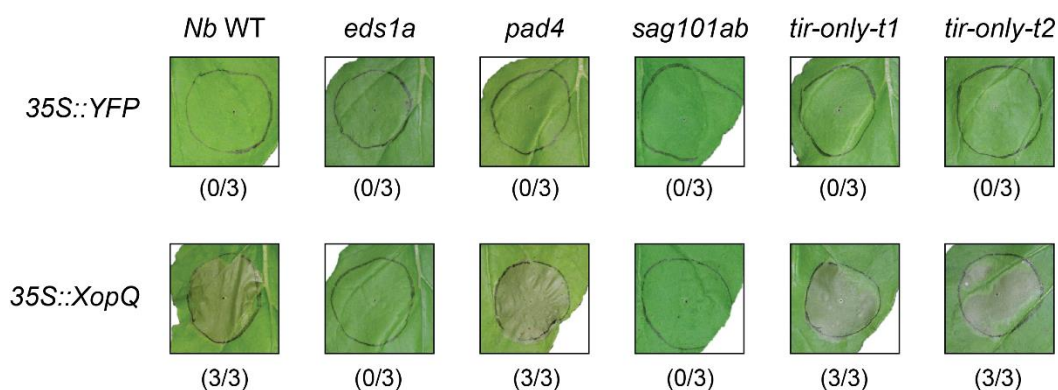


Figure 11: *Nicotiana benthamiana* *tir-only* mutant XopQ-triggered cell death assay

Macroscopic cell death induced by *Agrobacterium*-mediated overexpression of XopQ (35S promoter driven) in *Nicotiana benthamiana* (*Nb*) WT, *eds1a*, *pad4*, *sag101ab* and the two conserved *tir-only* triple mutants (*tir-only-t1*, *tir-only-t2*). Overexpression of YFP served as a negative control. Pictures were taken three days after *Agrobacterium* infiltration. In total, three biological replicates were performed, numbers below pictures indicate the number of replicates with cell death symptoms.

To further test the involvement of conserved *TIR-ONLYs* in *N. benthamiana* immunity, I performed an *Xcv* infection assay, including *Xcv* WT (carrying XopQ) and the $\Delta xopQ$ strain lacking XopQ to assess TNL-triggered and basal immunity, respectively. As a control, bacterial titers were determined directly after the infiltration, which did not vary across treatments, indicating equal infections (Figure 12). At 3 dpi, *Xcv* WT growth was restricted in WT, *pad4* and the two *tir-only* mutants (*tir-only-d1* and *tir-only-d2*), while it could grow up to non-recognized *Xcv* $\Delta xopQ$ titers in the *eds1a* and *sag101ab* mutants, again highlighting the importance of SAG101 for TNL immunity in *N. benthamiana* (Figure 12). *Xcv* $\Delta xopQ$ infected all *N. benthamiana* genotypes to a similar extent at 3 dpi (Figure 12), showing no indication of basal resistance against *Xcv*, as expected (Gantner *et al.*, 2019). In conclusion, the conserved *TIR-ONLYs* were not involved in *Xcv* immunity in *N. benthamiana*. Taken together, the data suggest that, as shown in *A. thaliana*, the conserved *TIR-onlys* are not directly involved in bacterial resistance pathways and do not behave like *EDSI* family mutants in *N. benthamiana*.

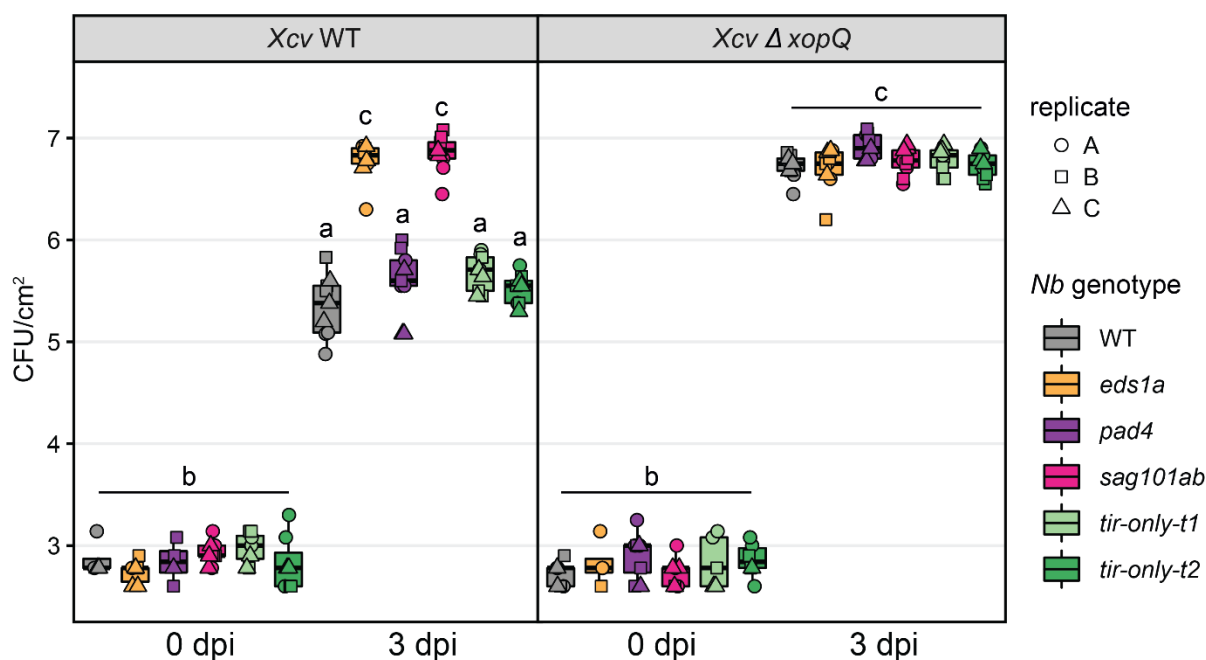


Figure 12: *Nicotiana benthamiana tir-only Xanthomonas campestris* immune assay

Xanthomonas campestris pv. *vesicatoria* (*Xcv*) growth assay in *Nicotiana benthamiana* (*Nb*) WT, *eds1a*, *pad4*, *sag101ab* and the two independent conserved *tir-only* triple mutants (*tir-only-t1*, *tir-only-t2*). Leaves were syringe-infiltrated with *Xcv* 85-10 (WT) and XopQ-knockout ($\Delta xopQ$) strains. Bacterial titers were determined at zero and six days post infection (dpi), the 0 dpi samples served as control for equal infiltrations. Boxplots show colony-forming units (CFU)/cm², colors indicate different *Nb* genotypes. The respective *Xcv* strains are shown above the boxplots. Shapes plotted over boxplots indicate individual CFU/cm² measurements, representing a total of three biological replicates. Genotype-treatment combinations sharing letters above boxplots do not show statistically significant differences (Tukey HSD test, $\alpha = 0.01$, $n = 9$).

2.2.4. Maize *ZmTNP-IIa* induces *EDS1*-independent cell death in *N. tabacum*

TNPs are present across land plants, with a small number of proteins predicted in most tested species (Figure 2). In contrast to conserved TIR-onlys, the TNP distribution does not follow the ones of EDS1, PAD4 or SAG101, with TNPs being retained in non-vascular plants that do not contain any EDS1 family member (Figure 2, (Baggs *et al.*, 2020; Lapin *et al.*, 2019)). I therefore hypothesized that TNPs would not rely on the EDS1 family in their potential functions. To enable the meaningful selection of candidate TNPs for further tests, it was crucial to reconstruct the internal TNP phylogeny to try and identify groups within the TNPs. For this, I generated a custom-built HMM based on the NB-ARC like domains of TNPs that were picked up by the TIR HMMs and clustered in the conserved group on the TIR and NB-ARC ML trees (Figure 2, Figure 3). Reciprocal BLAST searches already indicated the presence of additional TNPs with TIR domains too distinct from the canonical TIR HMMs to be picked up. This assumption was confirmed as the custom TNP HMM identified a total of 77 TNPs across the 39 tested plant species (Figure 2, Figure 13). I then build an ML tree based on the NB-ARC-like domains of these 77 TNPs, as NB-ARCs usually provide higher resolution than the TIR domain and were more easily identifiable with the custom HMM (Figure 13). Three major clades, with one split into two subclades were present on that tree. Clade I, Clade IIa and Clade IIb match the previously described TNP clades (Zhang *et al.*, 2017b), while Clade III is first described here and contains exclusively Bryophyte TNPs (Figure 13, (Johannndrees *et al.*, 2021)). Clade IIa, expectedly lacks Eudicot TNPs, but contains Monocot, Magnoliid and *Ceratophyllum* TNPs (Figure 13, (Zhang *et al.*, 2017b)). Clade I and Clade IIb contain TNPs from various land plants, mostly represented by a similar number of TNPs in both major clades (e.g.: *Arabidopsis* 1:1, *Hordeum* 1:1, *Nicotiana* 2:2) (Figure 13). Representative TNPs could now be selected for further experiments to reflect the maximum diversity across TNPs and to test if TNPs diverged functionally based on their internal phylogeny.

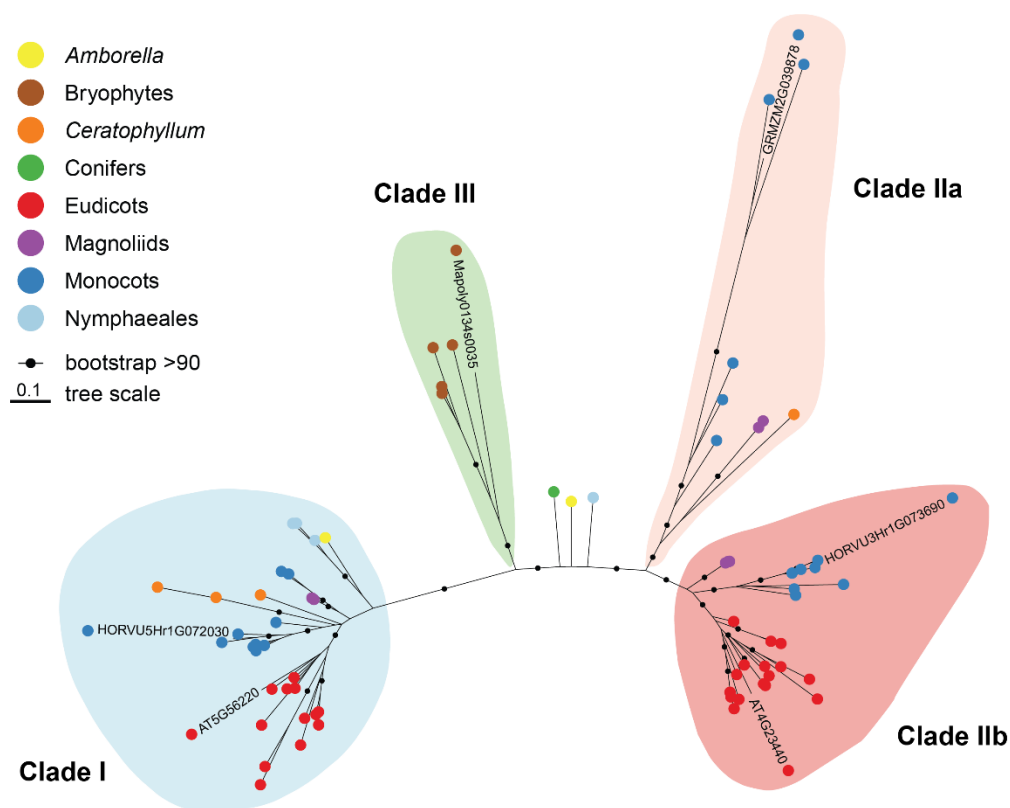


Figure 13: Internal TNP phylogeny based on their NB-ARC-like domains

TNP-specific NB-ARC domains were identified using a custom HMM (Table 2) on the 39 plant species shown on the tree in Figure 3. The Maximum-Likelihood tree was generated using IQ-TREE. Dots represent individual TNP NB-ARC domains, their color shows the phylogenetic origin. Branches with bootstrap support >90 are marked with black dots. Four conserved TNP clades are highlighted with colored shapes, representative TNPs within these clades used in further experiments are labeled with their complete protein identifier.

As described above, TNPs were selected from the conserved clades, including *A. thaliana* AT5G56220 (*AfTNP-I*) and *H. vulgare* HORVU5Hr1G072030 (*HvTNP-I*) from Clade I, *A. thaliana* AT4G23440 (*AfTNP-IIb*) and barley HORVU3Hr1G073690 (*HvTNP-IIb*) from Clade IIb, *Marchantia polymorpha* Mapoly0134s0035 (*MpTNP-III*) from the Bryophyte-specific Clade III, and *Zea mays* (maize) GRMZM2G039878 (*ZmTNP-IIa*) from Clade IIa. The representative TNPs were cloned from cDNA (all *A. thaliana*, *H. vulgare* and *M. polymorpha* TNPs) or recombinantly synthesized (*ZmTNP-IIa*) and overexpressed as C-terminal YFP fusion proteins in leaves of *N. tabacum* cv. Samsun WT or a corresponding *RNAi:EDS1* line (Duxbury *et al.*, 2020) via *Agrobacterium*-mediated transient expression. Cell death was visually assessed at 5 dpi, with

C-terminally YFP-tagged *AtRPP1*^{Wsb} and *ATR1*^{Emoy2}-SH expression as positive control for *EDS1*-dependent cell death (Krasileva *et al.*, 2010). YFP overexpression served as negative control for unspecific cell death induced by *Agrobacterium* infiltrations. Only the expression of *ZmTNP-IIa* and no other TNP induced cell death in *N. tabacum* (Figure 14). Strikingly, in contrast to *EDS1*-dependent *AtRPP1*^{Wsb}, cell death induced by *ZmTNP-IIa* was also observed in the *RNAi:EDS1* line (Figure 14). These results indicate autoactive and *EDS1*-independent cell death activity of *ZmTNP-IIa* in *N. tabacum*. It also suggests that TNPs from different clades vary in their molecular function or pre-requisites for cell death induction.

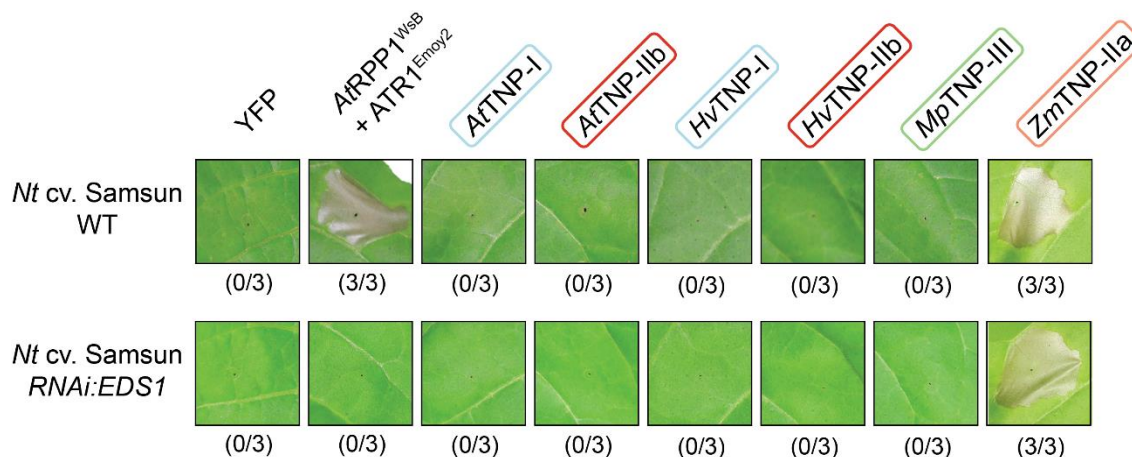


Figure 14: Cell Death induced by overexpression of maize *ZmTNP-IIa*

Macroscopic cell death induced by *Agrobacterium*-mediated overexpression (all constructs were 35S promoter driven) of YFP-tagged TNPs representing the four conserved TNP clades (*AtTNP-I* = AT5G56220 and *HvTNP-I* = HORVU5Hr1G072030 from Clade I, *AtTNP-IIb* = AT4G23440 and *HvTNP-IIb* = HORVU3Hr1G073690 from Clade IIb, *MpTNP-III* = Mapoly0134s0035 from Clade III, *ZmTNP-IIa* = GRMZM2G039878 from Clade IIa) in *Nicotiana tabacum* (*Nt*) c.v. “Samsun” WT and *RNAi:EDS1* lines. YFP and *AtRPP1*^{Wsb} together with the recognized effector *ATR1*^{Emoy2} were expressed as negative and positive controls, respectively. Pictures were taken five days after *Agrobacterium* infiltration. In total, three biological replicates were performed, numbers below pictures indicate the number of replicates with cell death symptoms.

To test if the putative catalytic glutamates conserved across TIRs (Figure 4) are important for cell death induced by *ZmTNP-IIa*, the two adjacent glutamates E130 and E131 in *ZmTNP-IIa* were mutated to alanines (*ZmTNP-IIa*^{E130A} and *ZmTNP-IIa*^{E131A}) (Figure 15). Additionally, a potential loss-of-function P-loop variant was generated by changing the amino acids G305, K306 and T307 to alanines (*ZmTNP-IIa*^{P-loop}). Cell death was abolished for both putative catalytic and the P-loop mutant variants, similar to the known P-loop loss-of-function *AtRPP1*^{WsB K293L} variant that was used as a control in the assay (Figure 15, (Krasileva *et al.*, 2010)). Similar results for the glutamate variants were reported for *N. tabacum* cv. Turk (Johannndrees *et al.*, 2021), excluding a cultivar-specific effect on cell death. Because none of the YFP-tagged *ZmTNP-IIa* variants could be detected by simple total protein extraction from infiltrated *N. tabacum* leaves, an α -GFP protein immunoprecipitation (IP) was performed to enrich tagged proteins with subsequent Western Blot for protein detection (Figure 15). After IP, all *ZmTNP-IIa* variants as well as the negative cell death control YFP were detected this way and shown to accumulate at 1 dpi (Figure 15). This indicated that loss of *ZmTNP-IIa* cell death is specific to mutations in the putative NADase catalytic residues and P-loop and not due to insufficient accumulation of the protein variants.

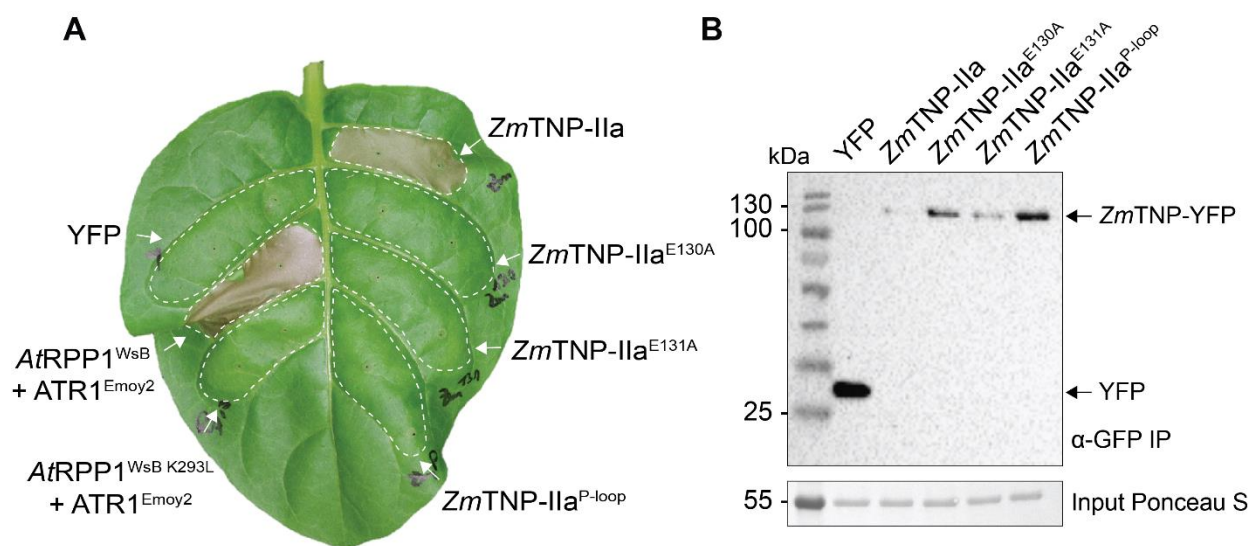


Figure 15: Importance of *ZmTNP-IIa* catalytic glutamates and P-loop for cell death

A Macroscopic cell death induced by *Agrobacterium*-mediated overexpression (all constructs were 35S promoter driven) of YFP-tagged *ZmTNP-IIa* WT, putative non-catalytic variants (*ZmTNP-IIa*^{E130A}, *ZmTNP-IIa*^{I31A}) and the P-loop mutant (G305A, K306A, T307A, called *ZmTNP-IIa*^{P-loop}) in *Nicotiana tabacum* (*Nt*) c.v. Samsun WT. YFP and *AtRPP1*^{WsB} as well as the P-loop mutant (*AtRPP1*^{WsB K293L}) together with the recognized effector *ATR1*^{Emoy2} were expressed as controls. Pictures were taken five days after *Agrobacterium* infiltration. In total, three biological replicates were performed, with similar results.

B Accumulation of *ZmTNP-IIa* variants in *Nt* WT leaves from experiments in **A** shown on immunoblots. Samples were taken from infiltrated leaf areas one day after *Agrobacterium* infiltration and subsequently YFP-tagged proteins were enriched via IP with α -GFP beads. Expected sizes for *ZmTNP-IIa*-YFP and free YFP as control are indicated on the right side. Ponceau S staining of the input samples used for IP served as control for equal loading. Protein standard sizes in kDa are indicated on the left side. Immunoblots were repeated with samples from two independent replicates, with similar results.

2.2.5. *Botrytis*-infected *N. benthamiana* *tnp* mutants develop smaller necrotic lesions

With the indication of *EDSI*-independent cell death functions of at least one TNP, it was of major interest to me to explore possible TNP functions in immunity and other pathways. For this, I generated *tnp* mutants in *N. benthamiana* using the same system as for the *tir-only* mutants. After genotyping, I was able to select two independent lines with homozygous mutations in all four *N. benthamiana* TNP genes (*tnp-q1* and *tnp-q2*) (Figure 16). All alleles introduced frameshifts and early stop codons, resulting in disruption of their corresponding TIR domains. The selected lines were propagated until the T3 generation and used for immune assays. Mutants did not show apparent phenotype when grown under greenhouse conditions (Figure 16). Similar results were obtained for *M. polymorpha* *tnp* mutants, which display a TIR-less plant (Johannndrees *et al.*, 2021). Taken together, this indicated that while TNPs are widely conserved across plants, they are not crucial for plant survival, even if all TIR proteins are removed (as in the case of the *M. polymorpha* *tnp* mutants).

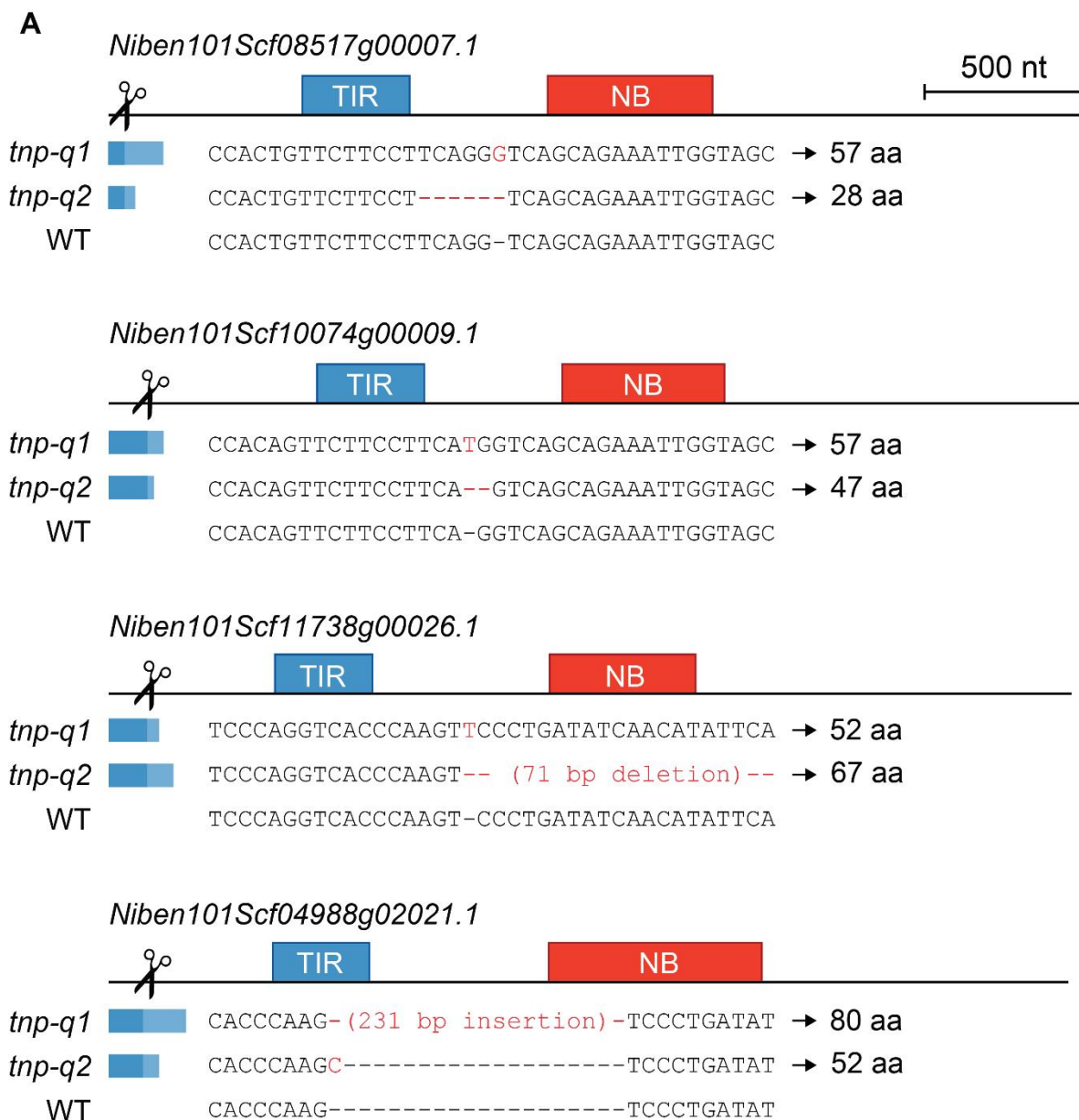
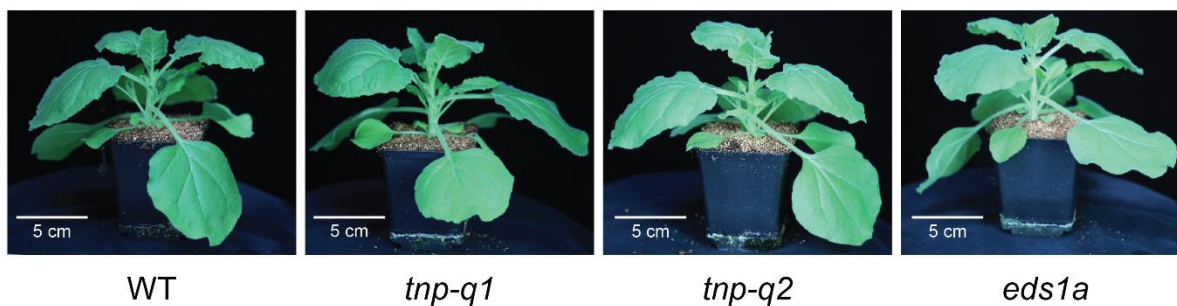
**B**

Figure 16: *Nicotiana benthamiana tnp* CRISPR/Cas9 mutants

A The four *Nicotiana benthamiana* TNP genes (Niben101Scf08517g00007.1, Niben101Scf10074g00009.1, Niben101Scf11738g00026.1, Niben101Scf04988g02021.1) targeted by CRISPR/Cas9 are indicated with a black line (representing their coding sequences), including a scale for size determination in nucleotides (nt). The scissor icon shows the gRNA target site in each gene, colored boxes on top indicate the location of TIR and NB-ARC-like (NB) domains. Blue bars underneath the genes indicate the “left-over” mRNA that is still translated in the mutants until a stop codon is introduced. The opaque part of the bar represents the frame-shift variant of the mRNA, induced by the mutation at the CRISPR site. The aligned sequences show the induced mutations on the DNA level and resulting protein sized are indicated in amino acids (aa) after each alignment.

B Pictures of 4-week-old *N. benthamiana* WT, the two independent *tnp* quadruple mutants (*tnp-q1*, *tnp-q2*) described in **A**, and *eds1a*. Plants were grown under long-day greenhouse conditions further described in the Material and Methods section.

First, the well-established *Xcv* infection and ion leakage assays were performed with the *tnp* quadruple mutants. Both *N. benthamiana tnp* lines allowed WT-like growth of avirulent *Xcv*, recognized by *NbRoq1* in *N. benthamiana* at both 3 and 6 dpi, while the *eds1a* mutant was fully susceptible to the bacterium (Figure 17). *Xcv ΔxopQ* grew to indistinguishable levels in all tested plants, including *tnp-q1* and *tnp-q2*, due to the previously described lack of basal resistance in *N. benthamiana* (Figure 17, (Gantner *et al.*, 2019)). Similarly, cell death induced by overexpression of XopQ was only impaired in *eds1a*, but not in the *tnp* quadruple mutants, where ion leakage values matched those of WT *N. benthamiana* (Figure 17). Collectively, these data suggest that TNPs are neither involved in TNL-triggered nor basal immune responses in *N. benthamiana* against *Xcv*. They further highlight their *EDS1*-independency, since TNPs must genetically function in different pathways as the *tnp* mutants did not phenocopy the *EDS1* family mutants.

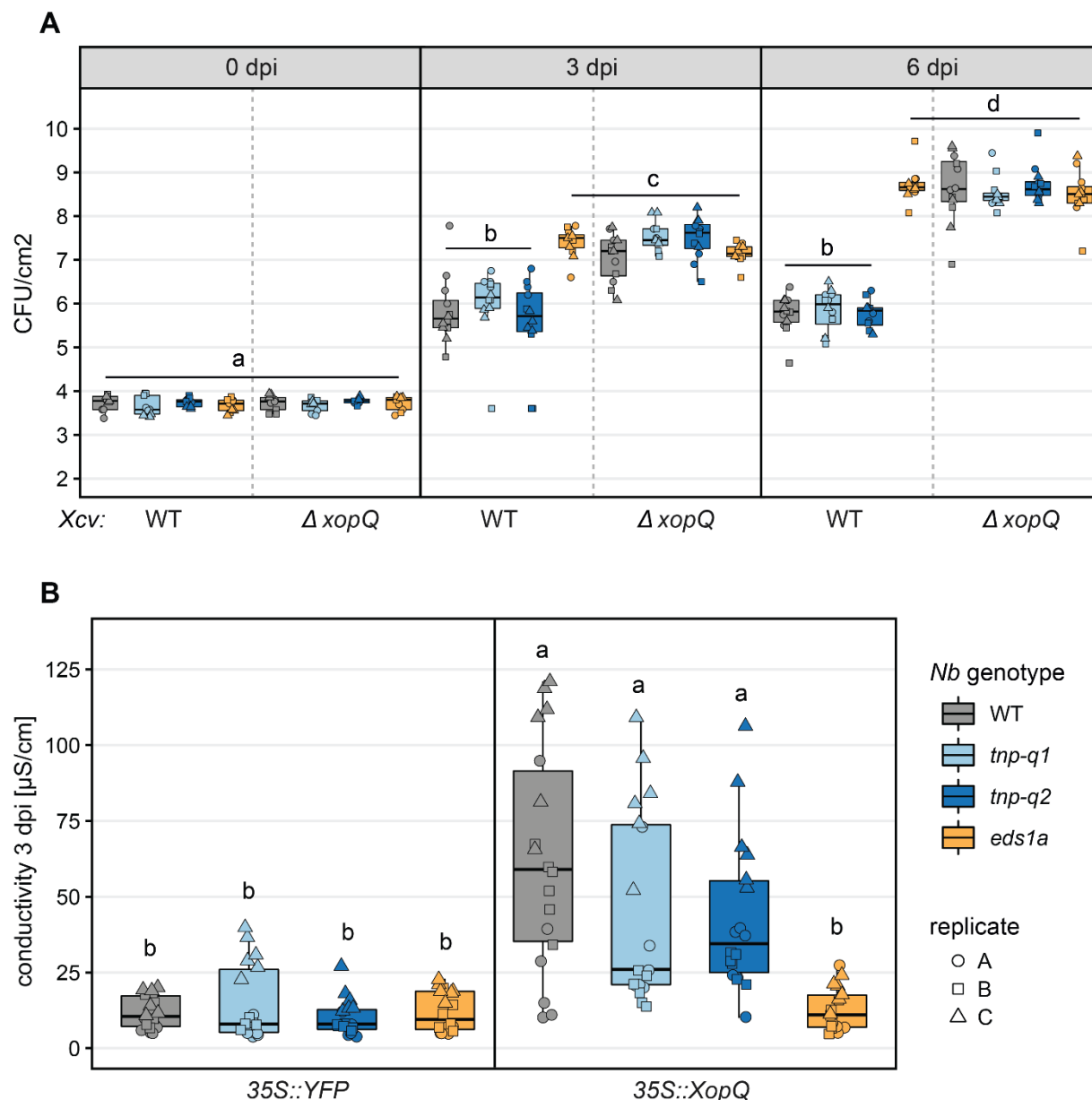


Figure 17: *Nicotiana benthamiana* *tnp* mutant infection and cell death assays

A *Xanthomonas campestris* pv. *vesicatoria* (*Xcv*) growth assay in *Nicotiana benthamiana* (*Nb*) WT, the two independent *tnp* quadruple mutants (*tnp-q1*, *tnp-q2*) and *eds1a*. Leaves were syringe-infiltrated with *Xcv* 85-10 (WT) and XopQ-knockout ($\Delta xopQ$) strains. Bacterial titers were determined at zero, three and six days post infiltration (dpi), the 0 dpi samples served as control for equal infiltrations. Boxplots show colony-forming units (CFU)/cm², colors indicate different *Nb* genotypes. The respective *Xcv* strains used are shown below the boxplots. Shapes plotted over boxplots indicate individual CFU/cm² measurements, representing a total of three biological replicates. Genotype-treatment combinations sharing letters above boxplots do not show statistically significant differences (Tukey HSD test, $\alpha = 0.01$, $n = 12$).

B Ion leakage assay to measure cell death triggered by *Agrobacterium*-mediated XopQ overexpression (35S promoter driven) in the same lines described in **A**. Ion leakage was determined by conductivity measurements three days after *Agrobacterium* infiltration. Overexpression of YFP served as a negative control. Shapes plotted over boxplots indicate individual ion leakage measurements, representing a total of three biological replicates. Genotype-treatment combinations sharing letters above boxplots do not show statistically significant differences (Tukey HSD test, $\alpha = 0.01$, $n = 18$).

In addition to the hemibiotrophic *Xcv*, *N. benthamiana* infection with the necrotrophic fungus *Botrytis cinerea* (strain B05.10) was performed (Figure 18). Both *tnp* quadruple mutants developed smaller lesions 48 hours after spore application to the *N. benthamiana* leaves, while *eds1a* showed WT-like lesion areas (Figure 18). Comparing lesions on WT and *eds1a* plants with the ones on the *tnp* lines, the data suggest that TNPs could, either directly or indirectly, contribute to an *EDSI*-independent necrotrophy-inducing pathway in *N. benthamiana*.

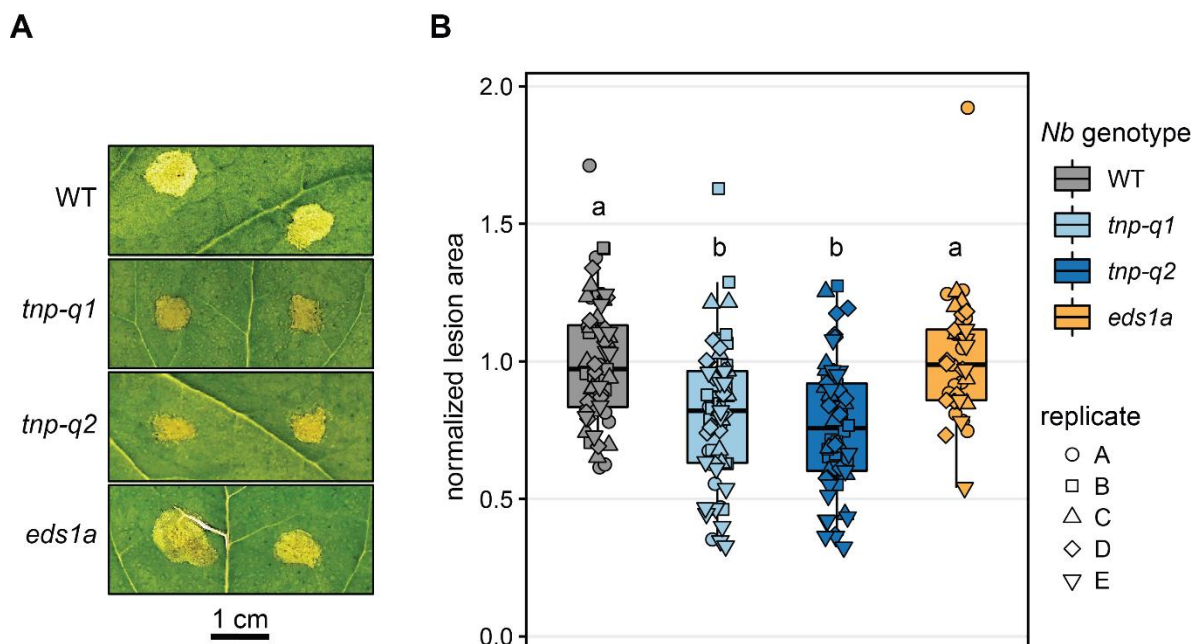


Figure 18: *Nicotiana benthamiana tnp* mutant *Botrytis cinerea* colonization assay

A Necrotic lesions induced by infection of *Nicotiana benthamiana* (*Nb*) WT, the two independent *tnp* quadruple mutant (*tnp-q1*, *tnp-q2*) and *eds1a* leaves with *Botrytis cinerea* strain B05.10. Plants were drop-inoculated, and pictures taken at 48 hours post infection (hpi).

B Quantification of lesion areas shown in **A**. Boxplots show lesion areas normalized to *Nb* WT leaves. Shapes plotted on top of boxplots indicate individual normalized lesion areas, representing a total of five biological replicates. Genotypes sharing letters above boxplots do not show statistically significant differences (Tukey HSD test, $\alpha = 0.01$, $n = 10-12$).

3. Discussion

3.1. TIR phylogeny reveals four interspecific conserved groups

3.1.1. Advantages of a phylogeny-based TIR protein grouping

Previous TIR protein annotations were based on the domain architectures of full-length proteins and did not consider the phylogenetic relationship of the contained TIR domains. Phylogenetic studies of TIRs were either limited to a small set of plant species (Nandety *et al.*, 2013) or provided a detailed view on one of the special TIR or NLR groups (Zhang *et al.*, 2017b). This led to common nomenclatures such as TX (for TIR-X), TN (for TIR-NB-ARC), TNL (for TIR-NB-ARC-LRR) and so on. However, this type of nomenclature can be misleading, as proteins with similar names might have different functions and are phylogenetically unrelated. For example, the *A. thaliana* TNP AT4G23440 described here as *AtTNP-IIb*, was previously called *AtTN17* (Nandety *et al.*, 2013), while a TIR-NB-ARC protein (*AtTN3*) with a TIR domain closely related to the ones from the canonical TNL proteins *AtRPS4* or *AtRPP1* are indistinguishable by their names (Nandety *et al.*, 2013). Because of the lacking distinction and categorization, one of the aims of this thesis was to provide a phylogeny-based grouping for plant TIR-domains. This relies solely on the TIR domains of the tested proteins, and not on additional domains. An up to date set of plant genomes and new phylogenetic tools allowed for a large-scale evolutionary analysis, of TIR domains, broadening previously described phylogeny. For the most unbiased set of plant TIRs, this study did not rely on previously published TIRs or on annotated proteins but used HMM-based protein prediction. Using this approach, a total of 2,348 TIRs were recovered in all 39 tested plant species, which laid the foundation for a more comprehensive categorization.

Conserved groups were defined as well-supported tree branches (bootstrap values >90) on the ML tree (Figure 2) sharing members of different plant clades or species. Four conserved groups could be recovered using this strategy, including two interspecific TNL groups, the Mesangiosperm conserved TIR-only and the most conserved group, represented by TNP proteins (Figure 2). These groups partially overlap with previously described TIR groups, including the TNPs (Meyers *et al.*, 2002; Zhang *et al.*, 2017b) and the two TNL groups (Zhang *et al.*, 2016). The conserved TIR-only group was not described as separate group, but as part of the TX proteins (Meyers *et al.*, 2002; Nandety *et al.*, 2013), containing other unrelated TIR-only proteins such as *AtRBA1*. By screening genomes of the recently sequenced Magnoliids *Cinnamomum* and *Persea* (Chaw *et al.*, 2019;

Rendon-Anaya *et al.*, 2019), as well as Nymphaeales and *Ceratophyllum* (Yang *et al.*, 2020), more precise claims could be drawn on the evolution of conserved TIR domains. This showed that the conserved TIR-only proteins are Mesangiosperm-specific, being present in the tested Monocots, Magnoliids and Eudicots, but not in the other clades.

3.1.2. Potential implications of TIR protein radiation

Apart from the four conserved groups described here, additional sets of TIR domains were identified, originating from a single species. These TIRs would all be very similar to each other, represented by short tree branches and high bootstrap values, but are not present across species (Figure 2). Similar groups could be identified on the NB-ARC phylogenetic tree, which in general has a similar structure as compared to the TIR tree (Figure 3). This indicates a degree of TIR and NB-ARC specification, evolving together as compound signaling domains. These proteins likely derived from a common ancestor through gene duplications, allowing the plants to enlarge their TIR repertoire. TIR radiations are also visible comparing TIR numbers, where Eudicot and Conifer species demonstrate extensive expansion. While it is hard to compare due to the variable nature of LRR domains, the proteins shared within those groups may contain different LRR or post-LRR domains, such as C-JID. This would lead to a set of proteins with similar TIR and NB-ARC parts, but variable C-termini with effector-recognizing capabilities adapted to bind diverse effector proteins. This would make sense, as TIRs are known signaling domains producing second messenger molecules that are recognized by EDS1 heterodimers to induce downstream signaling (Huang *et al.*, 2022; Jia *et al.*, 2022). Signaling could thereby converge on well-preserved TIR domains, triggered by specific effector binding. In contrast to Conifers and Eudicots, Monocots did not expand their TIR repertoire, indicated by small numbers and loss of TNLs across the tested species (Figure 1, Figure 2), which was also shown in previous publications (Meyers *et al.*, 1999; Shao *et al.*, 2016; Urbach & Ausubel, 2017). It is thought that Monocots have in turn expanded their CNL repertoire to recognize a wide variety of effector molecules (Liu *et al.*, 2021; Meyers *et al.*, 1999). It remains unclear what shifts the balance between TNL or CNL receptor numbers, but species with a complete EDS1 family, including most Eudicots but not Caryophyllales, tend to accumulate more TIR proteins, while species lacking the SAG101 signaling branch have lower TIR numbers and lack TNLs (Monocots), or retained only the TNL #1 group of TNLs (Caryophyllales) (Figure 1, Figure 2, (Zhao *et al.*, 2021)). It is unclear if presence of SAG101

dictates the presence of canonical TNLs, or the other way around, but a previous study aimed to test this (Liu *et al.*, 2021). However, because of the usually high numbers of TNLs, this is hard to predict, as pseudogenization may mask the absence of TNLs. It is unknown how TIR signaling functions in Conifers, which contain a multitude of TIRs and TNLs, yet lack SAG101 (Figure 2, (Lapin *et al.*, 2019)). However, the tested Conifers have extended numbers of PAD4 paralogs, which is unusual for a downstream signaling component but may compensate for missing SAG101 (Figure 2). However, these findings are limited by the fact that both tested Conifers (*Pinus*, *Picea*) are trees, which may have an immune system that greatly differs from the annual model plant *A. thaliana*, from which most of our knowledge of plant immunity has been gathered. It would be necessary to include other Gymnosperms in the analysis to draw a more precise conclusion of their TIR evolution.

3.1.3. Using phylogeny to predict TIR-EDS1 co-evolutionary patterns

By extending the phylogenetic analysis to EDS1 family members (Figure 2, (Johannrees *et al.*, 2021)), I was able to compare TIR and EDS1 co-evolution in plants in order to observe potential patterns. I aimed to use the conserved TIR groups to identify a minimal TIR-EDS1 signaling module. This was not previously possible, as the two global co-presence patterns were never directly compared. Among the conserved TIR proteins, there were two distinct opposite trends in co-occurrence with EDS1. Conserved TIR-onlys are co-present with EDS1 and PAD4 in Mesangiosperms, while TNPs seem to have evolved EDS1-independently, as they are also found in non-seed plants, which do not contain EDS1, PAD4 or SAG101 (Figure 2, (Lapin *et al.*, 2020; Lapin *et al.*, 2019)). While SAG101 is also absent from Monocots, all tested species contain EDS1 and PAD4, which is surprising, as the EDS1-PAD4 heterodimer is an essential part of TNL-triggered immunity in *A. thaliana*. One hypothesis is that CNLs may function through EDS1-PAD4 in Monocots, as was shown for the *A. thaliana* CNL *AtRPS2*, which is partially dependent on PAD4 (Bhandari *et al.*, 2019). However, this was not yet shown in Monocots, and may be due to the special nature of the *A. thaliana* immune system, which includes EDS1/PAD4-dependent basal resistance involving salicylic acid mediated signaling against virulent pathogens (Bhandari *et al.*, 2019; Dongus & Parker, 2021). The data shown here would favor the involvement of Monocot EDS1-PAD4 in TIR-only immunity, as these components are always co-present (Figure 2). Both on a global level for multiple species (Figure 5, (Johannrees *et al.*, 2021)) as well as for *A. thaliana*

and *H. vulgare* (Figure 6), an immune-related *TIR-ONLY* transcriptional induction could be observed. The strikingly low basal expression values of *TIR-ONLYs* contrasting with all other *TIR* groups as well as *NLRs* in general, suggests that their promoters are under tight control to prevent expression in untriggered tissues. It also likely excludes their involvement as sensor proteins, such as the unrelated *AtRBA1* TIR-only protein, as conserved *TIR-ONLY* transcripts can only be detected when the pathogens already started to colonize the host (Figure 6). This favors a role as signal amplifiers or downstream components, specifically induced upon immune activation. Inducible *TIR* genes have been reported previously, as potent signaling amplifiers in PTI (Tian *et al.*, 2021), but this has not been shown for the conserved *TIR-ONLYs* specifically.

In contrast to TIR-onlys, multiple species that have either lost EDS1 components, such as the aquatic plants *W. australiana* or *Ceratophyllum* (Figure 2, (Baggs *et al.*, 2020; Johannndrees *et al.*, 2021)), or likely never contained them, like *M. polymorpha* and other Bryophytes, contain TNPs (Figure 2). This indicates that in multiple incidents, without EDS1 present, TNPs have persisted in plant genomes. This conservation can be observed across clades within most tested plants, independent of their lifestyles, as trees, annual plants, and permanently submerged water plants all contain TNPs (Figure 2). TNP distribution therefore indicates a conserved and EDS1-independent function. TNPs can not generally be placed in immunity by analyzing their expression patterns. *TNPs* were induced by immune triggers in *H. vulgare*, but unresponsive in other species (Figure 5), which may be the result of limited RNAseq datasets available for *H. vulgare*. Both RNAseq samples originated from fungal infections, while the datasets for other species reflect a much broader range of biotic stresses (Table 3). In general, the expression analysis would suggest a TNP function outside of immunity.

Internal TNP clades were previously proposed (Zhang *et al.*, 2017b) and could be recovered here, with the addition of the Bryophyte-specific Clade III (Figure 13). The two major TNP Clades I and II likely originated from whole genome duplications and Clade III possibly represents the ancestral group, which was previously not identified, since only *M. polymorpha* was included in the analysis (Zhang *et al.*, 2017b). It remains unknown what distinguishes Clade IIa from the more widespread Clade IIb and why there are no Eudicot proteins found in Clade IIa.

3.2. Differential EDS1 requirements for plant TIR-induced cell death

3.2.1. Conserved monocot TIR-onlys induce cell death dependent on EDS1

Full-length TNLs triggered by their cognate effectors, their truncated TIR domains or TIR-only proteins were shown to induce cell death when overexpressed in *N. benthamiana*. This was also shown for the conserved TIR-only from *B. distachyon* (*BdTIR*), which induces *EDS1*-dependent cell death (Wan *et al.*, 2019). However, this has not been generalized to other conserved TIR-onlys. The data presented here suggest that induction of cell death by conserved TIR-onlys is a common feature of this TIR group. *EDS1*-dependence is unsurprising, as the conserved TIR-onlys evolved together with *EDS1*-PAD4 (Figure 2) and overall, the investigated motifs are similar to the ones from canonical TIR proteins (Figure 4).

In addition to the catalytic glutamate residue, which was shown to be important for *BdTIR* enzymatic activity (Wan *et al.*, 2019) and abolished *OsTIR* and *HvTIR*-induced cell death, I identified a glycine residue which was crucial for *OsTIR*-mediated cell death (Figure 7). The glycine residue originates from the predicted DE interface, and is conserved across TIR groups, with the exception of TNPs (Figure 4). This residue was previously shown to be required for cell death and immune responses in several TNLs by mediating TIR-TIR interactions (Zhang *et al.*, 2017a). A similar structural assembly could be assumed for the conserved TIR-only proteins, which can not rely on additional domains for protein-protein interactions and lack clear homology to the AE interface found in *AtRPP1*^{WsB}. However, the exact TIR-TIR interactions and complex stoichiometry remain elusive until the first structures are solved for conserved TIR-onlys.

The observed cell death induced by conserved TIR-onlys is a robust test for their activities, which is established for many TIR proteins. While being used as an output in this study, induction of cell death is likely not the native function of conserved TIR-onlys in immunity. This is due to their early transcriptional upregulation, which also occurs in compatible interactions like *A. thaliana* infections with *Pst* DC3000 EV (Figure 5), *XopQ* overexpression still triggering cell death in *N. benthamiana tir-only* mutants (Figure 11), and their co-occurrence with *EDS1*-PAD4 (Figure 2). It is more reasonable to assume that TIR-onlys are involved in basal resistance or PTI immune responses, potentially leading to transcriptional changes, which are also dependent on *EDS1*-PAD4 in *AtRPS4-AtRRS1* immunity (Bhandari *et al.*, 2019; Cui *et al.*, 2017). Only a prolonged expression, or ETI-specific expression would reason for an involvement of conserved TIR-onlys as cell death executors.

Finally, conserved TIR-onlys are likely to produce a similar set of metabolites as canonical TNLs or *AtRBA1*. This was shown for *Bd*TIR (Huang *et al.*, 2022) and because of their high level of conservation can be assumed for other members of the protein group. *Bd*TIR was able to induce the formation of the EDS1-PAD4 heterodimer *in vitro*, which underlines the conserved nature of the TIR-EDS1-PAD4 signaling node, in which a Monocot TIR-only can induce binding of *A. thaliana* EDS1 and PAD4 (Huang *et al.*, 2022). Similar activities are expected for the conserved TIR-onlys described here, but this has to be shown in future experiments. It would also be interesting to additionally test the ability of conserved TIR-onlys to synthesize cNMPs, as they have a native TIR-only domain architecture, in contrast to the tested truncated *LuL7*^{TIR} (Yu *et al.*, 2022), which originally occurs as part of a full-length TNL.

3.2.2. *Zm*TNP-IIa is an autoactive *EDS1*-independent cell death inducer

In contrast to conserved TIR-onlys, none of the TNPs tested in this study triggered cell death in *N. benthamiana* (Johannndrees *et al.*, 2021), which is why *N. tabacum* cv. Samsun was used for TNP experiments. The reason for lack of cell death remains unclear, but like its wild relative *N. benthamiana*, *N. tabacum* is a well-established host plant for cell death assays including effector-triggered *AtRPP1*^{W_sB} (Krasileva *et al.*, 2010). Across the four internal TNP clades (Figure 13) members were picked to test induction of cell death upon overexpression, but only the maize Clade IIa TNP *Zm*TNP-IIa induced cell death (Figure 14).

In striking contrast to all other so far studied plant TIRs, *Zm*TNP-IIa triggers cell death in an *EDS1*-independent fashion, as shown in an *RNAi:EDS1* line. While not a full knock-out, this line was previously shown to completely lack canonical TIR-triggered cell death (Duxbury *et al.*, 2020) and did not trigger cell death when overexpressing *AtRPP1*^{W_sB} together with *ATR1*^{Emoy2} (Figure 14, Figure 15). *Zm*TNP-IIa is the only tested TNP that induced cell death in tobacco and accumulates at 1 dpi (Figure 15). The other TNPs are likely instable or inactive on their own. *A. thaliana* TNPs *At*TNP-I and *At*TNP-IIb (previously named *At*TN17 and *At*TN21) were tested in a prior publication and reported to induce cell death in *N. benthamiana* (Nandety *et al.*, 2013). However, in that publication pictures and or protein accumulation were not included, and results could not be replicated here (Figure 14) marking *Zm*TNP-IIa the only TNP to reliably induce *EDS1*-independent cell death to date. This resembles cell death triggered by the human *Hs*SARM1, which was also shown to be *EDS1*-independent in plants (Horsefield *et al.*, 2019). It is hypothesized that instead

of production of specific catalytic metabolites that are recognized by plant signaling components, *HsSARM1* can induce plant cell death via NAD⁺-degradation, ultimately leading to necrosis similar to its function in human cells (Essuman *et al.*, 2017; Horsefield *et al.*, 2019). *ZmTNP-IIa* could function via a similar mechanism, as two putative catalytic glutamates are crucial for its cell death activity (Figure 15), meaning it is likely able to hydrolyze NAD⁺. It would therefore be unlikely that *ZmTNP-IIa* produces metabolites that are specifically recognized by EDS1 heterocomplexes, which is in line with EDS1-independent evolution (Figure 2) and the vastly changed putative catalytic region of TNPs (Figure 4).

Interestingly, in contrast to full-length TNLs, which need an effector-trigger to oligomerize and induce cell death (Ma *et al.*, 2020; Martin *et al.*, 2020), *ZmTNP-IIa* is active without an external trigger. In addition to glutamate residues, a mutated P-loop renders *ZmTNP-IIa* inactive, like *AtRPP1*^{WsB K293L} (Figure 15). While the *ZmTNP-IIa*^{P-loop} variant is stable (Figure 15), P-loop mutations may interfere with the formation of a higher order activated TNP-complex. These complexes were shown to exist in bacterial NACHT-TPR domain proteins, which interact via their NACHT domains (Kibby *et al.*, 2022). Similarly, NB-ARC and TPR domains could bring TNPs together, arranging their TIR domains to become enzymatically active, which would resemble conserved activation mechanisms of TNLs and *HsSARM1* (Kibby *et al.*, 2022; Ma *et al.*, 2020; Martin *et al.*, 2020; Shi *et al.*, 2022), both relying on additional intermolecular contact points. P-loop assisted TNP complex formation would explain that both TIR enzymatic residues as well as an intact P-loop are important for *ZmTNP-IIa*-mediated cell death induction (Figure 15).

3.3. High-order conserved TIR mutants to identify potential functions

3.3.1. TIR-onlys might act redundantly in immunity

Conserved TIR-onlys co-occur with EDS1 and PAD4 in Mesangiosperms (Figure 2), are transcriptionally upregulated by biotic immune triggers (Figure 5, Figure 6) and induce *EDS1*-dependent cell death (Figure 7). It was therefore reasonable to assume they would play a role in immune responses against invading pathogens. For this, CRISPR mutants were generated in *A. thaliana* and *N. benthamiana*, because of their differential employment of the EDS1 heterodimers and helper NLRs in immunity. In *A. thaliana* EDS1-SAG101-NRG1 mainly mediate host cell death, while EDS1-PAD4-ADR1 induce pathogen restriction, including basal resistance against virulent pathogens (Saile *et al.*, 2020; Sun *et al.*, 2021). Whereas in *N. benthamiana*, which lacks basal resistance outputs, EDS1-PAD4-ADR1 have no known contribution to resistance against avirulent pathogens, which is only mediated via the EDS1-SAG101-NRG1 node (Gantner *et al.*, 2019; Lapin *et al.*, 2019). Therefore, the two host species were suitable candidates to test TIR-only involvement in different EDS1 contexts.

The *tir-only* mutant lines were generated via plant CRISPR/Cas9 mutagenesis systems, which were shown to edit plants with a high efficiency, allowing simultaneous mutations of various target loci (Ordon *et al.*, 2020; Ordon *et al.*, 2017; Stuttmann *et al.*, 2021). The used vectors tend to induce small insertions and deletions, which was also observed in the lines described here (Figure 8, Figure 10). This did not result in complete knockout with large deletions of entire genes. However, mutations induced frameshifts early enough to inhibit proper translation of the TIR domains. The exception being the *N. benthamiana* gene Niben101Scf34945g00001, which is probably not correctly annotated in the version used, and it could not be properly targeted. However, a large part of the TIR domain does still contain a frameshift, likely rendering the resulting proteins non-functional (Figure 8, Figure 10).

All *A. thaliana* and *N. benthamiana* *tir-only* lines behaved like WT in the *Pst* and *Xcv* infection assays, respectively (Figure 9, Figure 12). Also, cell death was still induced by overexpression of XopQ in the *N. benthamiana* *tir-only* mutants (Figure 11). This led to the conclusion that in both plants, conserved *TIR-ONLYs* are not directly involved in resistance against the tested bacterial strains. There are multiple possibilities why a potential phenotype might not be detectable using the generated lines, including possible redundancy of TIR-only proteins. It was previously shown that in *A. thaliana*, a multitude of *TIRs*, including *TIR-ONLYs* are upregulated in immunity (Figure

6, (Tian *et al.*, 2021)). Due to their presence in a multitude of Mesangiosperms, conserved TIR-onlys might act as signaling boosters for TNLs, which could not be confirmed in the *A. thaliana* and *N. benthamiana* immune and cell death assays (Figure 9, Figure 11, Figure 12). With their repertoire of 134 and 37 TIRs (Figure 1), among them 29 and 4 TIR-onlys (Johannndrees *et al.*, 2021) in *A. thaliana* and *N. benthamiana*, other TIR proteins may compensate for mutated conserved TIR-onlys. In the *tir-only* mutants, it would therefore be interesting to test the global expression patterns of other genes coding for TIR proteins by RNAseq. This would give an indication of whether redundancy masks a possible phenotype in the analyzed *tir-only* mutant lines and identify new CRISPR/Cas9 targets for an extended mutant analysis. Additionally, *tir-only* colonization phenotypes in immunity could be more time-sensitive than corresponding *eds1* phenotypes, which are robust across time points (Figure 9, Figure 12, (Bhandari *et al.*, 2019; Gantner *et al.*, 2019; Lapin *et al.*, 2019)). This would make sense in light of the early and abrupt transcriptional induction of *TIR-ONLYs* upon infection (Figure 6), which could be tested by including earlier time points in the infection assays. Performing priming assays to see if systemic acquired resistance, which is a *pad4* phenotype in *A. thaliana* (Pruitt *et al.*, 2021), is impaired in the *tir-onlys* would be another option.

3.3.2. TNPs likely have immune-unrelated functions

As TNPs occur in a variety of land plants, with or without EDS1 family proteins (Figure 2), it did not seem crucial to compare plants with different immune systems, but rather to screen plants covering a large phylogenetic span, to compare TNP conservation. Therefore, *TNPs* were targeted via CRISPR/Cas9 in *N. benthamiana* (Figure 10) and *M. polymorpha* (Johannndrees *et al.*, 2021), which represent a Eudicot and Bryophyte, respectively. Since a sole *TNP* gene is the only predicted *TIR* gene in the entire *M. polymorpha* genome, the *tnp* mutants also represent a *TIR*-less plants (Johannndrees *et al.*, 2021), which enabled the analysis of possible basal functions of TNPs and TIRs. Similar to the *tir-only* lines, the two *N. benthamiana tnp* lines both contain mostly small deletions and insertions, leading to frameshifts in all four TNP genes, before translation of the TIR domains would occur (Figure 10). This likely renders all resulting truncated TNP proteins non-functional in both quadruple lines.

Taken together with the findings in this study, viability of *N. benthamiana* and *M. polymorpha tnp* mutants indicates that *TNPs* are likely not involved in processes crucial for plant survival, at least under optimal growth conditions (Figure 10, (Johannndrees *et al.*, 2021)). Whether this holds true for plants that are challenged with nutrient or other abiotic stresses, remains to be elucidated. Information from the RNAseq datasets further indicates no involvement of *TNPs* in biotic stresses since their genes are not universally upregulated by immune triggers (Figure 5). Experiments with biotic triggers, indicate that bacterial resistance is not impaired in the *N. benthamiana tnp* lines, as they behaved like their WT sister lines (Figure 16). This stands in contrast to the *eds1a* mutant, which allows *Xcv* WT growth up to $\Delta xopq$ levels (Figure 16), indicating a complete loss of induced ETI and highlights the *EDS1*-independent nature of *TNPs*. Based on the *N. benthamiana* mutants, it is therefore highly unlikely that they work in the same pathways. *Xcv* was described as hemibiotrophic pathogen, with the infection assays described here only testing the biotrophic phase of its interaction with the host. To allow a broader view on biotic interactions, the *tnp* lines were also tested using infections with the necrotrophic fungus *Botrytis cinerea*.

Interestingly, *N. benthamiana tnp* lines developed smaller necrotic lesions, when infected with *B. cinerea*, which again was in contrast to the *eds1a* mutant with WT-like lesion sizes (Figure 18). *EDS1* signaling components were shown to be hijacked by *B. cinerea*, contributing to infection (El Oirdi & Bouarab, 2007), which makes sense, considering that inducing cell death against a necrotroph is counterproductive. *B. cinerea* induces PTI responses by nlp recognition (Ono *et al.*, 2020), including ROS-bursts as one of the earliest PTI responses. Accordingly, ROS burst assays were performed to see if *tnp* mutants might induce enhanced PTI responses, which could explain decreased *B. cinerea* virulence. However, *tnp* mutants were indistinguishable from the WT in these experiments (Johannndrees *et al.*, 2021), which excluded enhanced ROS production as a possible explanation. Further experiments must be performed, to determine whether other PTI components, such as MAP kinases or Callose deposition might be negatively regulated by *TNPs*. Apart from enhanced immunity, another explanation for smaller lesions would be attenuated necrosis in the *tnp* mutants. This could either be caused by more structural hindrance by for example by cell wall restructuring, which was previously shown to impact *B. cinerea* growth in *A. thaliana* (Guzha *et al.*, 2022; Lionetti *et al.*, 2017), or the fungus may hijack an internal cell death pathway, which is disrupted in the *tnp* mutants. Like *HsSARM1* in human (Essuman *et al.*, 2017), *TNPs* may represent an internal, developmental cell death machinery, which the fungus is able to exploit for induction of necrosis in the infected tissues. This hypothesis may explain the striking conservation

of TNPs in most land plants, where they could serve developmental functions. Examination of a public gene expression browser (eFP) revealed specific expression of the *A. thaliana* TNPs in root cap cells, a root compartment significantly shaped by specific induction of cell death to shed cells during growth (Feng *et al.*, 2022). The *tnp* mutants described here and in the accompanying publication (Johandrees *et al.*, 2021) lay the foundation for characterization of potential developmental phenotypes to solve TNP functions.

3.4. Co-evolutionary patterns and potential origins of plant TIRs

During recent years, TIR domains have been intensively studied in multiple domains of life, including bacteria, archaea, animals and plants. Strikingly, cell death activities and roles in immunity are conserved features of TIRs in all of those organisms and across diverse full-length domain architectures of the TIR proteins (Lapin *et al.*, 2022). While TIR domains overall vary in sequence conservation and some structural components have changed, most of the studied TIR domains have an NADase activity, defined by catalytic glutamate residues (Essuman *et al.*, 2018; Horsefield *et al.*, 2019; Wan *et al.*, 2019). Enzymatic regulation, and identity of produced metabolites are intensively studied, yet not much is known about the large-scale phylogeny of plant TIR proteins. This study provides a comprehensive examination of plant TIR evolution by identifying TIRs across plants and showing co-evolutionary trends with EDS1.

While many TIRs, including TNLs, are co-present with EDS1 and species with a complete EDS1-SAG101 branch have enlarged TIR repertoires, TNPs developed in an EDS1-independent fashion. This divides plant TIRs based on their EDS1-dependency. It was interesting to see that the co-occurrence of certain TIRs with EDS1 can predict their EDS1-dependency, as conserved TIR-onlys are *EDS1*-dependent, while TNPs are *EDS1*-independent cell death inducers (Figure 19). This confirmed the beginning hypothesis that dependency on a signaling pathway might be predicted based on phylogeny and co-occurrence and suggests a TIR-EDS1 co-evolution. These two different TIR groups also asked the question of TIR origins in plants.

It remains hard to predict reliably, but certain features of plant TNPs point to a bacterial origin. While designing the gRNAs for CRISPR mutations in *M. polymorpha*, *A. thaliana* and *N. benthamiana*, and cloning the CDS of TNPs for *H. vulgare*, it became apparent that all of these *TNP* genes lack introns, an unusual feature for eukaryotic genes (Zou *et al.*, 2011). In addition, the presence of TPR repeats in TNPs first described here is more unusual for eukaryotic proteins, especially for plant proteins, which are much more likely to be associated with LRR domains (Figure 2, (Lapin *et al.*, 2022)). Finally, using the custom-built plant TNP NB-ARC HMM, I was able to identify bacterial homologs, which resemble the TIR-NB-TPR domain architecture. Prokaryotic genomes do not contain introns and the presence of TNP proteins in bacteria confirmed my suspicion that plant TNPs may be of bacterial origin. This requires further validation, as TNPs could so far only be identified in a small subset of bacteria belonging to the Actinobacteria, which is likely due to a small number of available genomes. However, these bacteria are reported to be

associated to roots, which could enable horizontal gene transfer between the bacteria and their host plant (Gao *et al.*, 2014). This hypothesis would provide a potential explanation for the existence of plant TNPs, which behave differently in many aspects compared to their more distant TIR relatives in plants.

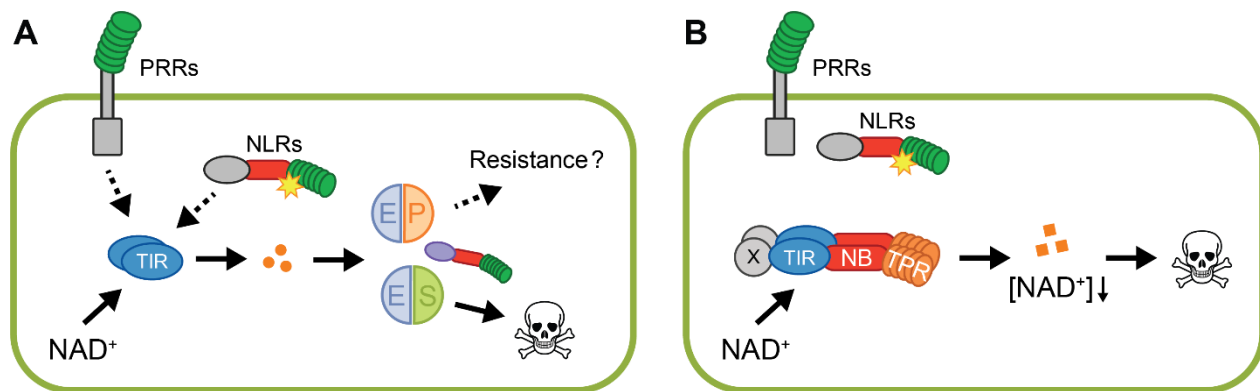


Figure 19: Differential *EDS1* requirement for cell death induced by conserved plant TIRs

A Conserved TIR-onlys induce *EDS1*-dependent cell death. Both PTI and ETI can transcriptionally activate conserved TIR-onlys, which require oligomerization and catalytic motifs. Conserved TIR-onlys can degrade NAD^+ and produce enzymatic metabolites that induce *EDS1*-RNL complex formation. While conserved TIR-onlys induce *EDS1*-dependent cell death in *Nicotiana benthamiana*, it remains unknown if they contribute to resistance against invading pathogens.

B TNPs induce *EDS1*-independent cell death. *TNPs* are not generally induced by PTI or ETI in tested plant species. *ZmTNP-IIa* requires conserved putative catalytic and P-loop residues to induce cell death in *Nicotiana tabacum*, which suggests TNP oligomerization and complex formation. Activated TNPs either produce metabolites distinct from canonical TNLs and conserved TIR-onlys or induce cell death via degradation of intracellular NAD^+ levels ($[\text{NAD}^+] \downarrow$), like *HsSARM1* in plants. TNPs evolved *EDS1*-independently and do not require *EDS1* to induce cell death in *N. tabacum*.

3.5. Future Perspectives

The comprehensive CRISPR/Cas9 mutants presented here lay the foundation of analysis of phylogenetically conserved TIR proteins in plants. In addition to the *A. thaliana* and *N. benthamiana* lines tested in this study, I also generated *eds1 pad4* mutant lines in *H. vulgare*. Research on Monocot immune systems focused mostly on identification of CNL-effector combinations in the past (Saur *et al.*, 2019a) and did not take into account that conserved TIR-onlys are present as well. Consequently, EDS1 proteins have only been examined in a few Monocot studies thus far (Chen *et al.*, 2018), as the canonical TNLs are missing and EDS1 components are most prominent for TNL signaling responses. With the *H. vulgare eds1 pad4* mutants and additional mutants in rice (Fernandes *et al.*, unpublished), future experiments will be enabled, comparing not only the *A. thaliana* and *N. benthamiana* immune systems, but extending research on Monocots. Using protoplasts assays, which are well established for barley and wheat (Saur *et al.*, 2019b), it could be tested if *HvTIR* and *OsTIR* are able to induce cell death in Monocot systems. In addition to *eds1 pad4* mutants in barley, during my PhD studies I also generated constructs targeting the *HvTIR* locus in barley and rice *tir-only* mutants were obtained from a company (BIOGLE GeneTech, China). As Monocots contain only conserved TIR-onlys and TNPs, these mutants would lack potential redundancies when it comes to immune outputs of TIR-onlys. They will therefore provide a suitable system to study conserved TIR-only functions in the future.

With more and more information on TIR-catalyzed enzymatic metabolites and the specifically induced EDS1 heterodimers, it would be interesting to test TNP enzymatic activities. Additionally, solving the TNP structure would provide insights into how differential EDS1-dependency might be regulated at a molecular level. It would be tempting to assume that differential TIR-TIR interactions or catalytic products distinguish between an EDS1-dependent and EDS1-independent plant TIR. TNPs provide suitable plant-based controls for production of EDS1-bound metabolites for future experiments to potentially narrow down the search for second messengers in plant immunity.

4. Material and Methods

4.1. Material

4.1.1. Species and Proteomes

The species used for phylogenetic analyses are listed with their full names in Table 1, including the proteome versions and sources that were used for protein predictions.

Table 1: Species and proteomes used for phylogenetic analyses

Species	Genome Version	Source	downloaded
<i>Amaranthus hypochondriacus</i>	v1.0.protein_primaryTranscriptOnly	Phytozome v12	19.10.2018
<i>Amborella trichopoda</i>	AMTR1.0.pep.all	Ensembl release 58	19.10.2018
<i>Ananas comosus</i>	v3.protein_primaryTranscriptOnly	Phytozome v12	19.10.2018
<i>Arabidopsis thaliana</i>	TAIR10.protein_primaryTranscriptOnly	Phytozome v12	19.10.2018
<i>Beta vulgaris</i>	RefBeet-1.2.2.pep.all	Ensembl release 58	19.10.2018
<i>Brachypodium distachyon</i>	v3.1.protein_primaryTranscriptOnly	Phytozome v12	19.10.2018
<i>Ceratophyllum demersum</i>	NA	Yang <i>et al.</i> 2020	26.03.2020
<i>Chara braunii</i>	GCA_003427395.1_Cbr_1.0_protein	Nishiyama <i>et al.</i> 2018	26.03.2020
<i>Chlamydomonas reinhardtii</i>	v5.5.protein_primaryTranscriptOnly	Phytozome v12	19.10.2018
<i>Cinnamomum micranthum</i>	NA	Chaw <i>et al.</i> 2019	26.03.2020
<i>Coccomyxa subellipsoidea C-169</i>	v2.0.protein_primaryTranscriptOnly	Phytozome v12	19.10.2018
<i>Daucus carota</i>	v2.0.protein_primaryTranscriptOnly	Phytozome v12	19.10.2018
<i>Dunaliella salina</i>	v1.0.protein_primaryTranscriptOnly	Phytozome v12	19.10.2018
<i>Eucalyptus grandis</i>	v2.0.protein_primaryTranscriptOnly	Phytozome v12	19.10.2018
<i>Euryale ferox</i>	NA	Yang <i>et al.</i> 2020	26.03.2020
<i>Hordeum vulgare</i>	Hv_IBSC_PGSB_v2.pep.all	Ensembl release 58	19.10.2018
<i>Linum usitatissimum</i>	v1.0.protein_primaryTranscriptOnly	Phytozome v12	19.10.2018

<i>Marchantia polymorpha</i>	v3.1.protein_primaryTranscriptOnly	Phytozome v12	19.10.2018
<i>Micromonas pusilla CCMP1545</i>	v3.0.protein_primaryTranscriptOnly	Phytozome v12	19.10.2018
<i>Mimulus guttatus</i>	v2.0.protein_primaryTranscriptOnly	Phytozome v12	19.10.2018
<i>Musa acuminata</i>	v1.protein_primaryTranscriptOnly	Phytozome v12	19.10.2018
<i>Nicotiana benthamiana</i>	NA	Kourelis <i>et al.</i> 2019	22.01.2020
<i>Nymphae colorata</i>	NA	Zhang <i>et al.</i> 2019	23.01.2020
<i>Oryza sativa</i>	v7.0.protein_primaryTranscriptOnly	Phytozome v12	19.10.2018
<i>Ostreococcus lucimarinus</i>	v2.0.protein_primaryTranscriptOnly	Phytozome v12	19.10.2018
<i>Panicum hallii</i>	v2.0.protein_primaryTranscriptOnly	Phytozome v12	19.10.2018
<i>Persea americana</i>	29305-CDS-prot	Rendón-Anaya 2019	26.03.2020
<i>Phaseolus vulgaris</i>	v2.1.protein_primaryTranscriptOnly	Phytozome v12	19.10.2018
<i>Physcomitrella patens</i>	v3.3.protein_primaryTranscriptOnly	Phytozome v12	19.10.2018
<i>Picea abies</i>	1.0-HC-pep	Congenie	19.10.2018
<i>Pinus taeda</i>	v1.01.scaffolds.trimmed all.maker.proteins.highq_whole	Congenie	19.10.2018
<i>Populus trichocarpa</i>	v3.0.protein_primaryTranscriptOnly	Phytozome v12	19.10.2018
<i>Prunus persica</i>	v2.1.protein_primaryTranscriptOnly	Phytozome v12	19.10.2018
<i>Selaginella moellendorffii</i>	v1.0.protein_primaryTranscriptOnly	Phytozome v12	19.10.2018
<i>Solanum lycopersicum</i>	ITAG2.4.protein primaryTranscriptOnly	Phytozome v12	19.10.2018
<i>Sphagnum fallax</i>	v0.5.protein_primaryTranscriptOnly	Phytozome v12	19.10.2018
<i>Vitis vinifera</i>	Genoscope.12X.protein primaryTranscriptOnly	Phytozome v12	19.10.2018
<i>Volvox carteri</i>	v2.1.protein_primaryTranscriptOnly	Phytozome v12	19.10.2018
<i>Zea mays</i>	AGPv4.pep.all	Ensembl release 58	19.10.2018

4.1.2. HMMs

Hidden-Markov Models (HMMs) used for protein domain predictions in full proteomes are listed in Table 2.

Table 2: HMMs used for protein domain predictions

Domain name	HMMER accession	downloaded
C-JID	PF20160.1	27.10.2020
DUF1863	PF08937.11	22.10.2018
LRR_1	PF00560.33	20.03.2020
LRR_2	PF07723.13	20.03.2020
LRR_3	PF07725.12	20.03.2020
LRR_4	PF12799.7	20.03.2020
LRR_5	PF13306.6	20.03.2020
LRR_6	PF13516.6	20.03.2020
LRR_8	PF13855.6	20.03.2020
LRR_9	PF14580.6	20.03.2020
NB-ARC	PF00931.22	20.03.2020
SEFIR	PF08357.11	22.10.2018
TIR	PF01582.20	18.10.2018
TIR_2	PF13676.6	19.10.2018
TIR_2	PF13676.5	06.09.2018
TIR-like	PF10137.9	22.10.2018
TPR_1	PF00515.29	18.06.2020
TPR_2	PF07719.18	18.06.2020
TPR_3	PF07720.13	18.06.2020
TPR_4	PF07721.15	18.06.2020
TPR_5	PF12688.8	18.06.2020
TPR_6	PF13174.7	18.06.2020
TPR_7	PF13176.7	18.06.2020
TPR_8	PF13181.7	18.06.2020
TPR_9	PF13371.7	18.06.2020
TPR_10	PF13374.7	18.06.2020
TPR_11	PF13414.7	18.06.2020
TPR_12	PF13424.7	18.06.2020
TPR_14	PF13428.7	18.06.2020
TPR_15	PF13429.7	18.06.2020
TPR_16	PF13432.7	18.06.2020
TPR_17	PF13431.7	18.06.2020
TPR_18	PF13512.7	18.06.2020
TPR_19	PF14559.7	18.06.2020
TPR_20	PF14561.7	18.06.2020
TPR_21	PF09976.10	18.06.2020

4.1.3. Public RNAseq datasets

Publicly available RNAseq datasets used for gene expression analysis in this study are listed in Table 3.

Table 3: RNAseq datasets used in this study

SRA accession	Host species	Description
SRP055503	<i>Arabidopsis thaliana</i>	<i>Botrytis cinerea</i> infected plants sampled at 0 and 14 hpi
SRP082532	<i>Arabidopsis thaliana</i>	flg22 infiltrated plants sampled at 0, 1 and 2 hpi
SRP151348	<i>Arabidopsis thaliana</i>	<i>Pst</i> DC3000 AvrRps4 infected plants sampled at 0, 8 and 24 hpi
SRP201971	<i>Arabidopsis thaliana</i>	flg22, nlp20 or chitin infiltrated seedlings sampled at 0, 1, 6 and 24 hpi
SRP075162	<i>Arabidopsis thaliana</i>	<i>Pst</i> DC3000 D28E infected plants sampled at 0, 2, 4, 6, 8, 10 and 12 hpi
SRP170258	<i>Nicotiana benthamiana</i>	<i>Phytophthora palmivora</i> infected plants sampled at 1, 2 and 3 dpi
SRP162149	<i>Nicotiana benthamiana</i>	<i>Agrobacterium</i> XopQ infiltrated leaves sampled at 24 hpi
SRP118889	<i>Nicotiana benthamiana</i>	<i>Pseudomonas fluorescens</i> infected leaves sampled at 6 hpi
SRP111697	<i>Hordeum vulgare</i>	<i>Blumeria graminis</i> infected leaves sampled at 0, 16, 20, 24, 32 and 48 hpi
SRP194287	<i>Hordeum vulgare</i>	<i>Bipolaris sorokiniana</i> infected roots sampled at 6 dpi
SRP049444	<i>Oryza sativa</i>	<i>Magnaporthe oryzae</i> infected leaves sampled at 24 hpi
SRP165938	<i>Oryza sativa</i>	<i>Tilletia horrida</i> infected leaves sampled at 8, 12, 24, 48, 72 hpi
SRP056884	<i>Oryza sativa</i>	<i>Xanthomonas oryzae</i> infected leaves sampled at 48 hpi

4.1.4. Oligonucleotides

The oligonucleotides used for molecular cloning, mutagenesis, genotyping and CRISPR/Cas9 gRNA generation are listed in Table 4. All oligonucleotides were custom ordered from Sigma-Aldrich.

Table 4: Oligonucleotides used in this study

ID	Orientation	Purpose	Sequence 5'-3'
nDL678	fw	<i>OsTIR</i> -NoStop CDS TOPO cloning	CACCATGTCGTCCACCGGGCTTTCC
nDL763	rv	<i>OsTIR</i> -NoStop CDS TOPO cloning	TGCCAGCCTGGACATGATCATAT
nDL684	fw	<i>HvTIR</i> -NoStop CDS TOPO cloning	CACCATGGCCTCAACCGGAGTTTC
nDL762	rv	<i>HvTIR</i> -NoStop CDS TOPO cloning	TGCGAGCCTTGAAACGATCG
nOJ017	fw	<i>OsTIR</i> SDM E133A	CGAGTATTGCCTCCGCGcGCTCGCCCT CCTCGTCGAGTC
nOJ018	rv	<i>OsTIR</i> SDM E133A	GACTCGACGAGGAGGGCGAGCgCGCGG AGGCAATACTCG
nOJ015	fw	<i>HvTIR</i> SDM E128A	CGGAGTACTGCCTCTGGGcGCTCGCCA TGCTCGTGGAGTC
nOJ016	rv	<i>HvTIR</i> SDM E128A	GACTCCACGAGCATGGCGAGCgCCCAG AGGCAGTACTCCG
nOJ045	fw	<i>OsTIR</i> SDM G188R	CGAGGTCAAGAACACAGTCcGCCTCAC CTACGACACAGCC
nOJ046	rv	<i>OsTIR</i> SDM G188R	GGCTGTGTCGTAGGTGAGGCgGACTGT GTTCTTGACCTCG
nOJ043	fw	<i>HvTIR</i> SDM G183R	CGAGGCCAAGAACACCGTcGCCTCAC CTACGACTCGGCC
nOJ044	rv	<i>HvTIR</i> SDM G183R	GGCCGAGTCGTAGGTGAGGCgGACGGT GTTCTTGGCCTCG
nOJ184	fw	<i>AtTNP-I</i> NoStop CDS BP cloning	GGGGACAAGTTTGTACAAAAAGCAGG CTTCATGAAGGGAATAGAAGAAGAAGC
nOJ185	rv	<i>AtTNP-I</i> NoStop CDS BP cloning	GGGGACCACTTTGTACAAGAAAGCTGG GTATATCTTGCTTCTCATTCTGACTA
nOJ182	fw	<i>AtTNP-IIb</i> NoStop CDS BP cloning	GGGGACAAGTTTGTACAAAAAGCAGG CTTCATGGATTCTCGAGGTGACAGTTC
nOJ183	rv	<i>AtTNP-IIb</i> NoStop CDS BP cloning	GGGGACCACTTTGTACAAGAAAGCTGG GTACGGTGAAGTGTATGAATCTGA
nDL682	fw	<i>HvTNP-I</i> NoStop CDS TOPO cloning	CACCATGGAAGGGGGGAGCAAAAA
nOJ088	rv	<i>HvTNP-I</i> NoStop CDS TOPO cloning	tgcGATTTTGTCTGCGGTACCTAACC
nDL686	fw	<i>HvTNP-IIb</i> NoStop CDS TOPO cloning	CACCATGGAGCTTCAAGAGGAAAGC
nOJ093	rv	<i>HvTNP-IIb</i> NoStop CDS TOPO cloning	tgcACTAAGGTGGACGTTTGTAAAG
nOJ086	fw	<i>MpTNP-III</i> NoStop CDS TOPO cloning	caccATGGATAATGGTTCCGCATCTG
nOJ087	rv	<i>MpTNP-III</i> NoStop CDS TOPO cloning	tgcGGCGTTGTTGCGAGCCCGGACC
nOJ347	fw	<i>ZmTNP-IIa</i> NoStop CDS BP cloning	GGGGACAAGTTTGTACAAAAAGCAGG CTTCATGGCAGCCGCTAGTTCAAGTGG

nOJ348	rv	<i>ZmTNP-IIa</i> NoStop CDS BP cloning	GGGGACCACTTTGTACAAGAAAGCTGG GTAAACACGAACAGTTTGTCTAAGA
EB-390	fw	<i>ZmTNP-IIa</i> SDM E130A	CAATCCGTACGCTGTAGCGGAGATCCA AGTGTTTC
EB-391	rv	<i>ZmTNP-IIa</i> SDM E130A	CACTTGGATCTCCGCTACAGCGTACGG ATTGGCTAAGC
EB-392	fw	<i>ZmTNP-IIa</i> SDM E131A	CCGTACGCTGTAGAGGCGATCCAAGTG TTCCCTCG
EB-393	rv	<i>ZmTNP-IIa</i> SDM E131A	GAGGAACACTTGGATCGCCTCTACAGC GTACGG
nOJ380	fw	<i>ZmTNP-IIa</i> SDM G305A, K306A, T307A	CAGCTTCCGGTACAGcCgcAgCTGAGT TGTTCTTGAGTTTG
nOJ381	rv	<i>ZmTNP-IIa</i> SDM G305A, K306A, T307A	CAAACCTCAAGAACCAACTCAGcTgcGg CTGTACCGGAAGCTG
nJAD075	fw	<i>NbTNP1</i> CRISPR gRNA	attgATTTGCAATCTTGATGGTAA
nJAD076	rv	<i>NbTNP1</i> CRISPR gRNA	aaacTTACCATCAAGATTGCAAAT
nJAD077	fw	<i>NbTNP2</i> CRISPR gRNA	attgACCAATTTCTGCTGACCTGA
nJAD078	rv	<i>NbTNP2</i> CRISPR gRNA	aaacTCAGGTCAGCAGAAATTGGT
nJAD079	fw	<i>NbTNP3</i> CRISPR gRNA	attGGTGCCTTAGATGCTAATTT
nJAD080	rv	<i>NbTNP3</i> CRISPR gRNA	aaacAAATTAGCATCTAAGGCAC
nJAD081	fw	<i>NbTNP4</i> CRISPR gRNA	attgTATGTTGATATCAGGGACTT
nJAD081	rv	<i>NbTNP4</i> CRISPR gRNA	aaacAAGTCCCTGATATCAACATA
nOJ001	fw	<i>NbTNP1</i> genotyping	GGAGAGTGTTCCCATCCGAA
nOJ002	rv	<i>NbTNP1</i> genotyping	AGTGCCCTTGAGAAATGT
nOJ003	fw	<i>NbTNP2</i> genotyping	TGTTATCTCCTTGGTTCCTCAA
nOJ004	rv	<i>NbTNP2</i> genotyping	GTGGGCAACTGAGGTAGGAG
nOJ005	fw	<i>NbTNP3</i> genotyping	GCACGACGTCAAGAAACCTAT
nOJ006	rv	<i>NbTNP3</i> genotyping	TGGGCAATGTTATAACTCGC
nOJ007	fw	<i>NbTNP4</i> genotyping	TACGACAGGAGATTGCCCTT
nOJ008	rv	<i>NbTNP4</i> genotyping	GATAAGCATCCGACAACCTGG

nDL806	fw	<i>AtTIR-ONLY1</i> CRISPR gRNA	attGTTGTTTAGCTGAACTGTTT
nDL807	rv	<i>AtTIR-ONLY1</i> CRISPR gRNA	aaacAAACAGTTCAGCTAAACAA
nDL808	fw	<i>AtTIR-ONLY2</i> CRISPR gRNA	attgACATGGGTTTGGGTAAGGTA
nDL809	rv	<i>AtTIR-ONLY2</i> CRISPR gRNA	aaacTACCTTACCCAAACCCATGT
nOJ122	fw	<i>AtTIR-ONLY1</i> genotyping	TCAAGCCCATTAATCCACGAA
nOJ123	rv	<i>AtTIR-ONLY1</i> genotyping	ACCGTTACAGCGACTTTAGAAG
nOJ124	fw	<i>AtTIR-ONLY2</i> genotyping	CCTCGTCTATTCAAAACTCTTCG
nOJ125	rv	<i>AtTIR-ONLY2</i> genotyping	GAGTCCGATGGCTTGACAT
nJAD083	fw	<i>NbTIR-ONLY1</i> CRISPR gRNA #1	attgTCTCCGGCTCGGGCGACAAA
nJAD084	rv	<i>NbTIR-ONLY1</i> CRISPR gRNA #1	aaacTTTGTGCGCCGAGCCGGAGA
nJAD089	fw	<i>NbTIR-ONLY1</i> CRISPR gRNA #2	attGCTCGGGCGACAAACGGAGC
nJAD090	rv	<i>NbTIR-ONLY1</i> CRISPR gRNA #2	aaacGCTCCGTTTGTGCGCCCGAG
nJAD085	fw	<i>NbTIR-ONLY2</i> CRISPR gRNA	attGCTCCGACGACAAATCGAGC
nJAD086	rv	<i>NbTIR-ONLY2</i> CRISPR gRNA	aaacGCTCGATTTGTGTCGTCGGAG
nJAD087	fw	<i>NbTIR-ONLY3</i> CRISPR gRNA	attGAAGAGGCCAAACAAACCGT
nJAD088	rv	<i>NbTIR-ONLY3</i> CRISPR gRNA	aaacACGGTTTGTGTTGGCCTCTT
nOJ009	fw	<i>NbTIR-ONLY1</i> genotyping	CCTTTCAAAGTTTACACCAGCC
nOJ010	rv	<i>NbTIR-ONLY1</i> genotyping	TCACGATACTGAGGGGAGAA
nOJ011	fw	<i>NbTIR-ONLY2</i> genotyping	AAAGGGCCATGCAACGTTC
nOJ012	rv	<i>NbTIR-ONLY2</i> genotyping	TCCAACAATGTATTTGCCTCCT
nOJ013	fw	<i>NbTIR-ONLY3</i> genotyping	AGTCGCTGTGTTTTCTCCAC
nOJ014	rv	<i>NbTIR-ONLY3</i> genotyping	CCACTTATCAGGATATCGCTAGT

4.1.5. Vectors

The vectors used and generated in this study are listed in Table 5.

Table 5: Vectors used in this study

ID	Vector	Purpose
	pENTR-D-TOPO	empty Gateway ENTRY vector (ThermoFisher) used for TOPO recombination with amplified PCR products
red301	pDONR221	empty Gateway DONOR vector used for BP recombination with amplified PCR products
red051	pXCSG_GW_YFP	empty Gateway DESTINATION vector containing a 35S promoter used for LR recombination ENTRY/DONOR vectors
pOJ042	pENTR_OsTIR-NoStop	for further cloning
pOJ050	pENTR_OsTIR-E133A NoStop	for further cloning
pOJ059	pENTR_OsTIR-G188R-NoStop	for further cloning
pOJ041	pENTR_HvTIR-NoStop	for further cloning
pOJ049	pENTR_HvTIR-E128A - NoStop	for further cloning
pOJ058	pENTR_HvTIR-G183R-NoStop	for further cloning
	pMGE311	empty vector for stable CRISPR/Cas9 transformation of <i>Nicotiana benthamiana</i>
	pDGE347	empty vector for stable CRISPR/Cas9 transformation of <i>Arabidopsis thaliana</i>
pOJ024	pMGE311_NbTNPs	CRISPR multiplex containing gRNAs for <i>NbTNPI-4</i>
pOJ025	pMGE311_NbTIRs	CRISPR multiplex containing gRNAs for <i>NbTIR1-3</i>
pOJ056	pDGE347_AtTNPs	CRISPR multiplex containing gRNAs for <i>AtTNP-I</i> and <i>AtTNP-IIb</i>
pOJ057	pDGE347_AtTIRs	CRISPR multiplex containing gRNAs for <i>AtTIR-ONLY1</i> and <i>AtTIR-ONLY2</i>
pOJ126	pDONR_AtTNP-I-NoStop	for further cloning
pOJ125	pDONR_AtTNP-IIb-NoStop	for further cloning
pOJ101	pENTR_HvTNP-I-NoStop	for further cloning
pOJ043	pENTR_HvTNP-IIb-NoStop	for further cloning
pOJ100	pENTR_MpTNP-III-NoStop	for further cloning
pOJ190	pDONR_ZmTNP-IIa-NoStop	for further cloning
pOJ192	pDONR_ZmTNP-IIa-E130A-NoStop	for further cloning
pOJ191	pDONR_ZmTNP-IIa-E131A-NoStop	for further cloning

green212	pXCSG_YFP	for transient expression in tobacco
pHL001	pXCSG_AtRPP1-WsB_YFP	for transient expression in tobacco
pOJ208	pXCSG_AtRPP1-K293L-YFP	for transient expression in tobacco
pOJ004	pXCSG_ATR1-Emoy2_SH	for transient expression in tobacco
pOJ048	pXCSG_OsTIR_YFP	for transient expression in tobacco
pOJ054	pXCSG_OsTIR-E128A_YFP	for transient expression in tobacco
pOJ185	pXCSG_OsTIR-G183R_YFP	for transient expression in tobacco
pOJ047	pXCSG_HvTIR_YFP	for transient expression in tobacco
pOJ053	pXCSG_HvTIR-E133A_YFP	for transient expression in tobacco
pOJ184	pXCSG_HvTIR-G188R_YFP	for transient expression in tobacco
pOJ134	pXCSG_AtTNP-I_YFP	for transient expression in tobacco
pOJ133	pXCSG_AtTNP-IIb_YFP	for transient expression in tobacco
pOJ109	pXCSG_HvTNP-I_YFP	for transient expression in tobacco
pOJ094	pXCSG_HvTNP-IIb_YFP	for transient expression in tobacco
pOJ105	pXCSG_MpTNP-III_YFP	for transient expression in tobacco
pOJ196	pXCSG_ZmTNP-IIa_YFP	for transient expression in tobacco
pOJ198	pXCSG_ZmTNP-IIa-E130A_YFP	for transient expression in tobacco
pOJ197	pXCSG_ZmTNP-IIa-E131A_YFP	for transient expression in tobacco
pOJ209	pXCSG_ZmTNP-IIa-G305A-K306A-T305A_YFP	for transient expression in tobacco

4.1.6. Plant Material

The plant genotypes used in this study and their sources are listed in Table 6.

Table 6: Plant lines used in this study

Species	Genotype	Reference
<i>Arabidopsis thaliana</i>	Col-0 WT	Dangl lab
<i>Arabidopsis thaliana</i>	Col-0 <i>eds1-12</i>	(Ordon <i>et al.</i> , 2017)
<i>Arabidopsis thaliana</i>	Col-0 <i>pad4-1</i>	(Glazebrook <i>et al.</i> , 1997)
<i>Arabidopsis thaliana</i>	Col-0 <i>sag101-3</i>	(Jirage <i>et al.</i> , 1999)
<i>Arabidopsis thaliana</i>	Col-0 <i>tir-only-d1</i>	this study
<i>Arabidopsis thaliana</i>	Col-0 <i>tir-only-d2</i>	this study
<i>Nicotiana benthamiana</i>	WT	MPIPZ, Cologne
<i>Nicotiana benthamiana</i>	<i>eds1a</i>	(Ordon <i>et al.</i> , 2017)
<i>Nicotiana benthamiana</i>	<i>pad4</i>	(Ordon <i>et al.</i> , 2017)
<i>Nicotiana benthamiana</i>	<i>sag101ab</i>	(Lapin <i>et al.</i> , 2019)
<i>Nicotiana benthamiana</i>	<i>tnp-q1</i>	this study
<i>Nicotiana benthamiana</i>	<i>tnp-q2</i>	this study
<i>Nicotiana benthamiana</i>	<i>tir-only-t1</i>	this study
<i>Nicotiana benthamiana</i>	<i>tir-only-t2</i>	this study
<i>Nicotiana tabacum</i>	c.v. Samsun WT	MPIPZ, Cologne
<i>Nicotiana tabacum</i>	c.v. Samsun <i>RNAi:EDS1</i>	Dangl lab, (Duxbury <i>et al.</i> , 2020)

4.1.7. Bacterial Strains

The bacterial strains used in this study including their genotypes and sources are listed in Table 7.

Table 7: Bacterial Strains used in this study

Species	Strain	Genotype
<i>Escherichia coli</i>	DH10B	F ⁻ <i>mcrA</i> Δ(<i>mrr-hsdRMS-mcrBC</i>) Φ80 <i>lacZ</i> ΔM15 Δ <i>lacX74 deoR recA1 endA1</i> <i>ara</i> Δ139 Δ(<i>ara, leu</i>)7697 <i>galU galK</i> λ ⁻ <i>rpsL</i> (Str ^R) <i>nupG</i>
<i>Escherichia coli</i>	DH5α	F ⁻ Φ80 <i>dlacZ</i> ΔM15 Δ(<i>lacZYA-argF</i>) U169 <i>deoR</i> <i>recA1 endA1 hsdR17</i> (r _k ⁻ , m _k ⁺) <i>phoA supE44</i> λ ⁻ <i>thi-1 gyrA96 relA1</i>
<i>Agrobacterium tumefaciens</i>	GV3101	pMP90RK (Deak <i>et al.</i> , 1986)
<i>Agrobacterium tumefaciens</i>	GV3101	pMP90 (Deak <i>et al.</i> , 1986)
<i>Pseudomonas syringae</i>	DC3000	pVSP61 EV (Hinsch & Staskawicz, 1996)
<i>Pseudomonas syringae</i>	DC3000	pVSP61 AvrRps4 (Hinsch & Staskawicz, 1996)
<i>Pseudomonas syringae</i>	DC3000	pVSP61 AvrRpt2 (Hinsch & Staskawicz, 1996)
<i>Xanthomonas campestris</i>	85-10	WT (Thieme <i>et al.</i> , 2005)
<i>Xanthomonas campestris</i>	85-10	Δ <i>xopQ</i> (Adlung <i>et al.</i> , 2016)

4.1.8. Antibiotics

Antibiotics and their concentrations used for bacterial selection are listed in Table 8. Antibiotics were purchased from Duchefa.

Table 8: Antibiotic concentrations for bacterial selection

Name	Stock Concentration	Working Concentration	Solvent
Kanamycin	50 mg/ml	25 mg/l	ddH ₂ O
Ampicillin	100 mg/ml	100 mg/l	ddH ₂ O
Spectinomycin	100 mg/ml	100 mg/l	ddH ₂ O
Rifampicin	100 mg/ml	40 mg/l	DMSO
Gentamycin	15 mg/ml	25 mg/l	ddH ₂ O
Carbenicillin	50 mg/ml	100 mg/l	ddH ₂ O
Streptomycin	150 mg/ml	150 mg/l	ddH ₂ O
Gentamycin*	25 mg/ml	25 mg/l	ddH ₂ O

* concentration for *Pst* selection.

4.1.9. Antibodies

Antibodies used for immunoblot analysis and their concentrations are listed in Table 9.

Table 9: Antibody concentrations used for immunoblots

Name	Source	Dilution	Supplier	Type
α -GFP	mouse monoclonal	1:5000	Sigma-Aldrich	primary
α -mouse IgG HRP	rabbit monoclonal	1:5000	Sigma-Aldrich	secondary

4.1.10. Media

Media compositions for bacterial and fungal cultivation are listed in Table 10.

Table 10: Media composition for bacterial and fungal cultivation

Name	Application	Composition
LB	<i>E. coli</i> cultivation	Tryptone: 10.0 g/l Yeast Extract: 5.0 g/l NaCl: 5.0 g/l pH 7.0 1.5 % (w/v) agar for plates
YEB	<i>A. tumefaciens</i> cultivation	Beef Extract: 5.0 g/l Yeast Extract: 1.0 g/l Peptone: 5.0 g/l Sucrose: 5.0 g/l 1 M MgSO ₄ : 2.0 ml/l pH 7.2 1.5 % (w/v) agar for plates
NYGA	<i>Xcv</i> and <i>Pst</i> cultivation	Peptone: 5.0 g/l Yeast Extract: 3.0 g/l Glycerol: 20.0 ml/l pH 7.0 1.5 % (w/v) agar for plates
PG	<i>Botrytis cinerea</i> cultivation	Potato Extract: 4.0 g/l Glucose: 20.0 g/l pH 5.6 1.5 % (w/v) agar for plates

4.2. Methods

4.2.1. Bioinformatic Methods

4.2.1.1. Prediction of protein domains in whole plant proteomes

For the analysis of TIR domains across plant proteomes, respective predicted proteomes were downloaded from public databases, as well as publications (Table 1). Proteomes of 39 plant species were screened for TIR domains using `hmmsearch` (HMMER 3.1b2, `--incE 0.01`) (Finn *et al.*, 2011) with TIR and the TIR-related TIR_2, TIR-like, DUF1863 and SEFIR HMMs downloaded from the Pfam database (Table 2). Potential TIR sequences identified by TIR and TIR-related HMMs (overlap >20 aa) were considered redundant and removed from the analysis. LRR and TPR domains were identified similarly, with their respective HMMs, while NB-ARC domains were identified using a single HMM. For the generation of the internal TNP phylogeny, a custom TNP HMM was generated using the `hmmbuild` algorithm (HMMER 3.1b2, `NSEQ = 77`) and used in a similar fashion on the whole plant proteomes.

4.2.1.2. Alignment and phylogenetic analysis of protein domains

Predicted protein domains were aligned using the MAFFT multiple sequence alignment (MSA) algorithm (v7.407, `fftms` with up to 1000 iterations) (Katoh *et al.*, 2002). The resulting MSAs were filtered and columns containing >40 % gaps were removed using the online Wasabi MSA browser (<http://was.bi/>) and exported. The filtered MSAs were then used to build phylogenetic trees with IQ-TREE (version 1.6.12, options: `-nt AUTO -ntmax 5 -alrt 1000 -bb 1000 -bnni`) (Chernomor *et al.*, 2016; Nguyen *et al.*, 2015). The resulting trees were annotated and additional information was added using the online phylogenetic tree manager iTOL v5 (Letunic & Bork, 2021) or the R package `ggtree` (Yu, 2020).

4.2.1.3. Analysis of public RNAseq datasets

Raw RNAseq data (Table 3) were directly downloaded from the NCBI Sequence Read Archive (SRA) using `sra toolkit` (SRA Toolkit Development Team, <https://github.com/ncbi/sra-tools>; v.2.10.0). Quality of the raw data was checked by running FastQC quality controls and possibly remaining adapters were trimmed from the reads with Trimmomatic (v0.38, options: `LEADING:5 TRAILING:5 SLIDINGWINDOW:4:15 MAXINFO:50:0.8 MINLEN:36`) (Bolger *et al.*, 2014).

Reads were quantified using Salmon (v.1.4.0, --fldMean=150 --fldSD=20 for single-end data and --validateMappings --gcBias for paired-end data) (Patro *et al.*, 2017). Genome versions used for transcript quantifications are: *A. thaliana*: TAIR10; *N. benthamiana*: v1.0.1, *H. vulgare*: IBSCv2; *O. sativa*: IRGSP-1.0. To convert reads into transcript-per-million (tpm), tximport library (v1.22.0) (Soneson *et al.*, 2015) was used. Values were normalized to Z-scores to allow comparisons between species. *NLR* genes were called using NLR-Annotator (Steuernagel *et al.*, 2020), while conserved *TIR* genes were annotated based on their phylogeny.

4.2.1.4. Generation of protein sequence motifs

TIR sequence logos were generated by extracting full TIR domain sequences based on the coordinates provided by hmmsearch. Per TIR group, all domains were aligned using mafft MSAs as described above and a sequence logo of the MSA was generated using the R package “ggseqlogo” (Wagih, 2017). Sequence logos were centered around known motifs in *AtRPP1*^{WSB} and plotted showing their chemical attributes.

4.2.2. Biochemical Methods**4.2.2.1. Total leaf protein extraction**

For immunoblot analysis of transiently expressed proteins in *N. benthamiana*, four 8 mm leaf disks were harvested from infiltrated leaf areas two days after *Agrobacterium* infiltrations and immediately frozen in liquid nitrogen in tubes containing ~5 metal beads. Frozen samples were homogenized using a Qiagen TissueLyser II at 30 Hz for 30 sec. The samples were resuspended in 8 M Urea buffer (50 mM Tris-HCl pH 6.8, 2 % (w/v) SDS, 8 M urea, 2 % (w/v) b-mercaptoethanol, 5 % (v/v) glycerol, protease inhibitor cocktail (Roche), 0.004 % (w/v) Bromophenol Blue) and boiled at 95 °C for 10 min, as previously described (Ma *et al.*, 2020). After centrifugation at 13,300 rpm for 1 min, the supernatant was used for SDS-PAGE.

4.2.2.2. Protein enrichment via immunoprecipitation (IP)

To enrich proteins YFP-tagged transiently expressed in *N. tabacum* leaves, immunoprecipitation was performed. For this, four 1 cm leaf disks were cut out from infiltrated leaf areas, placed in a tube with ~5 metal beads and immediately frozen in liquid nitrogen. The frozen samples were homogenized using a Qiagen TissueLyser II at 30 Hz for 30 sec. 1.5 ml of extraction buffer (10 % (v/v) glycerol, 100 mM TRIS-HCl pH 7.5, 5 mM MgCl₂, 300 mM NaCl, 10 mM DTT, 0.5 IGEPAL® CA-630, 1 x plant protease inhibitors, 2 % (w/v) Poly(vinylpolypyrrolidone)) were added and tubes incubated on an inverting wheel at 4 °C, 50 rpm for 10 min. The dissolved samples were centrifuged at 4,500 g at 4 °C for 35 min. The supernatant was passed through Miracloth into a new tube and a 50 µl input sample was taken, mixed with 50 µl Lämmli buffer (60 mM TRIS pH 6.8, 4 % (w/v) SDS, 200 mM DTT, 20 % (w/v) glycerol, 0.2 % (w/v) bromophenol blue) and boiled at 95 °C for 10 min. The remaining sample was mixed with 20 µl GFP Trap® agarose bead slurry (Chromotek) and incubated on an inverting wheel at 4 °C, 50 rpm for 2 h. Afterwards, tubes were centrifuged at 500 g, 4 °C for 1 min to pellet the GFP trap beads. Supernatant was removed and the beads resuspended in 1 ml IP-buffer (10 % (v/v) glycerol, 100 mM TRIS-HCl pH 7.5, 5 mM MgCl₂, 300 mM NaCl, 0.5 IGEPAL® CA-630, 1 x plant protease inhibitors) and transferred to a Protein LoBind tube (Eppendorf). Beads were washed three times with IP-buffer, centrifuging at 500 g, 4 °C for 1 min each time to pellet the beads. After the last centrifugation, the supernatant was removed, 50 µl Lämmli buffer added, and the samples boiled at 95 °C for 10 min. Prior to SDS-PAGE, input and IP protein samples were centrifuged at 13,300 rpm for 1 min.

4.2.2.3. SDS PAGE

For protein separation SDS-PAGE was run using the BioRad Mini-PROTEAN system. Samples dissolved in Lämmli buffer were loaded on 1.0 mm Any kD 15-well precast gels (BioRad). Gels were run in 1x TRIS-Glycine-SDS running buffer (250 mM TRIS, 1.92 M Glycine, 1 % (w/v) SDS) at 200 V for 30 min. Empty wells were loaded with Lämmli buffer to ensure equal running and PageRuler Prestained Protein Ladder (ThermoFisher) was used as size standard.

4.2.2.4. Immunoblot Analysis

After SDS-PAGE, separated proteins were transferred onto a BioRad 0.2 µm nitrocellulose membrane using the BioRad Mini Trans-Blot system. Gels were stacked onto the membrane and submerged into 1x transfer buffer (25 mM TRIS, 192 mM glycine, 0.1 % (w/v) SDS, 20 % (v/v) methanol). The transfer was carried out at 110 V for 70 min at 4°C. After transfer, membranes were blocked with 5 % (w/v) milk powder dissolved in TBS-T buffer (10 mM TRIS, 150 mM NaCl, 0.05 % (v/v) Tween-20, pH 7.5) at 4 °C overnight. Blocked membranes were then incubated in primary antibody solution containing 3 % (w/v) milk powder dissolved in TBS-T for 1 h at room temperature (concentrations indicated in Table 9). Afterwards, membranes were washed three times with TBS-T at room temperature, before adding the secondary antibody solution (Table 9), which also contained 3 % milk powder in TBS-T. After incubation for 1 h, the membranes were washed again three times using TBS-T. For detection of HRP-labeled antibodies, membranes were covered in ~100 µl Clarity™ Western ECL Substrate (BioRad). Chemiluminescence was detected using a BioRad ChemiDoc™ XRS+ detection system.

4.2.3. Molecular Biological Methods

4.2.3.1. Plant RNA extraction and cDNA synthesis

For cloning of CDS into vectors for further cloning, total RNA was extracted from 1-2 week-old rice and barley plants, as well as 4 week-old *A. thaliana* and *M. polymorpha* plants. RNA was extracted using the Bio-Budget Plant RNA Kit, following the manufacturer's instructions. Extracted RNA was dissolved in 30 μ l ddH₂O. The resulting RNA concentration was measured using a NanoDrop 1000 (ThermoFisher) photo spectrometer. To remove potential DNA contaminations, 1 μ g of RNA was incubated with DNase I (ThermoFisher) at 37 °C for 1 h, the reaction mix is listed in Table 11. After incubation, DNase was deactivated by adding 1 μ l 50 mM EDTA and incubation at 65 °C for 10 min. The DNase-treated RNA was used for reverse transcription with the RevertAid H Minus cDNA synthesis Kit (ThermoFisher), components of the reaction mix are listed in Table 12. The reaction mix was incubated at 42 °C for 60 min, followed by an inactivation step at 70 °C for 10 min. The resulting cDNA was stored at -20 °C until further use for PCR amplification of CDS for TOPO and BP cloning.

Table 11: DNase I Reaction Mix.

Component	Volume
RNA (200 ng/ μ l)	5.0 μ l
DNase I (1 U/ μ l)	1.0 μ l
DNase I buffer (10x)	1.0 μ l
RiboLock	0.25 μ l
ddH ₂ O	to 10.0 μ l

Table 12: Reverse Transcriptase Reaction Mix.

Component	Volume
DNase-treated RNA	10.0 μ l
Oligo dT ₁₈ (100 nM)	1.0 μ l
RevertAid™ H Minus buffer (5x)	4.0 μ l
RiboLock	0.5 μ l
dNTPs (10 mM)	2.0 μ l
RevertAid™ H Minus RT	1.0 μ l
ddH ₂ O	to 20.0 μ l

4.2.3.2. Polymerase Chain Reaction (PCR)

For plant genotyping purposes, the non-proofreading Phire HS II DNA Polymerase (ThermoFisher) was used, with the reaction mix and PCR program indicated in Table 13 and Table 14. For cloning, proofreading polymerases Phusion (NEB) and PrimeStar II HS (Takara Bio) were used. The standard cloning PCR mix for both polymerases is described in Table 15, the standard PCR program shown in Table 16.

Table 13: Plant Genotyping PCR Reaction Mix.

Component	Volume
Phire Green buffer (5x)	4.0 μ l
dNTPs (2.5 μ M)	0.4 μ l
Primer fw (10 μ M)	1.0 μ l
Primer rv (10 μ M)	1.0 μ l
Phire HS II Polymerase	0.2 μ l
gDNA (from Sucrose extraction)	1.0 μ l
ddH ₂ O	to 20.0 μ l

Table 14: Plant Genotyping PCR Program.

Step	Temperature	Time	Cycles
Initiation	98 °C	30 sec	1x
Denaturation	98 °C	10 sec	35x
Annealing	60 °C	15 sec	35x
Elongation	72 °C	15 sec/kb	35x
Final Elongation	72 °C	5 min	1x

Table 15: Standard PCR Reaction Mix.

Component	Volume
Phire Green buffer (5x)	4.0 μ l
dNTPs (2.5 μ M)	0.4 μ l
Primer fw (10 μ M)	1.0 μ l
Primer rv (10 μ M)	1.0 μ l
Phire HS II Polymerase	0.2 μ l
gDNA (from Sucrose extraction)	1.0 μ l
ddH ₂ O	to 20.0 μ l

Table 16: Standard PCR Program.

Step	Temperature	Time	Cycles
Initiation	98 °C	30 sec	1x
Denaturation	98 °C	10 sec	35x
Annealing	60 °C	15 sec	35x
Elongation	72 °C	15 sec/kb	35x
Final Elongation	72 °C	5 min	1x

4.2.3.3. Agarose Gel Electrophoresis

For visualization of PCR products and vector digests, DNA was mixed with 6x DNA loading dye (40 % (w/v) sucrose, 0.5 % (w/v) Orange G) and loaded on a 1 % (w/v) agarose gel in TAE buffer (40 mM TRIS, 20 mM acetic acid, 1 mM EDTA, pH 8.5) supplied with 0.2 mg/l ethidium bromide. Electrophoresis was performed at 120-140 V for 30-45 min and bands visualized using a UV trans-illuminator (Intas).

4.2.3.4. DNA purification from Agarose Gels

After agarose gel electrophoresis, confirmed DNA bands were cut from the gel and the DNA purified from the gel pieces using the NucleoSpin® Gel and PCR Clean-up kit (Macherey-Nagel), following the manufacturer's instructions. Instead of the supplied TE buffer, DNA was dissolved in 15-30 µl ddH₂O and stored at -20 °C until further use.

4.2.3.5. Generation of Gateway expression vectors

All plant expression vectors used in this thesis were generated using the Gateway cloning system supplied by ThermoFisher Scientific. *TNP* and *TIR-ONLY* coding sequences (CDS) without Stop codons were amplified from cDNA (*A. thaliana* Col-0, *O. sativa* cv. Kitaake, *H. vulgare* cv. Golden Promise, *M. polymorpha* Tak1) using oligonucleotides (custom oligos ordered from Sigma-Aldrich) with TOPO (fw: 5'-CACC-3') or BP *attB* (fw: 5'-GGGGACAAGTTTGTACAAAAAAGCAGGCTTCATG-3', rv: 5'-GGGGACCACTTTGTACAAGAAAGCTGGGTA-3') overhangs for the generation of pENTR-D-TOPO or pDONR221 based vectors, respectively (Table 5). The *ZmTNP-IIa* CDS was synthesized (TWIST Bioscience) with codon-optimization for *N. benthamiana* (Johannndrees *et al.*, 2021). All CDS were amplified using proof-reading polymerases Phusion (NEB) or PrimeStar HS (Takara Bio). After PCRs were confirmed on agarose gels, the PCR products were cleaned up and used for TOPO or BP reaction, following the manufacturer's protocol. Reaction mixes are listed in Table 17 and Table 18, respectively. TOPO reactions were incubated for 10 min, BP reactions for 1 h at room temperature, respectively. Reaction mixes were used for transformation of competent *E. coli* (DH10B or DH5α) and subsequently confirmed via enzyme digests and Sanger sequencing. Recombination of the CDS into the pXCSG_GW_YFP expression vector was performed by LR reactions, the reaction mix is described in Table 19. Expression vectors containing *AtRPP1*^{Wsb} and *ATR1*^{Emoy2} were previously published (Ma *et al.*, 2020).

Table 17: TOPO Reaction Mix.

Component	Volume
pENTR™/D-TOPO	0.5 µl
TOPO-PCR product	0.5 µl
salt solution	1.0 µl
ddH ₂ O	to 6.0 µl

Table 18: BP Reaction Mix.

Component	Volume/Amount
<i>attB</i> -PCR product	10-100 ng
pDONR221	50 ng
TE buffer	to 4.0 µl
BP Clonase™ Enzyme mix II	1.0 µl

Table 19: LR Reaction Mix.

Component	Volume/Amount
entry vector	50 ng
destination vector	50 ng
TE buffer	1.5 µl
LR Clonase™ Enzyme mix II	0.5 µl
ddH ₂ O	to 4.0 µl

4.2.3.6. Plasmid isolation and restriction enzyme digests

Generated vectors were isolated from *E. coli* strains DH10B and DH5 α using the NucleoSpin Plasmid kit (Macherey-Nagel), following the manufacturer’s instructions, with the exception that isolated plasmids were dissolved in 50 μ l ddH₂O instead of the provided TE buffer. Resulting DNA concentrations were measured using a NanoDrop 1000 photo spectrometer (ThermoFisher) and plasmids were stored at -20 °C. Isolated plasmids were digested using restriction enzymes (NEB) with the supplied buffers, the standard digestion mix is described in Table 20. Mixes were incubated at 37 °C for 1 h, before running on an agarose gel and checking correct DNA fragment sizes.

Table 20: Plasmid restriction digest Reaction Mix.

Component	Volume
Plasmid DNA	200-500 ng
Buffer (10x)	1.0 μ l
Restriction enzyme	0.3 μ l
ddH ₂ O	to 10.0 μ l

4.2.3.7. Sanger Sequencing

Sequencing of vectors and plant genotyping PCR products was carried out by Eurofins Genomics using the Mix2Seq Kit, following the manufacturer’s instructions.

4.2.3.8. Site-directed mutagenesis (SDM)

For specific mutations within the CDS of *TIR* genes, site-directed mutagenesis (SDM) was employed. Entry or expression vectors served as templates and a PCR was carried out using altered oligonucleotides, containing the desired mutations (Table 4). For this, the proof-reading polymerases Phusion (NEB) or PrimeStar HS (Takara Bio) were used, reaction mix, and PCR program are listed in Table 21 and Table 22, respectively. Template DNA was digested by adding 1 μ l of DpnI restriction enzyme (NEB) to the PCR mixes and incubation at 37 °C for 3 h. 5 μ l of the digested reaction mix were used for *E. coli* (DH10B or DH5 α) transformation, correct mutations were checked by Sanger sequencing.

Table 21: SDM PCR Reaction Mix.

Component	Volume
Buffer (5x)	4.0 μ l
dNTPs (2.5 μ M)	1.6 μ l
Primer fw (10 μ M)	1.0 μ l
Primer rv (10 μ M)	1.0 μ l
Polymerase	0.3 μ l
Plasmid to mutate	10 ng
ddH ₂ O	to 40.0 μ l

Table 22: SDM PCR Program.

Step	Temperature	Time	Cycles
Initiation	98 °C	1 min	1x
Denaturation	98 °C	10 sec	20x
Annealing	55 °C (1 °C/s ramp)	15 sec	20x
Elongation	72 °C	1 min/kb	20x
Final Elongation	72 °C	15 min	1x

4.2.3.9. Generation of Golden Gate CRISPR/Cas9 vectors

Guide RNAs (gRNAs) for CRISPR/Cas9 mutagenesis were designed using the online gRNA prediction tool CRISPR-P 2.0 (<http://crispr.hzau.edu.cn/CRISPR2/>) using *TNP* and *TIR-ONLY* CDS from *A. thaliana* and *N. benthamiana* as input. Potential gRNA candidates with high predicted efficiencies were then manually blasted against the reference genomes to check for possible off-targets. Only gRNAs without off-target hits were selected and ordered as oligonucleotides (from Sigma-Aldrich) with (fw: 5'-ATTG-3', rv: 5'-AAAC-3') overhangs for Golden Gate cloning (Table 4). The two complement gRNA oligos were hybridized at a concentration of 10 μ M for each oligo using a thermal cycler (Eppendorf Mastercycler), the hybridization temperature program is described in Table 23. Hybridized oligonucleotides were then diluted 1:200 (final concentration 50 fmol/ μ l) and used for Golden Gate integration into gRNA “shuttle vectors” (Ordon *et al.*, 2020; Ordon *et al.*, 2017), the reaction mix and cut/ligation program are described in Table 24 and Table

25, respectively. After Golden Gate cloning, 2.5 μ l of the reaction mix were used for transformation of *E. coli*, which were incubated in 4 ml of restrictive LB medium overnight at 37 °C in a shaking incubator, without plating out. Polyclonal plasmids were extracted the next day by miniprep and directly used for Golden Gate recombination with the multiplex gRNA constructs (vectors listed in Table 5), the reaction mix and cut/ligation program are shown in Table 26 and Table 27, respectively. Again, 2.5 μ l of the reaction mix were used for transformation of *E. coli*, this time plating out the regenerated bacteria on selective plates and incubation overnight at 37 °C. The resulting multiplex vectors were transformed into *Agrobacterium* GV3101 (pMP90) strains and used for plant transformation.

Table 23: gRNA Oligonucleotide Hybridization Program.

Temperature	Duration
95 °C	5 min
90 °C	2 min
85 °C	2 min
...	2 min
20 °C	2 min
15 °C	2 min
4 °C	15 min

Table 24: gRNA Shuttle Vector Golden Gate Reaction Mix.

Component	Volume
gRNA shuttle vector	60 ng
Hybridized gRNA oligo pair (50 fmol/ μ l)	1.0 μ l
Ligation buffer (10x)	1.0 μ l
BSA (1 mg/ml)	1.0 μ l
BpiI (ThermoFisher)	0.5 μ l
T4 Ligase (NEB, 1 U/ μ l)	0.5 μ l
ddH ₂ O	to 10.0 μ l

Table 25: gRNA Shuttle Vector cut/ligation Program.

Step	Temperature	Time	Cycles
Cut	37 °C	2 min	10x
Ligation	16 °C	5 min	10x
Inactivation (T4)	50 °C	10 min	1x
Inactivation (BpiI)	80 °C	10 min	1x

Table 26: CRISPR Multiplex Vector Golden Gate Reaction Mix.

Component	Volume
Recipient multiplex vector	320 ng
Each gRNA shuttle vector	40 ng
Ligation buffer (10x)	2.0 µl
BSA (1 mg/ml)	2.0 µl
Eco3II (ThermoFisher)	1.0 µl
T4 Ligase (NEB, 30 U/µl)	1.0 µl
ddH ₂ O	to 20.0 µl

Table 27: CRISPR Multiplex Vector cut/ligation Program.

Step	Temperature	Time	Cycles
Cut	37 °C	2 min	30x
Ligation	16 °C	5 min	30x
Inactivation (T4)	50 °C	10 min	1x
Inactivation (BpiI)	80 °C	10 in	1x

4.2.3.10. *In silico* Sequence Generation

Vector maps for TOPO, LR and BP reactions were generated using SeqBuilder Pro 15 (DNASTAR). SeqBuilder Pro 15 was also used to plan enzymatic restriction digests. Sanger sequencing reads were aligned to the *in silico* generated sequences and checked for correctness using SeqMan Pro 15 (DNASTAR).

4.2.4. Bacterial Methods

4.2.4.1. *E. coli* Cultivation and Transformation

E. coli strains DH10B and DH5 α were grown at 37 °C in LB liquid medium or on plates supplied with antibiotics (Table 8) to ensure maintenance of desired plasmids. For transformation of chemically competent *E. coli*, 50 μ l of bacterial cells were thawed on ice and 1-10 μ l plasmid or reaction mix was added, incubating for 30 min on ice. To perform heat-shock transformation, tubes were then placed into a water bath at 42 °C for 45 sec and immediately placed on ice afterwards. Then, 800 μ l LB medium was added to the transformed cells and bacteria were regenerated at 37 °C shaking for 1 h. After regeneration, bacteria were pelleted at 11,000 rpm for 30 sec and resuspended in ~100 μ l LB to be plated onto LB plates containing antibiotics for plasmid selection. Plates were incubated at 37 °C overnight until colonies were visible and used for inoculation of liquid cultures.

4.2.4.2. *A. tumefaciens* Cultivation and Transformation

Agrobacterium was grown in liquid YEB medium or on plates containing Rifampicin, Gentamycin, and the respective antibiotics (Table 8) for plasmid maintenance. Transformation of competent *Agrobacterium* cells was performed by electroporation. For this, 50 μ l of cell suspension was thawed on ice and 0.5 μ l of desired plasmid was added. The mixture was incubated on ice for 10 min before being transferred into an electroporation cuvette (2 mm gap, cell projects). Electroporation was carried out using a BioRad Gene Pulser Xcell with the *Agrobacterium* pre-set. After pulsing, 800 μ l of YEB medium were added to the cuvette and cells transferred into a new tube and incubated on a shaking incubator at 28 °C, 600 rpm for 2 h. Afterwards, 50 μ l of the regenerated *Agrobacterium* cultures were plated onto YEB plates containing respective antibiotics and incubated at 28 °C for 2 days until colonies were visible.

4.2.4.3. *Xcv* Cultivation

Xanthomonas campestris pv. *vesicatoria* 85.10 strains were grown in liquid NYGA medium or NYGA plates supplied with Rifampicin. Plates were incubated at 28 °C until densely covered in bacteria. Liquid cultures were started from these plates and incubated at 28 °C in a shaking incubator at 200 rpm overnight prior to infection experiments.

4.2.4.4. *Pst* Cultivation

Pseudomonas syringae pv. *tomato* (*Pst*) DC3000 strains were grown in liquid NYGA medium or on NYGA plates supplied with Rifampicin and Kanamycin to select for *Pst* DC3000 and the pVSP61 vectors, respectively. Plates were incubated at 28 °C until densely covered in bacteria. Liquid cultures were started from these plates and incubated at 28 °C in a shaking incubator at 200 rpm overnight prior to infection experiments.

4.2.5. Plant Methods

4.2.5.1. Plant Cultivation

For immune assays, *A. thaliana* seeds were sown on moist soil fertilized with 10 mg/l Confidor WG70 (Bayer) and covered with a plastic lid. Trays were placed into a growth chamber with 10 h light, 14 h dark, ~150 $\mu\text{mol/m/s}$, 22 °C, 65 % humidity growing conditions. *A. thaliana* seeds intended for plant propagation were grown in “speed breeding” chambers with 22 h light, 2 h dark, ~150 $\mu\text{mol/m/s}$, 22 °C, 65 % humidity growing conditions. Lids were removed ~5 days after placing the trays into the growth chambers. When plants were setting seeds, irrigation was stopped, and plants wrapped in paper bags until dried completely and seeds were harvested.

N. benthamiana and *N. tabacum* plants were grown in a greenhouse compartment with 16 h light, 8 h dark, growing conditions. Four- to five-week-old plants were used for the immune assays. Plants for seed production were further grown until seed pods were completely dry and harvested off the plant for seed collection.

4.2.5.2. Stable Transformation of *A. thaliana* (Floral Dip)

For stable transformation of *A. thaliana* plants, the floral dip method was used (Clough & Bent, 1998; Logemann *et al.*, 2006). Flowering plants grown under “speed breeding” conditions were cut to remove the inflorescence once, allowing them to re-grow for higher flower numbers. Approximately 5-week-old flowering plants were used for transformation. For this, an *Agrobacterium* solution containing 5 % sucrose, 0.01 % Silwet L-77 and *Agrobacterium* carrying the desired vector for transformation at an OD₆₀₀ of 1.5 was generated and put into a small autoclave bag. Inflorescences were submerged in the *Agrobacterium* solution for ~45 sec and dried off on a paper towel to remove excess bacteria. The plants were then covered with plastic bags and put in the dark for 1 day, before the plastic bags were removed and the plants were placed back into the “speed breeding” chambers until setting seeds.

4.2.5.3. Stable Transformation of *N. benthamiana*

Stable transformation of *N. benthamiana* was performed as previously described in (Ordon, 2019) ([dx.doi.org/10.17504/protocols.io.sbaeiaie](https://doi.org/10.17504/protocols.io.sbaeiaie)). *Agrobacterium* strains carrying the desired CRISPR constructs were grown in liquid YEB medium at 28 °C in a shaking incubator until cultures were densely grown. 100 ml induction medium (YEB medium with 20 µM Acetosyringone) were inoculated with 1 ml of the pre-culture and incubated at 28 °C shaking at 200 rpm overnight. 40 ml of the culture were pelleted at 4,000 rpm for 20 min and the pellet resuspended in 20 ml MMA medium (1x MS salts (+MES), 20 g/l sucrose, pH 5.7) without antibiotics. The optical density (OD₆₀₀) was measured and adjusted to 0.8 in a total of 50 ml MMA medium. Six fully expanded leaves from four-to-five-week-old *N. benthamiana* plants were harvested and the middle vein removed using a razor blade. Leaf halves were sterilized in a 1.2 % (v/v) NaOCl, 0.01 % (v/v) Tween-20 solution for 30 sec until washed twice in sterile ddH₂O, 0.01 % (v/v) Tween-20. Leaves were cut into small (~1x1 cm) pieces, placed in a sterile petri dish, covered in *Agrobacterium* solution, and incubated for 30 min. Then, leaves were transferred onto Whatman paper wetted with sterile ddH₂O in a square petri dish, which was sealed with 3M Micropore tape, covered in aluminum foil, and incubated in the light culture room for 2 days. Afterwards, leaf cuts were transferred into sterilizing solution (ddH₂O, 250 mg/l Cefotaxime, 100 mg/l Kanamycin), dried on Whatman paper and transferred onto MS-II plates (1x MS salts, 1.0 mg/l 6-Benzylaminopurine, 0.1 mg/l Naphthalene acetic acid, 200 mg/l Cefotaxime, 100 mg/l Kanamycin). Plates were sealed with 3M Micropore tape and incubated in the light culture room for 5-6 weeks. After plantlets developed on the MS-II plates, they were cut off using a razor blade and transferred onto MS-III medium (1x MS salts, 200 mg/l Cefotaxime, 100 mg/l Kanamycin) in “Weck” jars to allow horizontal growth and rooting of the plantlets. Jars were placed in the light culture room for 1-3 weeks until roots appeared. Plantlets were transferred into pots and placed in the greenhouse until setting seeds. Presence of the Cas9 constructs was tested via CNL assay (Stuttman *et al.*, 2021) and PCRs.

4.2.5.4. Plant Genomic DNA Extraction for Genotyping

For crude large-scale plant genotyping, *A. thaliana* and *N. benthamiana* genomic DNA was extracted using the sucrose method as previously described (Berendzen *et al.*, 2005). A small amount of leaf tissue was placed into a collection tube (Qiagen) with a metal bead inside. To this, 200 μ l of Sucrose solution (50 mM TRIS-HCl pH 7.5, 300 mM NaCl, 300 mM sucrose) were added and samples were homogenized using a TissueLyser II (Qiagen). Tubes were then centrifuged at 1,000 rpm for 1 min, their lids removed, and the tubes placed into a water bath at 97 °C and incubated for 15 min. After boiling, the samples were immediately placed on ice for at least 30 min before being used for genotyping PCRs. Samples were stored at 4 °C when not used directly after DNA extraction.

4.2.5.5. Transient protein expression in tobacco plants

Agrobacterium strains transformed with the desired vectors were grown on YEB plates containing respective antibiotics (Table 8) overnight at 28 °C. Bacteria were collected from plates by adding 3 ml infiltration solution (10 mM MgCl₂, 10 mM MES/KOH pH 5.6, 150 nM Acetosyringone) in which they were resuspended. The optical density (OD₆₀₀) was measured using a photo spectrometer (BioPhotometer, Eppendorf) and adjusted to an OD₆₀₀ of 0.5 per strain in each mix. For *N. benthamiana* infiltrations, an *Agrobacterium* strain expressing the viral DNA silencing repressor P90 was added at an OD₆₀₀ of 0.2, which was omitted for *N. tabacum* infiltrations, since it causes autoimmunity. *N. benthamiana* and *N. tabacum* leaves were infiltrated using a needleless syringe, the infiltrated leaf area was marked with a permanent marker.

4.2.5.6. Ion leakage assay

Three days after infiltration with *Agrobacterium*, six 8 mm disks were cut out from infiltrated *N. benthamiana* leaf areas using a cork borer. Leaf disks were washed in ~10 ml ddH₂O for 30 min on a rotating plate at room temperature. After washing, the leaf disks were individually transferred to 24-well plates containing 1 ml ddH₂O per well. Conductivity of the water in each well was measured directly after transfer and after 6 h of incubation at room temperature using a Horiba Twin ModelB-173 conductometer.

4.2.5.7. *Xcv* infection assay in *N. benthamiana*

Xanthomonas campestris pv. *vesicatoria* (*Xcv*) was grown on NYGA plates supplied with Rifampicin until densely covered in bacteria. From those plates, liquid cultures were started and incubated overnight at 28 °C, 200 rpm in a shaking incubator. Cultures were centrifuged at 4,000 rpm for 2 min, the pellet was resuspended in 10 mM MgCl₂ and the optical density (OD₆₀₀) was measured using a photo spectrometer (BioPhotometer, Eppendorf). Cultures were diluted to an OD₆₀₀ of 0.0005 and incubated in the dark for 1 h. *N. benthamiana* leaves were infiltrated using a needleless syringe, infiltration spots were labeled using a permanent marker. After allowing the leaves to dry, one 8 mm leaf disk was harvested per *Xcv* – *N. benthamiana* genotype combination, placed into a tube containing 1 ml 0.001 % Silwet L-77 in ddH₂O and incubated on a shaking incubator at 28 °C, 300 rpm for 1 h. For each leaf disk, 10 µl undiluted bacterial suspension were plated onto NYGA plates containing Rifampicin. Plates were incubated for 2 days at 28 °C when colonies were visible and colony-forming units (CFUs) calculated. Infiltrated plants were placed in a long-day chamber at 25 °C for 6 days and three 8 mm leaf disks sampled per treatment at 3 and 6 days. CFUs were determined as before, including dilutions.

4.2.5.8. *Botrytis* growth assay in *N. benthamiana*

Botrytis cinerea strain B05.10 was grown on PG plates for 20 days before harvesting spores. Spores were diluted to a concentration of 5x10⁵ conidiospores/ml in PG liquid medium. Four- to five-week-old *N. benthamiana* leaves were drop-inoculated by pipetting 10 µl of the spore suspension on each side of the middle vein. Infected leaves were incubated for 48 hours in the dark at room temperature, ensuring high humidity in the closed trays. Lesion areas were measured by using ImageJ (Schindelin *et al.*, 2012) tools on photographs of the infected leaf areas.

4.2.5.9. *Pst* growth assay in *A. thaliana*

Pseudomonas syringae pv. *tomato* (*Pst*) DC3000 was grown on NYGA plates supplied with Rifampicin and antibiotics for plasmid selection until densely covered in bacteria. Liquid cultures were started from those plates and incubated overnight at 28 °C, 200 rpm in a shaking incubator. Cultures were centrifuged at 4,000 rpm for 2 min, the pellet was resuspended in 1 mM MgCl₂ and the optical density (OD₆₀₀) was measured using a photo spectrometer (BioPhotometer, Eppendorf). Cultures were diluted to an OD₆₀₀ of 0.0005 and incubated in the dark for 1 h. *A. thaliana* leaves were infiltrated using a needleless syringe, using two infiltration spots to fill the entire leaf. Infiltrated leaves were marked using a permanent marker. Infiltrated plants were placed in a growth chamber at 25 °C for three days. Six 4 mm leaf disks were taken per *Pst* – *A. thaliana* genotype combination and two leaf disks placed into a single tube containing 1 ml 0.001 % (v/v) Silwet L-77 in ddH₂O and incubated on a shaking incubator at 28 °C, 300 rpm for 1 h. Bacterial dilutions were plated onto NYGA plates with Rifampicin and respective antibiotic and incubated at 28 °C for two days. Colonies were counted and colony-forming units (CFUs) calculated.

5. References

- Adachi, H., Kamoun, S., & Maqbool, A. (2019). A resistosome-activated 'death switch'. *Nat Plants*, 5(5), 457-458. doi:10.1038/s41477-019-0425-9
- Adlung, N., Prochaska, H., Thieme, S., Banik, A., Blüher, D., John, P., . . . Bonas, U. (2016). Non-host Resistance Induced by the Xanthomonas Effector XopQ Is Widespread within the Genus Nicotiana and Functionally Depends on EDS1. *Frontiers in Plant Science*, 7, 1796. Retrieved from <https://www.frontiersin.org/article/10.3389/fpls.2016.01796>
- Albert, I., Bohm, H., Albert, M., Feiler, C. E., Imkampe, J., Wallmeroth, N., . . . Nurnberger, T. (2015). An RLP23-SOBIR1-BAK1 complex mediates NLP-triggered immunity. *Nat Plants*, 1, 15140. doi:10.1038/nplants.2015.140
- Anderson, K. V., Bokla, L., & Nusslein-Volhard, C. (1985). Establishment of dorsal-ventral polarity in the Drosophila embryo: the induction of polarity by the Toll gene product. *Cell*, 42(3), 791-798. doi:10.1016/0092-8674(85)90275-2
- Axtell, M. J., & Staskawicz, B. J. (2003). Initiation of RPS2-specified disease resistance in Arabidopsis is coupled to the AvrRpt2-directed elimination of RIN4. *Cell*, 112(3), 369-377. doi:10.1016/s0092-8674(03)00036-9
- Baggs, E. L., Monroe, J. G., Thanki, A. S., O'Grady, R., Schudoma, C., Haerty, W., & Krasileva, K. V. (2020). Convergent Loss of an EDS1/PAD4 Signaling Pathway in Several Plant Lineages Reveals Coevolved Components of Plant Immunity and Drought Response[OPEN]. *The Plant Cell*, 32(7), 2158-2177. doi:10.1105/tpc.19.00903
- Baggs, E. L., Tiersma, M. B., Abramson, B. W., Michael, T. P., & Krasileva, K. V. (2022). Characterization of defense responses against bacterial pathogens in duckweeds lacking EDS1. *New Phytol.* doi:10.1111/nph.18453
- Bayless, A. M., & Nishimura, M. T. (2020). Enzymatic Functions for Toll/Interleukin-1 Receptor Domain Proteins in the Plant Immune System. *Frontiers in Genetics*, 11, 539. Retrieved from <https://www.frontiersin.org/article/10.3389/fgene.2020.00539>
- Berendzen, K., Searle, I., Ravenscroft, D., Koncz, C., Batschauer, A., Coupland, G., . . . Ulker, B. (2005). A rapid and versatile combined DNA/RNA extraction protocol and its application to the analysis of a novel DNA marker set polymorphic between Arabidopsis thaliana ecotypes Col-0 and Landsberg erecta. *Plant Methods*, 1(1), 4. doi:10.1186/1746-4811-1-4
- Bernoux, M., Ve, T., Williams, S., Warren, C., Hatters, D., Valkov, E., . . . Dodds, P. N. (2011). Structural and functional analysis of a plant resistance protein TIR domain reveals interfaces for self-association, signaling, and autoregulation. *Cell Host Microbe*, 9(3), 200-211. doi:10.1016/j.chom.2011.02.009
- Bhandari, D. D., Lapin, D., Kracher, B., von Born, P., Bautor, J., Niefind, K., & Parker, J. E. (2019). An EDS1 heterodimer signalling surface enforces timely reprogramming of immunity genes in Arabidopsis. *Nat Commun*, 10(1), 772. doi:10.1038/s41467-019-08783-0
- Bi, G., Su, M., Li, N., Liang, Y., Dang, S., Xu, J., . . . Zhou, J. M. (2021). The ZAR1 resistosome is a calcium-permeable channel triggering plant immune signaling. *Cell*, 184(13), 3528-3541 e3512. doi:10.1016/j.cell.2021.05.003
- Bolger, A. M., Lohse, M., & Usadel, B. (2014). Trimmomatic: a flexible trimmer for Illumina sequence data. *Bioinformatics*, 30(15), 2114-2120. doi:10.1093/bioinformatics/btu170

- Bonardi, V., Tang, S., Stallmann, A., Roberts, M., Cherkis, K., & Dangl, J. L. (2011). Expanded functions for a family of plant intracellular immune receptors beyond specific recognition of pathogen effectors. *Proc Natl Acad Sci U S A*, *108*(39), 16463-16468. doi:10.1073/pnas.1113726108
- Castel, B., Ngou, P. M., Cevik, V., Redkar, A., Kim, D. S., Yang, Y., . . . Jones, J. D. G. (2019). Diverse NLR immune receptors activate defence via the RPW8-NLR NRG1. *New Phytol*, *222*(2), 966-980. doi:10.1111/nph.15659
- Chaw, S. M., Liu, Y. C., Wu, Y. W., Wang, H. Y., Lin, C. I., Wu, C. S., . . . Tsai, I. J. (2019). Stout camphor tree genome fills gaps in understanding of flowering plant genome evolution. *Nat Plants*, *5*(1), 63-73. doi:10.1038/s41477-018-0337-0
- Chen, G., Wei, B., Li, G., Gong, C., Fan, R., & Zhang, X. (2018). TaEDS1 genes positively regulate resistance to powdery mildew in wheat. *Plant Mol Biol*, *96*(6), 607-625. doi:10.1007/s11103-018-0718-9
- Chernomor, O., von Haeseler, A., & Minh, B. Q. (2016). Terrace Aware Data Structure for Phylogenomic Inference from Supermatrices. *Syst Biol*, *65*(6), 997-1008. doi:10.1093/sysbio/syw037
- Cirl, C., Wieser, A., Yadav, M., Duerr, S., Schubert, S., Fischer, H., . . . Miethke, T. (2008). Subversion of Toll-like receptor signaling by a unique family of bacterial Toll/interleukin-1 receptor domain-containing proteins. *Nat Med*, *14*(4), 399-406. doi:10.1038/nm1734
- Clabbers, M. T. B., Holmes, S., Muusse, T. W., Vajjhala, P. R., Thygesen, S. J., Malde, A. K., . . . Ve, T. (2021). MyD88 TIR domain higher-order assembly interactions revealed by microcrystal electron diffraction and serial femtosecond crystallography. *Nat Commun*, *12*(1), 2578. doi:10.1038/s41467-021-22590-6
- Clough, S. J., & Bent, A. F. (1998). Floral dip: a simplified method for *Agrobacterium*-mediated transformation of *Arabidopsis thaliana*. *Plant J*, *16*(6), 735-743. doi:10.1046/j.1365-313x.1998.00343.x
- Couto, D., & Zipfel, C. (2016). Regulation of pattern recognition receptor signalling in plants. *Nat Rev Immunol*, *16*(9), 537-552. doi:10.1038/nri.2016.77
- Cui, H., Gobbato, E., Kracher, B., Qiu, J., Bautor, J., & Parker, J. E. (2017). A core function of EDS1 with PAD4 is to protect the salicylic acid defense sector in *Arabidopsis* immunity. *New Phytol*, *213*(4), 1802-1817. doi:10.1111/nph.14302
- Cui, H., Tsuda, K., & Parker, J. E. (2015). Effector-triggered immunity: from pathogen perception to robust defense. *Annu Rev Plant Biol*, *66*, 487-511. doi:10.1146/annurev-arplant-050213-040012
- Deak, M., Kiss, G. B., Koncz, C., & Dudits, D. (1986). Transformation of *Medicago* by *Agrobacterium* mediated gene transfer. *Plant Cell Rep*, *5*(2), 97-100. doi:10.1007/BF00269243
- Dongus, J. A., Bhandari, D. D., Penner, E., Lapin, D., Stolze, S. C., Harzen, A., . . . Parker, J. E. (2022). Cavity surface residues of PAD4 and SAG101 contribute to EDS1 dimer signaling specificity in plant immunity. *Plant J*, *110*(5), 1415-1432. doi:10.1111/tpj.15747
- Dongus, J. A., & Parker, J. E. (2021). EDS1 signalling: At the nexus of intracellular and surface receptor immunity. *Curr Opin Plant Biol*, *62*, 102039. doi:10.1016/j.pbi.2021.102039
- Duxbury, Z., Wang, S., MacKenzie, C. I., Tenthorey, J. L., Zhang, X., Huh, S. U., . . . Jones, J. D. G. (2020). Induced proximity of a TIR signaling domain on a plant-mammalian NLR chimera activates defense in plants. *Proc Natl Acad Sci U S A*, *117*(31), 18832-18839. doi:10.1073/pnas.2001185117

- Dyrka, W., Lamacchia, M., Durrens, P., Kobe, B., Daskalov, A., Paoletti, M., . . . Saupe, S. J. (2014). Diversity and variability of NOD-like receptors in fungi. *Genome Biol Evol*, 6(12), 3137-3158. doi:10.1093/gbe/evu251
- Eastman, S., Smith, T., Zaydman, M. A., Kim, P., Martinez, S., Damaraju, N., . . . Guo, M. (2021). A phyto-bacterial TIR domain effector manipulates NAD(+) to promote virulence. *New Phytol*. doi:10.1111/nph.17805
- El Oirdi, M., & Bouarab, K. (2007). Plant signalling components EDS1 and SGT1 enhance disease caused by the necrotrophic pathogen *Botrytis cinerea*. *New Phytol*, 175(1), 131-139. doi:10.1111/j.1469-8137.2007.02086.x
- Essuman, K., Summers, D. W., Sasaki, Y., Mao, X., DiAntonio, A., & Milbrandt, J. (2017). The SARM1 Toll/Interleukin-1 Receptor Domain Possesses Intrinsic NAD⁺ Cleavage Activity that Promotes Pathological Axonal Degeneration. *Neuron*, 93(6), 1334-1343.e1335. doi:10.1016/j.neuron.2017.02.022
- Essuman, K., Summers, D. W., Sasaki, Y., Mao, X., Yim, A. K. Y., DiAntonio, A., & Milbrandt, J. (2018). TIR Domain Proteins Are an Ancient Family of NAD⁺-Consuming Enzymes. *Current Biology*, 28(3), 421-430.e424. doi:10.1016/j.cub.2017.12.024
- Feng, Q., De Rycke, R., Dagdas, Y., & Nowack, M. K. (2022). Autophagy promotes programmed cell death and corpse clearance in specific cell types of the Arabidopsis root cap. *Curr Biol*, 32(9), 2110-2119 e2113. doi:10.1016/j.cub.2022.03.053
- Fields, J. K., Gunther, S., & Sundberg, E. J. (2019). Structural Basis of IL-1 Family Cytokine Signaling. *Front Immunol*, 10, 1412. doi:10.3389/fimmu.2019.01412
- Figley, M. D., Gu, W., Nanson, J. D., Shi, Y., Sasaki, Y., Cunnea, K., . . . Ve, T. (2021). SARM1 is a metabolic sensor activated by an increased NMN/NAD(+) ratio to trigger axon degeneration. *Neuron*, 109(7), 1118-1136 e1111. doi:10.1016/j.neuron.2021.02.009
- Finn, R. D., Clements, J., & Eddy, S. R. (2011). HMMER web server: interactive sequence similarity searching. *Nucleic Acids Res*, 39(Web Server issue), W29-37. doi:10.1093/nar/gkr367
- Gantner, J., Ordon, J., Kretschmer, C., Guerois, R., & Stuttmann, J. (2019). An EDS1-SAG101 Complex Is Essential for TNL-Mediated Immunity in *Nicotiana benthamiana*. *The Plant Cell*, 31(10), 2456-2474. doi:10.1105/tpc.19.00099
- Gao, C., Ren, X., Mason, A. S., Liu, H., Xiao, M., Li, J., & Fu, D. (2014). Horizontal gene transfer in plants. *Funct Integr Genomics*, 14(1), 23-29. doi:10.1007/s10142-013-0345-0
- Gay, N. J., & Keith, F. J. (1991). Drosophila Toll and IL-1 receptor. *Nature*, 351(6325), 355-356. doi:10.1038/351355b0
- Glazebrook, J., Zook, M., Mert, F., Kagan, I., Rogers, E. E., Crute, I. R., . . . Ausubel, F. M. (1997). Phytoalexin-deficient mutants of Arabidopsis reveal that PAD4 encodes a regulatory factor and that four PAD genes contribute to downy mildew resistance. *Genetics*, 146(1), 381-392. doi:10.1093/genetics/146.1.381
- Guo, H., Ahn, H. K., Sklenar, J., Huang, J., Ma, Y., Ding, P., . . . Jones, J. D. G. (2020). Phosphorylation-Regulated Activation of the Arabidopsis RRS1-R/RPS4 Immune Receptor Complex Reveals Two Distinct Effector Recognition Mechanisms. *Cell Host Microbe*, 27(5), 769-781 e766. doi:10.1016/j.chom.2020.03.008
- Guzha, A., McGee, R., Scholz, P., Hartken, D., Ludke, D., Bauer, K., . . . Ischebeck, T. (2022). Cell wall-localized BETA-XYLOSIDASE4 contributes to immunity of Arabidopsis against *Botrytis cinerea*. *Plant Physiol*, 189(3), 1794-1813. doi:10.1093/plphys/kiac165
- Hinsch, M., & Staskawicz, B. (1996). Identification of a new Arabidopsis disease resistance locus, RPs4, and cloning of the corresponding avirulence gene, avrRps4, from *Pseudomonas syringae* pv. pisi. *Mol Plant Microbe Interact*, 9(1), 55-61. doi:10.1094/mpmi-9-0055

- Horsefield, S., Burdett, H., Zhang, X., Manik, M. K., Shi, Y., Chen, J., . . . Kobe, B. (2019). NAD⁺ cleavage activity by animal and plant TIR domains in cell death pathways. *Science*, 365(6455), 793. doi:10.1126/science.aax1911
- Huang, S., Jia, A., Song, W., Hessler, G., Meng, Y., Sun, Y., . . . Chai, J. (2022). Identification and receptor mechanism of TIR-catalyzed small molecules in plant immunity. *Science*, 377(6605), eabq3297. doi:10.1126/science.abq3297
- Jacob, P., Kim, N. H., Wu, F., El-Kasmi, F., Chi, Y., Walton, W. G., . . . Dangl, J. L. (2021). Plant "helper" immune receptors are Ca(2+)-permeable nonselective cation channels. *Science*, 373(6553), 420-425. doi:10.1126/science.abg7917
- Jia, A., Huang, S., Song, W., Wang, J., Meng, Y., Sun, Y., . . . Chai, J. (2022). TIR-catalyzed ADP-ribosylation reactions produce signaling molecules for plant immunity. *Science*, 377(6605), eabq8180. doi:10.1126/science.abq8180
- Jirage, D., Tootle, T. L., Reuber, T. L., Frost, L. N., Feys, B. J., Parker, J. E., . . . Glazebrook, J. (1999). Arabidopsis thaliana PAD4 encodes a lipase-like gene that is important for salicylic acid signaling. *Proc Natl Acad Sci U S A*, 96(23), 13583-13588. doi:10.1073/pnas.96.23.13583
- Johandrees, O., Baggs, E. L., Uhlmann, C., Locci, F., Läßle, H. L., Melkonian, K., . . . Lapin, D. (2021). Differential EDS1 requirement for cell death activities of plant TIR-domain proteins. *bioRxiv*, 2021.2011.2029.470438. doi:10.1101/2021.11.29.470438
- Jones, J. D., & Dangl, J. L. (2006). The plant immune system. *Nature*, 444(7117), 323-329. doi:10.1038/nature05286
- Jones, J. D., Vance, R. E., & Dangl, J. L. (2016). Intracellular innate immune surveillance devices in plants and animals. *Science*, 354(6316). doi:10.1126/science.aaf6395
- Kadota, Y., Sklenar, J., Derbyshire, P., Stransfeld, L., Asai, S., Ntoukakis, V., . . . Zipfel, C. (2014). Direct regulation of the NADPH oxidase RBOHD by the PRR-associated kinase BIK1 during plant immunity. *Mol Cell*, 54(1), 43-55. doi:10.1016/j.molcel.2014.02.021
- Katoh, K., Misawa, K., Kuma, K., & Miyata, T. (2002). MAFFT: a novel method for rapid multiple sequence alignment based on fast Fourier transform. *Nucleic Acids Res*, 30(14), 3059-3066. doi:10.1093/nar/gkf436
- Kawasaki, T., & Kawai, T. (2014). Toll-like receptor signaling pathways. *Front Immunol*, 5, 461. doi:10.3389/fimmu.2014.00461
- Kibby, E. M., Conte, A. N., Burroughs, A. M., Nagy, T. A., Vargas, J. A., Aravind, L., & Whiteley, A. T. (2022). Bacterial NLR-related proteins protect against phage. *bioRxiv*, 2022.2007.2019.500537. doi:10.1101/2022.07.19.500537
- Krasileva, K. V., Dahlbeck, D., & Staskawicz, B. J. (2010). Activation of an Arabidopsis Resistance Protein Is Specified by the in Planta Association of Its Leucine-Rich Repeat Domain with the Cognate Oomycete Effector *The Plant Cell*, 22(7), 2444-2458. doi:10.1105/tpc.110.075358
- Kumar, S., Stecher, G., Suleski, M., & Hedges, S. B. (2017). TimeTree: A Resource for Timelines, Timetrees, and Divergence Times. *Mol Biol Evol*, 34(7), 1812-1819. doi:10.1093/molbev/msx116
- Lapin, D., Bhandari, D. D., & Parker, J. E. (2020). Origins and Immunity Networking Functions of EDS1 Family Proteins. *Annual Review of Phytopathology*, 58(1), 253-276. doi:10.1146/annurev-phyto-010820-012840
- Lapin, D., Johandrees, O., Wu, Z., Li, X., & Parker, J. E. (2022). Molecular innovations in plant TIR-based immunity signaling. *Plant Cell*, 34(5), 1479-1496. doi:10.1093/plcell/koac035

- Lapin, D., Kovacova, V., Sun, X., Dongus, J. A., Bhandari, D., von Born, P., . . . Parker, J. E. (2019). A Coevolved EDS1-SAG101-NRG1 Module Mediates Cell Death Signaling by TIR-Domain Immune Receptors. *The Plant Cell*, *31*(10), 2430-2455. doi:10.1105/tpc.19.00118
- Lemaitre, B., Nicolas, E., Michaut, L., Reichhart, J. M., & Hoffmann, J. A. (1996). The dorsoventral regulatory gene cassette spatzle/Toll/cactus controls the potent antifungal response in *Drosophila* adults. *Cell*, *86*(6), 973-983. doi:10.1016/s0092-8674(00)80172-5
- Letunic, I., & Bork, P. (2021). Interactive Tree Of Life (iTOL) v5: an online tool for phylogenetic tree display and annotation. *Nucleic Acids Res*, *49*(W1), W293-W296. doi:10.1093/nar/gkab301
- Li, L., Li, M., Yu, L., Zhou, Z., Liang, X., Liu, Z., . . . Zhou, J. M. (2014). The FLS2-associated kinase BIK1 directly phosphorylates the NADPH oxidase RbohD to control plant immunity. *Cell Host Microbe*, *15*(3), 329-338. doi:10.1016/j.chom.2014.02.009
- Lionetti, V., Fabri, E., De Caroli, M., Hansen, A. R., Willats, W. G., Piro, G., & Bellincampi, D. (2017). Three Pectin Methyltransferase Inhibitors Protect Cell Wall Integrity for Arabidopsis Immunity to Botrytis. *Plant Physiol*, *173*(3), 1844-1863. doi:10.1104/pp.16.01185
- Liu, Y., Zeng, Z., Zhang, Y. M., Li, Q., Jiang, X. M., Jiang, Z., . . . Shao, Z. Q. (2021). An angiosperm NLR atlas reveals that NLR gene reduction is associated with ecological specialization and signal transduction component deletion. *Mol Plant*. doi:10.1016/j.molp.2021.08.001
- Logemann, E., Birkenbihl, R. P., Ulker, B., & Somssich, I. E. (2006). An improved method for preparing *Agrobacterium* cells that simplifies the Arabidopsis transformation protocol. *Plant Methods*, *2*, 16. doi:10.1186/1746-4811-2-16
- Lu, D., Wu, S., Gao, X., Zhang, Y., Shan, L., & He, P. (2010). A receptor-like cytoplasmic kinase, BIK1, associates with a flagellin receptor complex to initiate plant innate immunity. *Proc Natl Acad Sci U S A*, *107*(1), 496-501. doi:10.1073/pnas.0909705107
- Ma, S., Lapin, D., Liu, L., Sun, Y., Song, W., Zhang, X., . . . Chai, J. (2020). Direct pathogen-induced assembly of an NLR immune receptor complex to form a holoenzyme. *Science*, *370*(6521), eabe3069. doi:10.1126/science.abe3069
- Martin, R., Qi, T., Zhang, H., Liu, F., King, M., Toth, C., . . . Staskawicz, B. J. (2020). Structure of the activated ROQ1 resistosome directly recognizing the pathogen effector XopQ. *Science*, *370*(6521), eabd9993. doi:10.1126/science.abd9993
- Meyers, B. C., Dickerman, A. W., Michelmore, R. W., Sivaramakrishnan, S., Sobral, B. W., & Young, N. D. (1999). Plant disease resistance genes encode members of an ancient and diverse protein family within the nucleotide-binding superfamily. *Plant J*, *20*(3), 317-332. doi:10.1046/j.1365-313x.1999.t01-1-00606.x
- Meyers, B. C., Morgante, M., & Michelmore, R. W. (2002). TIR-X and TIR-NBS proteins: two new families related to disease resistance TIR-NBS-LRR proteins encoded in Arabidopsis and other plant genomes. *The Plant Journal*, *32*(1), 77-92. doi:https://doi.org/10.1046/j.1365-313X.2002.01404.x
- Monteiro, F., & Nishimura, M. T. (2018). Structural, Functional, and Genomic Diversity of Plant NLR Proteins: An Evolved Resource for Rational Engineering of Plant Immunity. *Annu Rev Phytopathol*, *56*, 243-267. doi:10.1146/annurev-phyto-080417-045817
- Nandety, R. S., Caplan, J. L., Cavanaugh, K., Perroud, B., Wroblewski, T., Michelmore, R. W., & Meyers, B. C. (2013). The Role of TIR-NBS and TIR-X Proteins in Plant Basal Defense Responses. *Plant Physiology*, *162*(3), 1459-1472. doi:10.1104/pp.113.219162

- Nanson, J. D., Rahaman, M. H., Ve, T., & Kobe, B. (2020). Regulation of signaling by cooperative assembly formation in mammalian innate immunity signalosomes by molecular mimics. *Semin Cell Dev Biol*, *99*, 96-114. doi:10.1016/j.semcdb.2018.05.002
- Neuwald, A. F. (2014). A Bayesian sampler for optimization of protein domain hierarchies. *J Comput Biol*, *21*(3), 269-286. doi:10.1089/cmb.2013.0099
- Ngou, B. P. M., Ahn, H. K., Ding, P., & Jones, J. D. G. (2021). Mutual potentiation of plant immunity by cell-surface and intracellular receptors. *Nature*, *592*(7852), 110-115. doi:10.1038/s41586-021-03315-7
- Nguyen, L. T., Schmidt, H. A., von Haeseler, A., & Minh, B. Q. (2015). IQ-TREE: a fast and effective stochastic algorithm for estimating maximum-likelihood phylogenies. *Mol Biol Evol*, *32*(1), 268-274. doi:10.1093/molbev/msu300
- Nimma, S., Gu, W., Maruta, N., Li, Y., Pan, M., Saikot, F. K., . . . Kobe, B. (2021). Structural Evolution of TIR-Domain Signalosomes. *Front Immunol*, *12*, 784484. doi:10.3389/fimmu.2021.784484
- Nishimura, M. T., Anderson, R. G., Cherkis, K. A., Law, T. F., Liu, Q. L., Machius, M., . . . Dangl, J. L. (2017). TIR-only protein RBA1 recognizes a pathogen effector to regulate cell death in *Arabidopsis*. *Proceedings of the National Academy of Sciences*, *114*(10), E2053. doi:10.1073/pnas.1620973114
- O'Neill, L. A. J., & Bowie, A. G. (2007). The family of five: TIR-domain-containing adaptors in Toll-like receptor signalling. *Nature Reviews Immunology*, *7*(5), 353-364. doi:10.1038/nri2079
- Ofir, G., Herbst, E., Baroz, M., Cohen, D., Millman, A., Doron, S., . . . Sorek, R. (2021). Antiviral activity of bacterial TIR domains via immune signalling molecules. *Nature*, *600*(7887), 116-120. doi:10.1038/s41586-021-04098-7
- Ono, E., Mise, K., & Takano, Y. (2020). RLP23 is required for Arabidopsis immunity against the grey mould pathogen *Botrytis cinerea*. *Sci Rep*, *10*(1), 13798. doi:10.1038/s41598-020-70485-1
- Ordon, J., Bressan, M., Kretschmer, C., Dall'Osto, L., Marillonnet, S., Bassi, R., & Stuttmann, J. (2020). Optimized Cas9 expression systems for highly efficient Arabidopsis genome editing facilitate isolation of complex alleles in a single generation. *Funct Integr Genomics*, *20*(1), 151-162. doi:10.1007/s10142-019-00665-4
- Ordon, J., Gantner, J., Kemna, J., Schwalgun, L., Reschke, M., Streubel, J., . . . Stuttmann, J. (2017). Generation of chromosomal deletions in dicotyledonous plants employing a user-friendly genome editing toolkit. *Plant J*, *89*(1), 155-168. doi:10.1111/tbj.13319
- Patro, R., Duggal, G., Love, M. I., Irizarry, R. A., & Kingsford, C. (2017). Salmon provides fast and bias-aware quantification of transcript expression. *Nat Methods*, *14*(4), 417-419. doi:10.1038/nmeth.4197
- Pruitt, R. N., Locci, F., Wanke, F., Zhang, L., Saile, S. C., Joe, A., . . . Nurnberger, T. (2021). The EDS1-PAD4-ADR1 node mediates Arabidopsis pattern-triggered immunity. *Nature*, *598*(7881), 495-499. doi:10.1038/s41586-021-03829-0
- Qi, T., Seong, K., Thomazella, D. P. T., Kim, J. R., Pham, J., Seo, E., . . . Staskawicz, B. J. (2018). NRG1 functions downstream of EDS1 to regulate TIR-NLR-mediated plant immunity in *Nicotiana benthamiana*. *Proc Natl Acad Sci U S A*, *115*(46), E10979-E10987. doi:10.1073/pnas.1814856115

- Rendon-Anaya, M., Ibarra-Laclette, E., Mendez-Bravo, A., Lan, T., Zheng, C., Carretero-Paulet, L., . . . Herrera-Estrella, L. (2019). The avocado genome informs deep angiosperm phylogeny, highlights introgressive hybridization, and reveals pathogen-influenced gene space adaptation. *Proc Natl Acad Sci U S A*, *116*(34), 17081-17089. doi:10.1073/pnas.1822129116
- Saile, S. C., Jacob, P., Castel, B., Jubic, L. M., Salas-González, I., Bäcker, M., . . . El Kasmi, F. (2020). Two unequally redundant "helper" immune receptor families mediate *Arabidopsis thaliana* intracellular "sensor" immune receptor functions. *PLOS Biology*, *18*(9), e3000783. doi:10.1371/journal.pbio.3000783
- Sarris, P. F., Cevik, V., Dagdas, G., Jones, J. D., & Krasileva, K. V. (2016). Comparative analysis of plant immune receptor architectures uncovers host proteins likely targeted by pathogens. *BMC Biol*, *14*, 8. doi:10.1186/s12915-016-0228-7
- Saur, I. M., Bauer, S., Kracher, B., Lu, X., Franzeskakis, L., Muller, M. C., . . . Schulze-Lefert, P. (2019a). Multiple pairs of allelic MLA immune receptor-powdery mildew AVR effectors argue for a direct recognition mechanism. *Elife*, *8*. doi:10.7554/eLife.44471
- Saur, I. M. L., Bauer, S., Lu, X., & Schulze-Lefert, P. (2019b). A cell death assay in barley and wheat protoplasts for identification and validation of matching pathogen AVR effector and plant NLR immune receptors. *Plant Methods*, *15*, 118. doi:10.1186/s13007-019-0502-0
- Schindelin, J., Arganda-Carreras, I., Frise, E., Kaynig, V., Longair, M., Pietzsch, T., . . . Cardona, A. (2012). Fiji: an open-source platform for biological-image analysis. *Nat Methods*, *9*(7), 676-682. doi:10.1038/nmeth.2019
- Schultink, A., Qi, T., Lee, A., Steinbrenner, A. D., & Staskawicz, B. (2017). Roq1 mediates recognition of the *Xanthomonas* and *Pseudomonas* effector proteins XopQ and HopQ1. *The Plant Journal*, *92*(5), 787-795. doi:https://doi.org/10.1111/tpj.13715
- Seidl, M. F., & Van den Ackerveken, G. (2019). Activity and Phylogenetics of the Broadly Occurring Family of Microbial Nep1-Like Proteins. *Annu Rev Phytopathol*, *57*, 367-386. doi:10.1146/annurev-phyto-082718-100054
- Shao, Z.-Q., Xue, J.-Y., Wu, P., Zhang, Y.-M., Wu, Y., Hang, Y.-Y., . . . Chen, J.-Q. (2016). Large-Scale Analyses of Angiosperm Nucleotide-Binding Site-Leucine-Rich Repeat Genes Reveal Three Anciently Diverged Classes with Distinct Evolutionary Patterns. *Plant Physiology*, *170*(4), 2095-2109. doi:10.1104/pp.15.01487
- Shen, C., Vohra, M., Zhang, P., Mao, X., Figley, M. D., Zhu, J., . . . Milbrandt, J. (2021). Multiple domain interfaces mediate SARM1 autoinhibition. *Proc Natl Acad Sci U S A*, *118*(4). doi:10.1073/pnas.2023151118
- Shi, Y., Kerry, P. S., Nanson, J. D., Bosanac, T., Sasaki, Y., Krauss, R., . . . Ve, T. (2022). Structural basis of SARM1 activation, substrate recognition, and inhibition by small molecules. *Mol Cell*, *82*(9), 1643-1659 e1610. doi:10.1016/j.molcel.2022.03.007
- Sohn, K. H., Segonzac, C., Rallapalli, G., Sarris, P. F., Woo, J. Y., Williams, S. J., . . . Jones, J. D. (2014). The nuclear immune receptor RPS4 is required for RRS1SLH1-dependent constitutive defense activation in *Arabidopsis thaliana*. *PLoS Genet*, *10*(10), e1004655. doi:10.1371/journal.pgen.1004655
- Soneson, C., Love, M. I., & Robinson, M. D. (2015). Differential analyses for RNA-seq: transcript-level estimates improve gene-level inferences. *F1000Res*, *4*, 1521. doi:10.12688/f1000research.7563.2
- Sporny, M., Guez-Haddad, J., Khazma, T., Yaron, A., Dessau, M., Shkolnisky, Y., . . . Opatowsky, Y. (2020). Structural basis for SARM1 inhibition and activation under energetic stress. *Elife*, *9*. doi:10.7554/eLife.62021

- Steuernagel, B., Witek, K., Krattinger, S. G., Ramirez-Gonzalez, R. H., Schoonbeek, H. J., Yu, G., . . . Wulff, B. B. H. (2020). The NLR-Annotator Tool Enables Annotation of the Intracellular Immune Receptor Repertoire. *Plant Physiol*, *183*(2), 468-482. doi:10.1104/pp.19.01273
- Stuttman, J., Barthel, K., Martin, P., Ordon, J., Erickson, J. L., Herr, R., . . . Bonas, U. (2021). Highly efficient multiplex editing: one-shot generation of 8x *Nicotiana benthamiana* and 12x *Arabidopsis* mutants. *Plant J*, *106*(1), 8-22. doi:10.1111/tpj.15197
- Sun, X., Lapin, D., Feehan, J. M., Stolze, S. C., Kramer, K., Dongus, J. A., . . . Parker, J. E. (2021). Pathogen effector recognition-dependent association of NRG1 with EDS1 and SAG101 in TNL receptor immunity. *Nat Commun*, *12*(1), 3335. doi:10.1038/s41467-021-23614-x
- Sun, X., Pang, H., Li, M., Chen, J., & Hang, Y. (2014). Tracing the origin and evolution of plant TIR-encoding genes. *Gene*, *546*(2), 408-416. doi:10.1016/j.gene.2014.04.060
- Sun, Y., Li, L., Macho, A. P., Han, Z., Hu, Z., Zipfel, C., . . . Chai, J. (2013). Structural basis for flg22-induced activation of the *Arabidopsis* FLS2-BAK1 immune complex. *Science*, *342*(6158), 624-628. doi:10.1126/science.1243825
- Tamborski, J., & Krasileva, K. V. (2020). Evolution of Plant NLRs: From Natural History to Precise Modifications. *Annual Review of Plant Biology*, *71*(1), 355-378. doi:10.1146/annurev-arplant-081519-035901
- Thieme, F., Koebnik, R., Bekel, T., Berger, C., Boch, J., Buttner, D., . . . Kaiser, O. (2005). Insights into genome plasticity and pathogenicity of the plant pathogenic bacterium *Xanthomonas campestris* pv. *vesicatoria* revealed by the complete genome sequence. *J Bacteriol*, *187*(21), 7254-7266. doi:10.1128/JB.187.21.7254-7266.2005
- Tian, H., Wu, Z., Chen, S., Ao, K., Huang, W., Yaghmaiean, H., . . . Zhang, Y. (2021). Activation of TIR signalling boosts pattern-triggered immunity. *Nature*, *598*(7881), 500-503. doi:10.1038/s41586-021-03987-1
- Toruno, T. Y., Stergiopoulos, I., & Coaker, G. (2016). Plant-Pathogen Effectors: Cellular Probes Interfering with Plant Defenses in Spatial and Temporal Manners. *Annu Rev Phytopathol*, *54*, 419-441. doi:10.1146/annurev-phyto-080615-100204
- Toshchakov, V. Y., & Neuwald, A. F. (2020). A survey of TIR domain sequence and structure divergence. *Immunogenetics*, *72*(3), 181-203. doi:10.1007/s00251-020-01157-7
- Urbach, J. M., & Ausubel, F. M. (2017). The NBS-LRR architectures of plant R-proteins and metazoan NLRs evolved in independent events. *Proc Natl Acad Sci U S A*, *114*(5), 1063-1068. doi:10.1073/pnas.1619730114
- van der Hoorn, R. A., & Kamoun, S. (2008). From Guard to Decoy: a new model for perception of plant pathogen effectors. *Plant Cell*, *20*(8), 2009-2017. doi:10.1105/tpc.108.060194
- Venugopal, S. C., Jeong, R. D., Mandal, M. K., Zhu, S., Chandra-Shekara, A. C., Xia, Y., . . . Kachroo, P. (2009). Enhanced disease susceptibility 1 and salicylic acid act redundantly to regulate resistance gene-mediated signaling. *PLoS Genet*, *5*(7), e1000545. doi:10.1371/journal.pgen.1000545
- Wagih, O. (2017). ggseqlogo: a versatile R package for drawing sequence logos. *Bioinformatics*, *33*(22), 3645-3647. doi:10.1093/bioinformatics/btx469
- Wagner, S., Stuttman, J., Rietz, S., Guerois, R., Brunstein, E., Bautor, J., . . . Parker, Jane E. (2013). Structural Basis for Signaling by Exclusive EDS1 Heteromeric Complexes with SAG101 or PAD4 in Plant Innate Immunity. *Cell Host & Microbe*, *14*(6), 619-630. doi:https://doi.org/10.1016/j.chom.2013.11.006

- Wan, L., Essuman, K., Anderson, R. G., Sasaki, Y., Monteiro, F., Chung, E.-H., . . . Nishimura, M. T. (2019). TIR domains of plant immune receptors are NAD⁺-cleaving enzymes that promote cell death. *Science*, *365*(6455), 799. doi:10.1126/science.aax1771
- Wang, G., Roux, B., Feng, F., Guy, E., Li, L., Li, N., . . . Zhou, J. M. (2015). The Decoy Substrate of a Pathogen Effector and a Pseudokinase Specify Pathogen-Induced Modified-Self Recognition and Immunity in Plants. *Cell Host Microbe*, *18*(3), 285-295. doi:10.1016/j.chom.2015.08.004
- Wang, J., Hu, M., Wang, J., Qi, J., Han, Z., Wang, G., . . . Chai, J. (2019a). Reconstitution and structure of a plant NLR resistosome conferring immunity. *Science*, *364*(6435). doi:10.1126/science.aav5870
- Wang, J., Wang, J., Hu, M., Wu, S., Qi, J., Wang, G., . . . Chai, J. (2019b). Ligand-triggered allosteric ADP release primes a plant NLR complex. *Science*, *364*(6435). doi:10.1126/science.aav5868
- Whitham, S., Dinesh-Kumar, S. P., Choi, D., Hehl, R., Corr, C., & Baker, B. (1994). The product of the tobacco mosaic virus resistance gene N: similarity to toll and the interleukin-1 receptor. *Cell*, *78*(6), 1101-1115. doi:10.1016/0092-8674(94)90283-6
- Wiermer, M., Feys, B. J., & Parker, J. E. (2005). Plant immunity: the EDS1 regulatory node. *Curr Opin Plant Biol*, *8*(4), 383-389. doi:10.1016/j.pbi.2005.05.010
- Williams, S. J., Sohn, K. H., Wan, L., Bernoux, M., Sarris, P. F., Segonzac, C., . . . Jones, J. D. G. (2014). Structural Basis for Assembly and Function of a Heterodimeric Plant Immune Receptor. *Science*, *344*(6181), 299. doi:10.1126/science.1247357
- Wirthmueller, L., Zhang, Y., Jones, J. D., & Parker, J. E. (2007). Nuclear accumulation of the Arabidopsis immune receptor RPS4 is necessary for triggering EDS1-dependent defense. *Curr Biol*, *17*(23), 2023-2029. doi:10.1016/j.cub.2007.10.042
- Wu, Z., Li, M., Dong, O. X., Xia, S., Liang, W., Bao, Y., . . . Li, X. (2019). Differential regulation of TNL-mediated immune signaling by redundant helper CNLs. *New Phytol*, *222*(2), 938-953. doi:10.1111/nph.15665
- Wu, Z., Tian, L., Liu, X., Zhang, Y., & Li, X. (2021). TIR signal promotes interactions between lipase-like proteins and ADR1-L1 receptor and ADR1-L1 oligomerization. *Plant Physiol*, *187*(2), 681-686. doi:10.1093/plphys/kiab305
- Yadav, M., Zhang, J., Fischer, H., Huang, W., Lutay, N., Cirl, C., . . . Svanborg, C. (2010). Inhibition of TIR domain signaling by TcpC: MyD88-dependent and independent effects on Escherichia coli virulence. *PLoS Pathog*, *6*(9), e1001120. doi:10.1371/journal.ppat.1001120
- Yamaoka, N., Yoshida, S., Motoyama, E., Takeuchi, Y., Takada, Y., & Fukunaga, N. (2000). Resistance induction in barley coleoptile cells by intracellular pH decline. *Plant Cell Physiol*, *41*(12), 1321-1326. doi:10.1093/pcp/pcd065
- Yang, Y., Sun, P., Lv, L., Wang, D., Ru, D., Li, Y., . . . Liu, J. (2020). Prickly waterlily and rigid hornwort genomes shed light on early angiosperm evolution. *Nat Plants*, *6*(3), 215-222. doi:10.1038/s41477-020-0594-6
- Yu, D., Song, W., Tan, E. Y. J., Liu, L., Cao, Y., Jirschtzka, J., . . . Chai, J. (2022). TIR domains of plant immune receptors are 2',3'-cAMP/cGMP synthetases mediating cell death. *Cell*, *185*(13), 2370-2386 e2318. doi:10.1016/j.cell.2022.04.032
- Yu, G. (2020). Using ggtree to Visualize Data on Tree-Like Structures. *Curr Protoc Bioinformatics*, *69*(1), e96. doi:10.1002/cpbi.96

-
- Yuan, M., Jiang, Z., Bi, G., Nomura, K., Liu, M., Wang, Y., . . . Xin, X. F. (2021). Pattern-recognition receptors are required for NLR-mediated plant immunity. *Nature*, *592*(7852), 105-109. doi:10.1038/s41586-021-03316-6
- Zhang, J., Li, W., Xiang, T., Liu, Z., Laluk, K., Ding, X., . . . Zhou, J. M. (2010). Receptor-like cytoplasmic kinases integrate signaling from multiple plant immune receptors and are targeted by a *Pseudomonas syringae* effector. *Cell Host Microbe*, *7*(4), 290-301. doi:10.1016/j.chom.2010.03.007
- Zhang, X., Bernoux, M., Bentham, A. R., Newman, T. E., Ve, T., Casey, L. W., . . . Kobe, B. (2017a). Multiple functional self-association interfaces in plant TIR domains. *Proceedings of the National Academy of Sciences*, *114*(10), E2046. doi:10.1073/pnas.1621248114
- Zhang, Y.-M., Xue, J.-Y., Liu, L.-W., Sun, X.-Q., Zhou, G.-C., Chen, M., . . . Hang, Y.-Y. (2017b). Divergence and Conservative Evolution of XTNX Genes in Land Plants. *Frontiers in Plant Science*, *8*, 1844. Retrieved from <https://www.frontiersin.org/article/10.3389/fpls.2017.01844>
- Zhang, Y., Xia, R., Kuang, H., & Meyers, B. C. (2016). The Diversification of Plant NBS-LRR Defense Genes Directs the Evolution of MicroRNAs That Target Them. *Molecular Biology and Evolution*, *33*(10), 2692-2705. doi:10.1093/molbev/msw154
- Zhao, T., Zwaenepoel, A., Xue, J. Y., Kao, S. M., Li, Z., Schranz, M. E., & Van de Peer, Y. (2021). Whole-genome microsynteny-based phylogeny of angiosperms. *Nat Commun*, *12*(1), 3498. doi:10.1038/s41467-021-23665-0
- Zipfel, C., Robatzek, S., Navarro, L., Oakeley, E. J., Jones, J. D., Felix, G., & Boller, T. (2004). Bacterial disease resistance in *Arabidopsis* through flagellin perception. *Nature*, *428*(6984), 764-767. doi:10.1038/nature02485
- Zou, M., Guo, B., & He, S. (2011). The roles and evolutionary patterns of intronless genes in deuterostomes. *Comp Funct Genomics*, *2011*, 680673. doi:10.1155/2011/680673

Acknowledgements

Jane, thanks for allowing me to graduate in your group and keeping me on the project since my Master's studies. You provided an open and free research atmosphere that allowed me to learn a lot of new methods and to go my own way. Also, thank you to the other members of my TAC committee, Tonni and Takaki, for the constant support and critical questions during the meetings.

Thank you to Prof. Dr. Gunther Döhlemann for agreeing to be the second reviewer and Prof. Dr. Stanislav Kopriva for chairing my Thesis Defense.

A special thank you goes to Dima, for the great supervision during my PhD, but also already during my Master's. Thanks for showing me how to work independently in the lab and for all the support with the bioinformatic analyses and during manuscript writing. I admire your seemingly never-ending drive for science and that your days seem to have 48 instead of 24 hours.

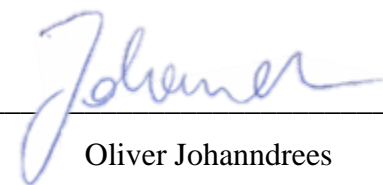
Furthermore, I would like to thank the JP group members, especially Jaqueline for helping me with countless Minipreps, PCRs, Cloning steps, Genotypings or simply watering my plants while on holidays. Thanks to Giuliana, Henni, Anthony, Fede, Junli, Fei, Joel, Charles, Anna, Lara and all other past JP members for joining me on my PhD journey. Thanks for the great working atmosphere and lots of feedback and help. I also want to thank my other office mates and the rest of the PSL Department.

Thanks to my family and friends for the constant support from home and for distracting me when I was too occupied with Science. Thank you for always being there for me.

Eidesstattliche Erklärung

Hiermit versichere ich an Eides statt, dass ich die vorliegende Dissertation selbstständig und ohne die Benutzung anderer als der angegebenen Hilfsmittel und Literatur angefertigt habe. Alle Stellen, die wörtlich oder sinngemäß aus veröffentlichten und nicht veröffentlichten Werken dem Wortlaut oder dem Sinn nach entnommen wurden, sind als solche kenntlich gemacht. Ich versichere an Eides statt, dass diese Dissertation noch keiner anderen Fakultät oder Universität zur Prüfung vorgelegen hat; dass sie - abgesehen von unten angegebenen Teilpublikationen und eingebundenen Artikeln und Manuskripten - noch nicht veröffentlicht worden ist sowie, dass ich eine Veröffentlichung der Dissertation vor Abschluss der Promotion nicht ohne Genehmigung des Promotionsausschusses vornehmen werde. Die Bestimmungen dieser Ordnung sind mir bekannt. Darüber hinaus erkläre ich hiermit, dass ich die Ordnung zur Sicherung guter wissenschaftlicher Praxis und zum Umgang mit wissenschaftlichem Fehlverhalten der Universität zu Köln gelesen und sie bei der Durchführung der Dissertation zugrundeliegenden Arbeiten und der schriftlich verfassten Dissertation beachtet habe und verpflichte mich hiermit, die dort genannten Vorgaben bei allen wissenschaftlichen Tätigkeiten zu beachten und umzusetzen. Ich versichere, dass die eingereichte elektronische Fassung der eingereichten Druckfassung vollständig entspricht.

Köln, 19. September 2022



Oliver Johandrees